ISSN: 2588-5596

JGT

Journal of Gas Technology

Volume 9 . Issue 1 . Summer 2024 . www.jgt.irangi.org

Journal of Gas Technology, JGT

Volume 9, Issue 1, Summer 2024

Publisher
Iranian Gas Institute

Contact Information
http://jgt.irangi.org
Email: ijgt.igi@gmail.com

EISSN: 2588-5596

Open Access Journal
Journal of Gas Technology is a peer reviewed, open access journal.

JOURNAL OF GAS TECHNOLOGY

Volume 9, Issue 1, Summer 2024

Annual Names of Reviewers

Ali Vatani
University of Tehran

Mastaneh Hajipour
Islamic Azad University, Science and Research Branch

Saeid Jamshidi
Sharif University of Technology

Morteza Zivdar
University of Sistan and Baluchestan

Amir Hossein Mohammadi
University of KwaZulu-Natal, South Africa

Alimorad Rashidi
Research Institute of Petroleum Industry

Davood Khoozan
Tarbiat Modares University

Omid Tavakoli
University of Tehran

Masoud Aghajani
Petroleum University of Technology

Hamid Reza Moghdam Zadeh
Islamic Azad University South Tehran Branch

Masoud Dorfeshan
Behbahan Khatam Alanbia University of Technology

Leila Moharrery
Islamic Azad University, Robat Karim Branch

Bita Zamiri
Amirkabir University of Technology

Saman Jahanbakhshi
University of Tehran

Robabeh Nasirian
Islamic Azad University, North Tehran Branch

Azadeh Hemati
Semnan University

Mahdi Elyasi Kojabad
Behbahan Khatam Alanbia University of Technology

Elham Jannatdoust
Urmia University of Technology

Ashkan Vatandoost
Mapsa Technology Center(MTC), MAPSA Company

Table of Contents

JOURNAL OF GAS TECHNOLOGY

Volume 9 / Issue 1 / Summer 2024 / Pages 5-18

Journal Home page: http://jgt.irangi.org

Evaluation of the Impact of Aqueous Phase Salinity on Carbon Dioxide Mineralization during Gas Sequestration

Bright Bariakpoa Kinate[1*], Ugwunna Dickson Amadi[2], Olalekan Kunle Akindele[3], Jeremiah Ifeanyi Okoroma[4]

1,4. Department of Petroleum Engineering, Rivers State University, Port Harcourt, Nigeria
2. Department of Petroleum and Gas, University of Salford, Manchester, UK
3. Department of Data Science, Artificial Intelligence and Modeling, University of Hull, UK

ARTICLE INFO

ORIGINAL RESEARCH ARTICLE

Article History:
Received: 12 July 2024
Revised: 17 August 2024
Accepted: 23 August 2024

Keywords:
Mineralization
Dissolution
Aquifer model
Phase Salinity
Sequestration

DOR: 20.1001.1/jgt.2024.2033713.1042

ABSTRACT

Aqueous phase salinity has a major effect on the quantity of carbon dioxide trapped by solubility trapping and may also affect mineral dissolution and precipitation. While carbon dioxide storage through structural, residual, dissolution and partly mineral trapping modes have a wide investigation, the mineral trapping potential and its influencing factors have not been explored. In this work, the effects of variable aqueous phase salinity on carbon dioxide mineralization were investigated. Numerical simulations were done using a geochemical simulator and three-dimensional homogeneous aquifer model of dimensions 30×30×10 (9000 grid blocks) and block width of 70 m was built. The generated grid was populated with petrophysical, grid and rock properties .Four models with similar rock and fluid characteristics were simulated for pure water and different salinity of 0.01 wt (10000 ppm), 0.015 wt (15000 ppm) and 0.02 wt (20000 ppm) respectively. Result shows a decrease in the moles of carbon dioxide solubilized with an increase in brine salinity level. Increase in brine salinity decreases the moles of carbon dioxide converted to aqueous ions and dissolution in resident brine. There was an increase in the rate of Kaolinite precipitation, Calcite precipitation and a decrease in the rate of Anorthite dissolution with increase in duration of carbon dioxide injection. The mineral mole changes for Anorthite increases with level of salinity and decreases with duration of carbon dioxide injection. Moreover, Calcite and Kaolinite mineral moles changes decreases with level of salinity and with duration of carbon dioxide injection. Calcite and Kaolinite decreases as aqueous phase salinity increases. This work has shown that formation minerals has different reactivity to salinity concentration which decides carbon dioxide trapping and storage capacity.

How to cite this article
B.B. Kinate, U.D. Amadi, O.K. Akindele, J.I. Okoroma, Evaluation of the Impact of Aqueous Phase Salinity on Carbondioxide Mineralization during Gas Sequestration. Journal of Gas Technology. 2024; 9(1): 5 -18. (https://jgt.irangi.org/article_717199.html)

* Corresponding author.
E-mail address: kinate.bright@ust.edu.ng, (B.B. Kinate).

Available online 10 September 2024

1. Introduction

Carbon dioxide (CO_2) is the major greenhouse gas (GHG), that arises mostly from the consumption of fossil fuels. Indisputably, sensible environmental difficulties such as climate changes and an increase in the global surface temperature are as a result of a rise in carbon dioxide emission (Abas and Khan, 2014; Olajire, 2018; Venkatraman and Alsberg, 2017; Liu et al., 2018; Singh, 2018). Geological carbon storage is one of the most promising strategies to decrease anthropogenic carbon emissions by trapping the carbon dioxide from big stationary sources and depositing it into deep geological formations (Pruess et al., 2003).

Among the numerous sorts of prospective storage locations, saline aquifers have been identified with the biggest storage capacity(Zhang et al., 2016).Generally carbon dioxide should be injected at depths below 800 m, where formation temperature and pressure would preserve the carbon dioxide in a dense supercritical phase (Pruess et al., 2003; Pentland et al., 2011). The brine-carbon dioxide density difference can then migrate toward the surface vertically. The movement can be minimized and carbon dioxide can be inhibited from leaking to the atmosphere via four basic trapping strategies, namely structural trapping (Hesse et al., 2008; Naylor et al., 2011; Iglauer et al., 2015), residual trapping which relies on the capillary forces (Pentland et al., 2011; Iglauer et al., 2011; Krevor et al., 2015; Rahman et al., 2016), dissolution trapping (Spycher et al., 2003) which is a function of carbon dioxide-brine interfacial area (Kumar et al., 2005) and mineral trapping (Xu et al., 2004; Gaus, 2010) which is a factor of the chemical reactions between reservoir rock minerals,fluids and the injected carbon dioxide (Xu et al., 2003; 2005).

The permanent storage of carbon dioxide in saline aquifer is connected with mineral trapping (Pruess, 2003; Gunter et al., 2004), where dissolved carbon dioxide reacts with the minerals present in the formation rock and with cations present in the pore water to form stable mineral precipitates, which bind injected carbon dioxide more tightly into the aquifer.

These geo-chemical reactions becomes the trapping processes for the injected carbon dioxide in saline aquifers and rely on a number of parameters, including the existing pressure and temperature of the formation, the mineralogy of the formation rock and the composition and salinity of the resident brine (Gaus, 2010).

During carbon dioxide storage, solubility and mineral trapping processes are connected in which solubility in brine have an impact on the rate of mineral trapping. As example, the higher the solubility, the more carbon dioxide that can react with formation minerals (Bachu, 2016; Kolster et al., 2018). Significantly, brine salinity has an effect on the amount of carbon dioxide trapped by solubility trapping (Saraji et al., 2014; Al-Yaseri et al., 2016; Arif et al., 2016a) and may positively or negatively influence mineral dissolution and precipitation. Carbon dioxide solubility in brine has been shown to decrease with increase in brine salinity (Al-khdheeawi et al., 2017; Al-khdheeawi et al., 2018). Kumar et al. (2020) opined that increase in brine salinity decreases the storage efficiency and mass of carbon dioxide dissolved in the aqueous phase but no significance effect on mineral precipitation in carbonate formation.

The objective of this study is to analyze the impact of different brine salinity level on carbon dioxide dissolution, carbon dioxide aqueous ions, mineral moles changes, carbon dioxide trapped for different mineral types (Anorthite, Calcite, and Kaolinite). CMG-GEM was used to built a three dimensional geological model of the aquifer and PR1978 EOS used for the thermodynamic properties evaluation. An injector well was built and completed in three layers at the bottom of the model and shut in after 10 simulation years of carbon dioxide injection and fate monitored for 190 simulation years. Then, the base model for water with no salinity was initiated and three models simulated for three different salinities and compared for the carbon dioxide mineralized for three different mineral types.

2. Methodology

2.1.Simulation and Input Data

CMG simulator and data on Aquifer properties (Aquifer depth, thickness , width, and length, Rock compressibility, Initial temperature and pressure, Permeability and porosity), Rock physics functions (saturations and phase relative permeabilities), Fluid properties (Methane and Carbon dioxide fractions, Aquifer temperature, Aquifer salinity), Injection well (Grids well completion, Well radius and skin, Maximum Bottom-hole pressure, Maximum injection rate), Mineral properties and kinetic parameters (Rate constant, Reactive surface area, Activation energy, Molecular weight and initial volume fraction) were used and presented in (Table 1 to Table 6).

Table 1. Aquifer Properties for the Initial Condition (Khan et al., 2015)

Property	Value
Aquifer depth	1265 m
Aquifer thickness (z direction)	300 m (10×30)
Aquifer length	2100 m (30×70)
Rock compressibility	4.5×10^{-7} per kPa
Initial reservoir temperature	45 °C
Initial reservoir pressure	12400 kPa
Permeability	165 mD
Porosity	0.21
Gas/Water contact	1250 m

Table 2. Data for GEM Fluid Model Creation (Khan et al., 2015)

Component	Mole fraction
CH_4	0.999
CO_2	0.001
Aquifer temperature	45 °C
Aquifer salinity	10000 ppm (base case)

Table 3. Properties and Kinetic Rate Parameters for Minerals (Khan et al., 2015)

Minerals	Rate Constant mol/m². s	Reactive Surface Area m²/m³	Activation Energy J/mole	Molecular Weight g/mol	Initial Volume Fraction
Calcite	-8.78	88	41870	100	0.0088
Anorthite	-12	88	67830	278	0.0088
Kaolinite	-13	17600	62760	258.1603	0.0176

Table 4. Water Relative Permeability Data

Sw	Krw	Krow
0.20	0.0000	1.0000
0.30	0.0002	0.5862
0.40	0.0039	0.3164
0.50	0.0198	0.1526
0.60	0.0625	0.0625
0.70	0.1526	0.0198
0.8	0.3164	0.0039
0.9	0.5862	0.0002
1	1.0000	0.0000

Table 5. Gas Relative Permeability Data

Sg	Krg	Krog
0.05	0.0005	0.7725
0.1	0.0037	0.5862
0.2	0.0273	0.3164
0.3	0.0857	0.1526
0.4	0.1875	0.0625
0.5	0.3357	0.0198
0.6	0.5273	0.0039
0.7	0.7537	0.0002
0.8	1.0000	0.0000

Table 6. Parameters of the Injection Well (Khan et al., 2015)

Property	Value
Grids well completion (I J K)	15, 15, 8-10
Injection duration	10 years
Well radius	0.0762 m
Skin	0
CO_2 mole fraction	1
Maximum Bottom-hole Pressure	28300 kPa
Maximum injection rate (SC)	89200 m^3/day

2.2. Transport Equation for Mineral and Aqueous Phase

The simulations were performed using the commercial compositional generalised equation of state simulator (CMG-GEM). The governing equations are given in equation (1), (2), (3) and (4);

For the components of the gaseous phase, the mass balance equation is given by;

$$\frac{\partial N_{ig}}{\partial t} = \nabla.\left(\frac{\rho_g k k_{rg} m_{ig,g}}{\mu_g}\right)(\nabla p + \nabla p_{cwg} - \rho_g g \nabla z) + \nabla.\left(\frac{\rho_w k k_{rw} m_{ig,w}}{\mu_w}\right)(\nabla p + \nabla p_{cwg} - \rho_w g \nabla z) + \nabla. J_{ig} + \sigma_{ig,aq} + q \quad (1)$$

For the components in the aqueous phase;

$$\frac{\partial N_{ia}}{\partial t} = \nabla.\left(\frac{\rho_w k w m_{ia,w}}{\mu_w}\right)(\nabla p - \rho_w g \nabla z) + \nabla. J_{ia} + \sigma_{ia,aq} + \sigma_{ia,mn} + q \quad (2)$$

For the minerals;

$$\frac{\partial N_{km}}{\partial t} = \sigma_{km,mn} \quad (3)$$

Where $\sigma_{km,mn}$ is mineral reaction rate, ρ_g is density of gas, ρ_w is density of water, ρ_{cwg} is capillary pressure between water and gas, J_{ig} is diffusion/dispersion of gas component, J_{ia} is diffusion/dispersion of aqueous component, N_{ig} is the number of moles of gas component i per grid volume, q is well molar flow rate of gas component, $m_{ig,g}$ is the mole fractions of gas component i in gas phase, $m_{ig,w}$ is the mole fractions of gas component i in aqueous phase, $m_{ia,w}$ is mole fraction of aqueous component i in aqueous phase, $\sigma_{ig,aq}$ is reaction rate between gaseous and aqueous component, $\sigma_{ia,aq}$ is reaction rate between aqueous and aqueous component, $\sigma_{ia,mn}$ is reaction rate between aqueous and mineral component, k is permeability, k_{rg} is gas relative permeability, k_{rw} is water relative permeability, t is time step, and z is depth and p is water pressure.

The first terms at left hand side of equations (1), (2) and (3) represent the accumulation.

The first and second terms at the right-hand side of equations (2), and (3) describe convective and diffusive transport respectively. q in equations (1) and (2) are the flow rates and, in this study, represent the CO_2 injection rate.

The mineral dissolution/precipitation due to chemical reactions with the components forming the aqueous phase in equations (3) is governed by:

$$R_i = A_i k_i \left(\frac{1 - Q_i}{k_{eq,i}}\right) \quad (4)$$

Where A_i is reactive surface area for mineral i, k_i is reaction rate constant, Q_i is activity product of mineral reaction i, and $k_{eq,i}$ is the equilibrium constant for mineral reaction.

The numerical method adopted for solving the above governing equations was the finite difference method with the adaptive-implicit discretisation. Newton's method was used to solve the equations describing the flow, the phase equilibrium, the chemical equilibrium and the mineral dissolution and precipitation rates.

Geochemical reactions

i. Intra-aqueous chemical equilibrium reactions

$$CO_{2(aq)} + H_2O = H^+ + HCO_3^-$$

$$CO_3^{2-} + H^+ = HCO_3^-$$

$$OH^- + H^+ = H_2O$$

ii. Mineral reactions

$$Calcite + H^+ = Ca^{2+} + HCO_3^-$$

$$Anorthite + 8H^+ = Ca^{++} + 2Al^{+++} + 2SiO_{2(aq)} + 4H_2O$$

$$Kaolinite + 6H^+ = 5H_2O + 2SiO_{2(aq)} + 2Al^{+++}$$

$Koalinite: Al_2Si_2O_5(OH)_4$

$Calcite: CaCO_3$

$Anorthite: CaAl_2Si_2O_8$

2.3. Simulation Approach

We used CMG-GEM and built-in grid building module "Builder" to generate the geological model of the aquifer. A three (3) dimensional homogeneous aquifer model of dimensions 30×30×10 (9000 grid blocks) and block width of 70 m was built. The generated grid was populated with petrophysical, grid and rock properties with

the data presented in (Table 1). Data in (Table 2) and (Table 3) were used for the calculation of the properties of CH_4 and CO_2 (critical pressure, critical temperature, acentric factors and binary interaction coefficients) and the mineral species present in the aquifer at initial condition with PR1978 selected as the EoS for thermodynamic properties calculation. The aquifer was assumed to be completely saturated with reservoir brine and has an insignificant concentration of trace gas (methane gas). Li-Nghiem's model was used for the calculation of Henry's constant for gas solubility in brine. The created fluid model was imported into the component section of GEM data file. Relative permeability data in (Table 4) and (Table 5) were used to define the relative permeability curves and the model was initialized with water-gas contact set at 1250 m above the reference depth which gave a model fully saturated with brine. Gas cap was initialized with supercritical CO_2 fraction of 0.001 and CH_4 fraction of 0.999 respectively.

An injector well 'CO_2_INJECTOR' was completed in three layers at the bottom of the model with the data presented in (Table 6). Pure supercritical CO_2 was injected at a maximum, constant surface gas rate of 89200 m^3/day with a bottomhole injection pressure limit of 28300 kPa for 10 years. The injector was shut-in after 10 years of CO_2 injection with the CO_2 fate monitored for 190 years. The base case model for pure water (zero salinity level) was initiated and three models with similar rock and fluid characteristics simulated for different salinity of 0.01 wt (10000 ppm), 0.015 wt (15000 ppm) and 0.02 wt (20000 ppm) in terms of NaCl concentration as brines and modeled with assumption that the total salinity is due only to Na+ and Cl- ions. The simulation work flow is shown in (Figure 1).

The 3D visualization of the reservoir model for case with no salinity, 10000 ppm, 15000 ppm and 20000 ppm salinities are presented in (Figure 2), (Figure 3), (Figure 4) and (figure 5).

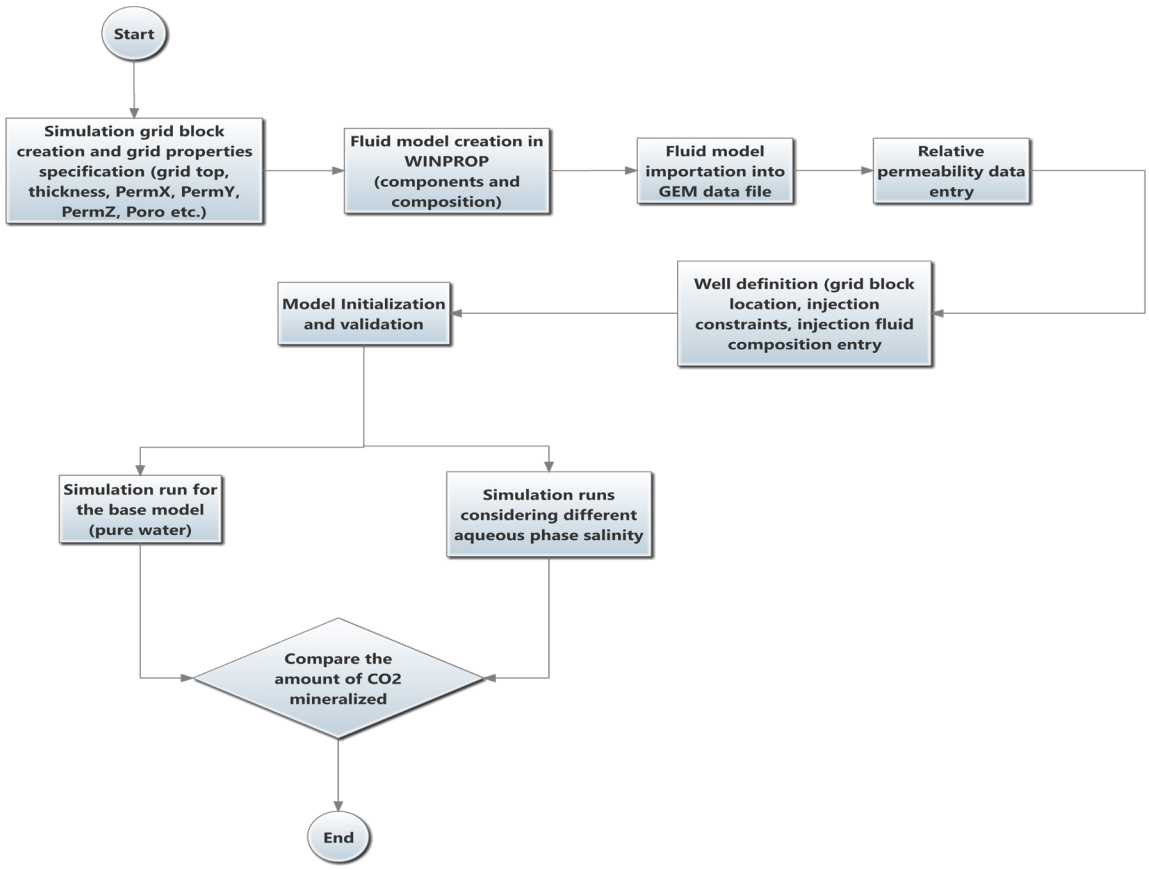

Figure 1. Simulation Work Flow

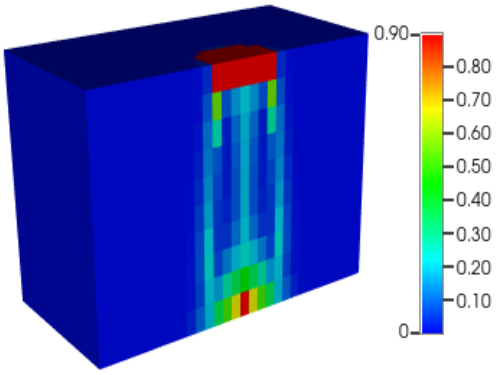

Figure 2. 3D Model for 0 ppm

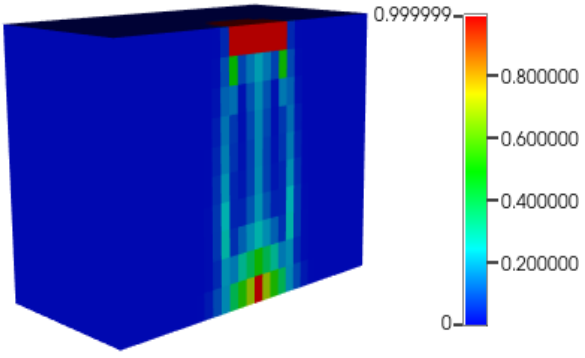

Figure 3. 3D Model for 10000 ppm

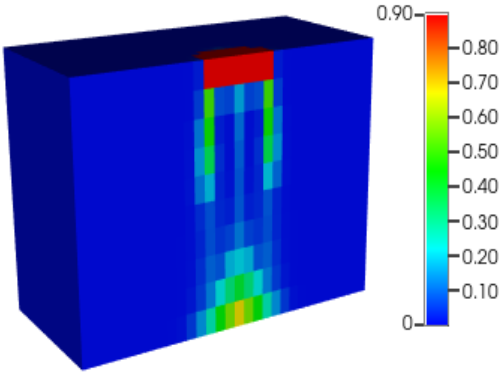

Figure 4. 3D Model for 15000 ppm

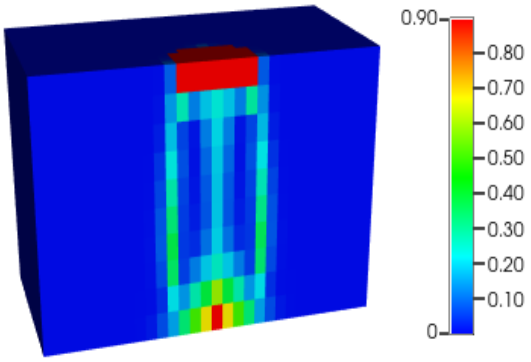

Figure 5. 3D Model for 20000 ppm

3. Results and Discussion

3.1. Amount of CO_2 Dissolved in Water

The amount of CO_2 dissolved in resident brine for pure water is presented in (Figure 6). Result reveals that a higher number of moles solubilised in the post-injection phase than the injection phase. The number of moles dissolved in the post-injection phase doubles the injection phase for each resident time. The CO_2 dissolved in moles increases with time (duration of injection) and decreases with increase in level of salinity. There was a significant difference in the CO_2 dissolved for each level of salinity with increase in time.

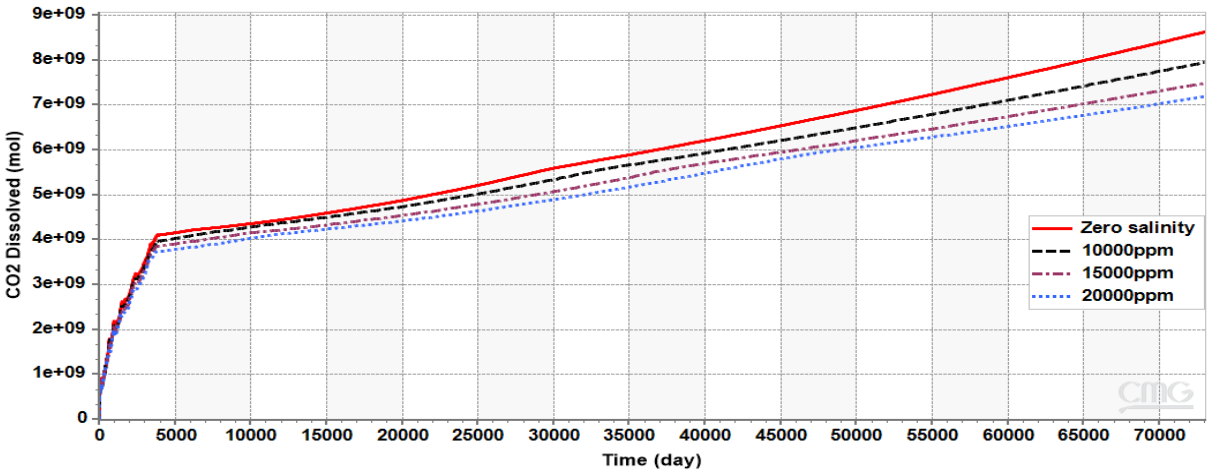

Figure 6. Aqueous Salinity on CO_2 Dissolution

3.2. Amount of CO_2 Converted to Aqueous Ions

The amount of supercritical CO_2 converted into aqueous ions, $CO_{2(aq)}$ is shown in (Figure 7). For zero salinity level, a lower number of moles of CO_2 were converted to $CO_{2(aq)}$ and later increases by one and half times the moles at 200 years. Increase in the salinity level with duration of injection decreases the level of CO_2 conversion to aqueous ion. There was no much difference between the CO_2 aqueous ions converted with increase in level of salinity for each salinity. The change in the CO_2 aqueous ions was almost the same with increase in time (duration of injection) for each level of salinity. There was a continues uniform trend for all the level of salinity with time.

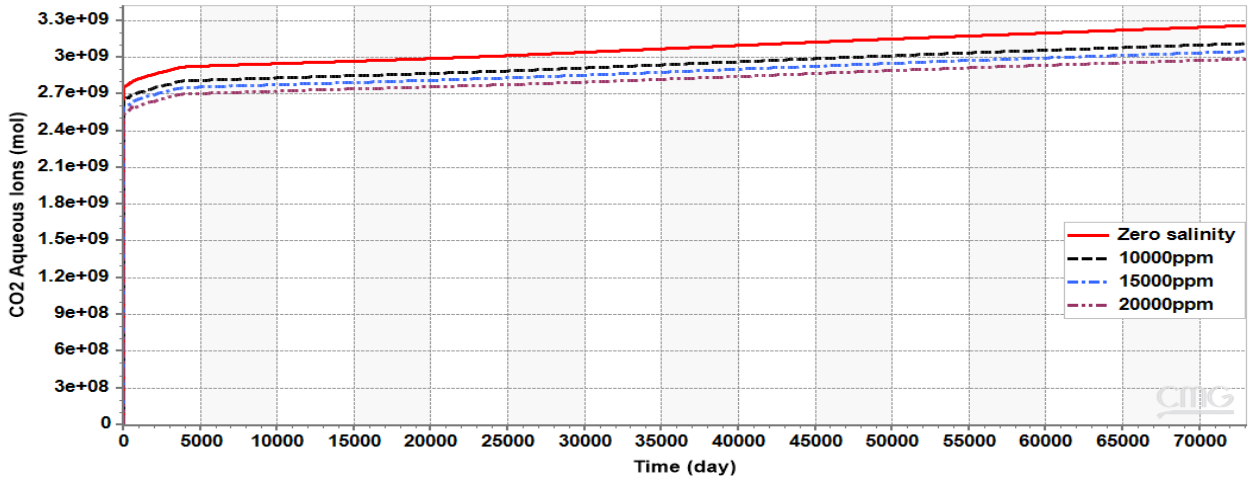

Figure 7.Aqueous Salinity on CO_2 Conversion to Aqueous Ions

3.3. Changes in Rock Mineralogy

The beginning of injection was characterised by saturation of the injected CO_2 through brine displacement away from the wellbore. Dissolution of CO_2 within formation water occurs through mass transfer from CO_2 phase to aqueous phase whenever the two phases are in contact. The dissolved CO_2 dissociates into ions, H^+ and bicarbonate, HCO_3^- and the process continues as long as there was free CO_2 phase and results in increasing HCO_3^-. The ions result in acid solutions and the possibility of attack on the initial minerals present in the formation. Resident minerals begin to dissolve as long as there is enough H^+ and generate ions (Ca^{2+} from Anorthite and Calcite, Al^{3+} from Anorthite and Kaolinite) in the system. The generated ions from the mineral dissolution process combined with bicarbonate HCO_3^- and precipitate Calcite and Kaolinite.

3.3.1. Mineral Mole Changes (Anorthite)

Changes in rock mineralogy for CO_2 injection in resident brine in the presence of various aqueous phase salinity for Anorthite are shown in (Figure 8). There was dissolution in mineral mole changes for Anorthite. The dissolution of Anorthite continue until the dissolutions of the other minerals (Calcite and Kaolinite) provide excess calcium ions (Ca^{2+}), which reverses the process to precipitation. There was a decrease in the moles of Anorthite dissolved from the injection to post-injection phase. Increase in the duration of injection decreases the mineral mole changes for each level of salinity. Increase in the level of salinity increases the mineral moles changes with time. There was a uniform decline in the mineral moles changes with increase in duration of injection.

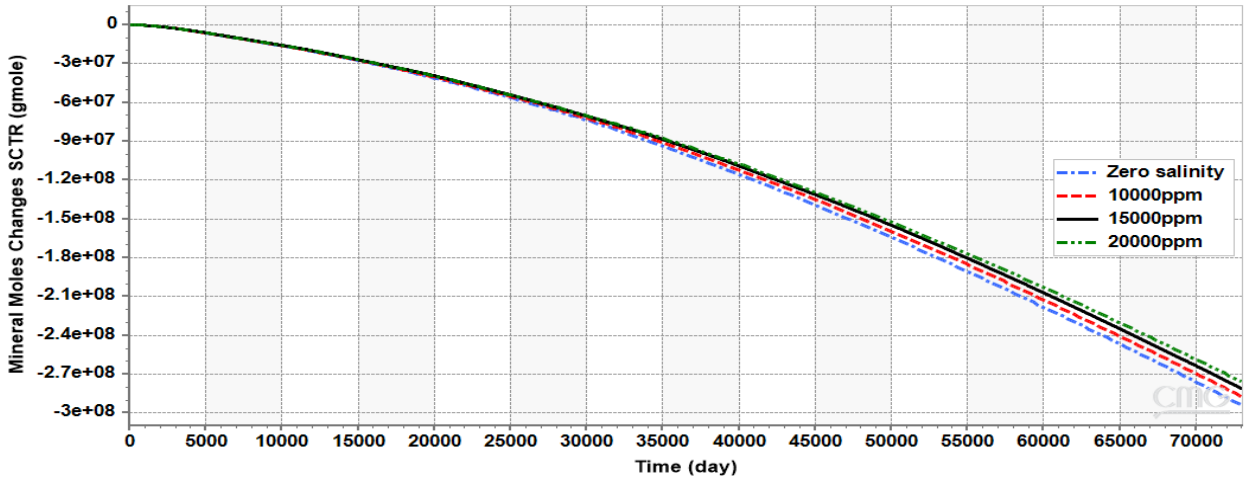

Figure 8. Aqueous Salinity on Mineral Mole Changes for Anorthite

3.3.2. Mineral Mole Changes (Calcite)

(Figure 9) shows the mineral mole changes of Calcite in resident brine of various salinities. There was continuous dissolution of Calcite minerals until the dissolution of Anorthite began to provide excess Ca^{2+} ions until precipitation occurs. The mineral mole changes of Calcite after dissolution increases with duration of injection for all salinity levels. The precipitation of Calcite (mineral mole changes) increases for all level of salinity with duration of injection. There was a uniform trend in the level of precipitation with time. Increase salinity level decreases level of Calcite precipitation.

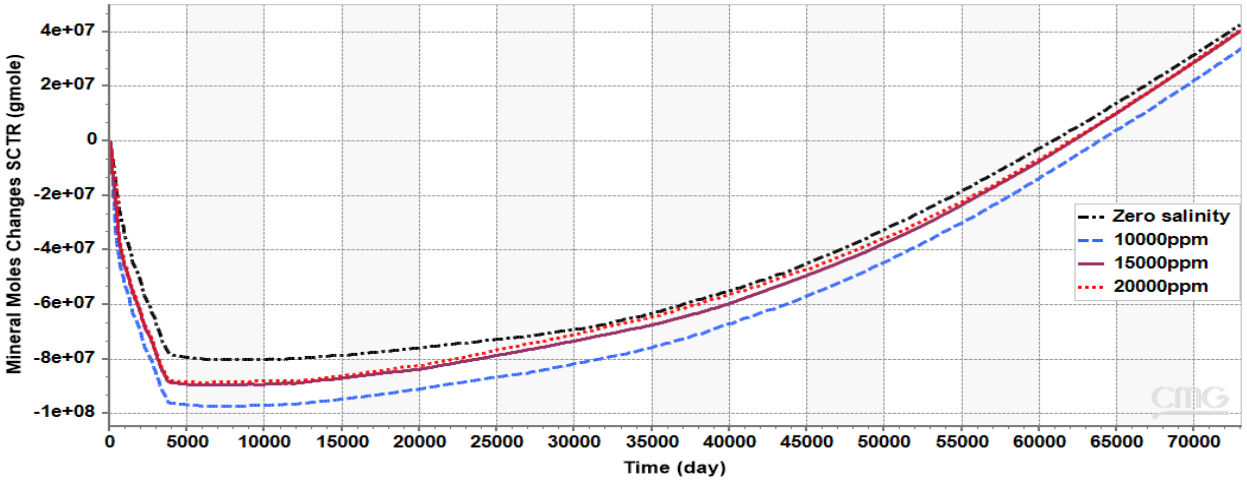

Figure 9.Aqueous Salinity on Mineral Mole Changes (Calcite)

3.3.3. Mineral Mole Mhanges (Kaolinite)

The total amount of Kaolinite precipitated in resident brine of different salinities is presented in (Figure 10). The present of excess Al^{3+} ion from Anorthite dissolution results in precipitation of Kaolinite. Increase in the level of salinity decreases the Kaolinite mineral moles changes with duration of injection. There was a uniform trend in level of Kaolinite precipitation with time. There was no significant change in mineral moles change from each level of salinity.

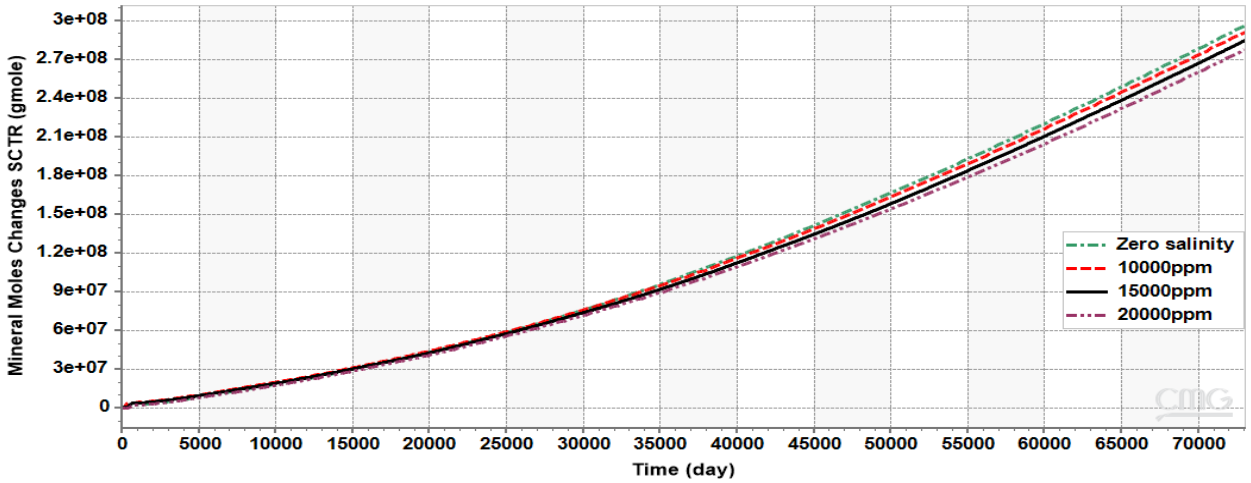

Figure 10. Aqueous Salinity on Mineral Mole Changes (Kaolinite)

3.4. Storage Capacity of CO_2 by Mineral Trapping

(Figure 11) shows aqueous phase salinities level on the storage capacity of CO_2 by mineral trapping mechanism.The results indicate a rise in the process of mineral dissolution during a period of 10 years of CO_2 injection, regardless of the salinity levels. CO_2 mineral trapped decreases with increase in level of salinity as shown in (Figure 11). While 10000 ppm gave the least CO_2 mineral trapped, 15000 ppm and 20000 ppm almost gave the same level of trapping with increase in duration of injection.

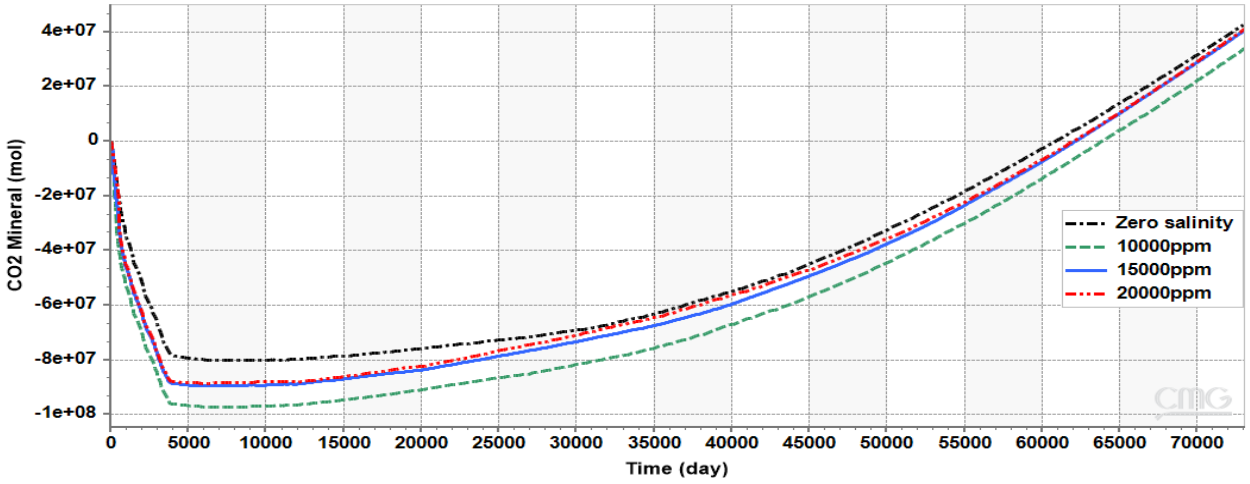

Figure 11. Aqueous Salinity on CO_2 Trapping by Mineralization

3.5.Comparison of Carbon dioxide Converted to Aqueous Ions

The carbon dioxide converted to aqueous ions for different salinity level is presented in (Figure 12). Increase in salinity level reduces the moles of carbon dioxide converted to aqueous ion.

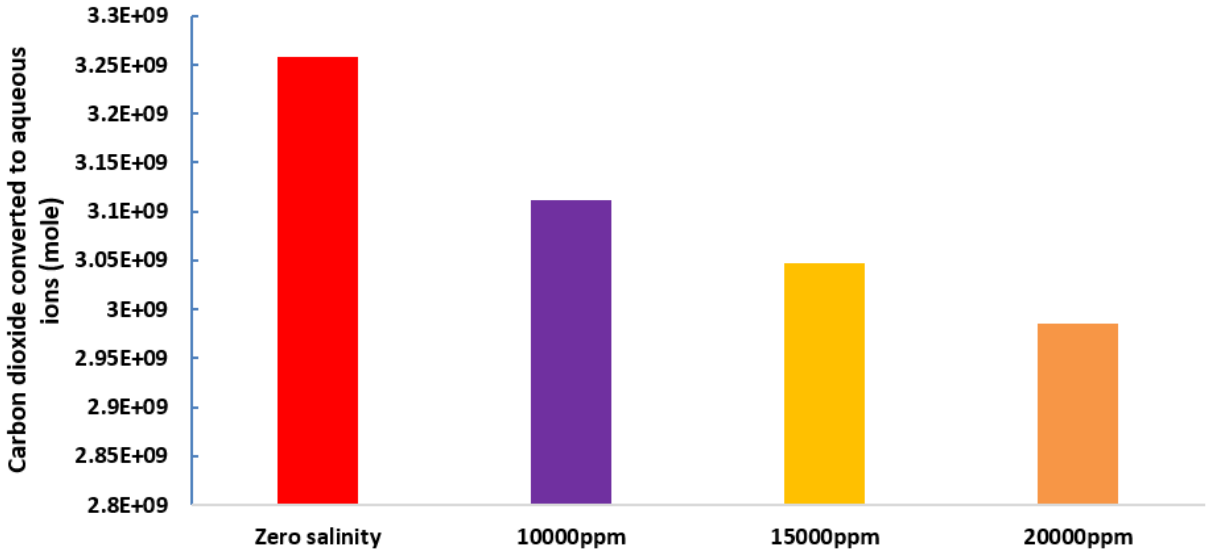

Figure 12. Carbon Dioxide Converted to Aqueous Ions for Different Salinity

3.6. Comparison of Mineral Mole Changes Due to Precipitation

The level of precipitation of the minerals for different salinities is presented in (Figure 13). Kaolinite has the highest precipitation level. The precipitation level of Kaolinite is about six(6) times the Calcite while Anorthite did not precipitate but dissolved.

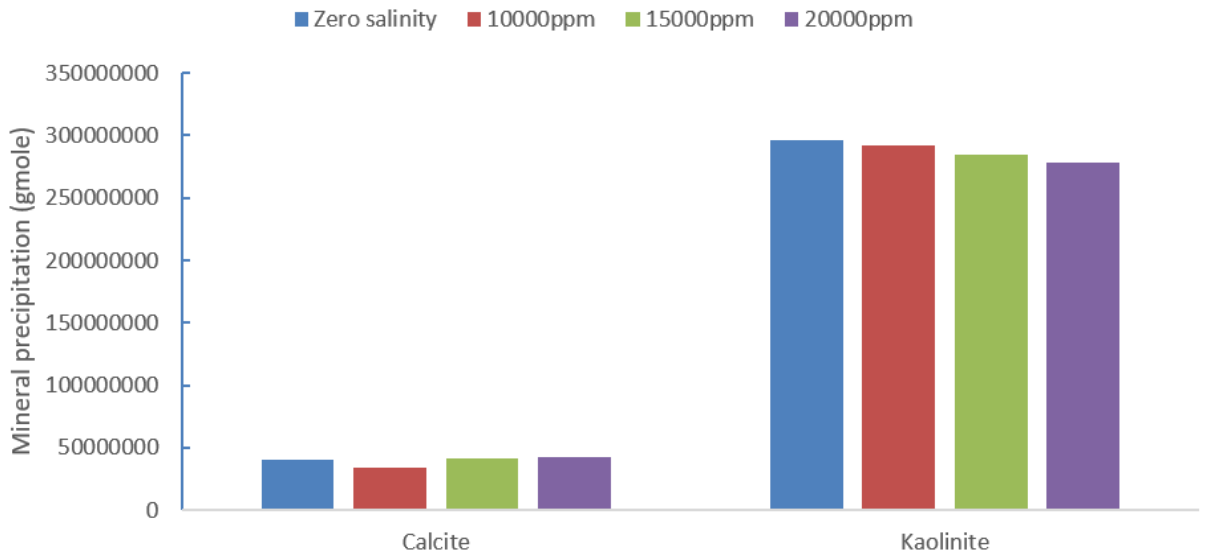

Figure 13. Precipitation Level of Minerals

3.7.Mineral Mole Changes Due to Dissolution (Anorthite)

(Figure 14) shows the mineral dissolution level at different salinities. Increase in salinity decreases the level of dissolution for Anorthite. The composition of the mineral is a vital factor for dissolution tendencies.

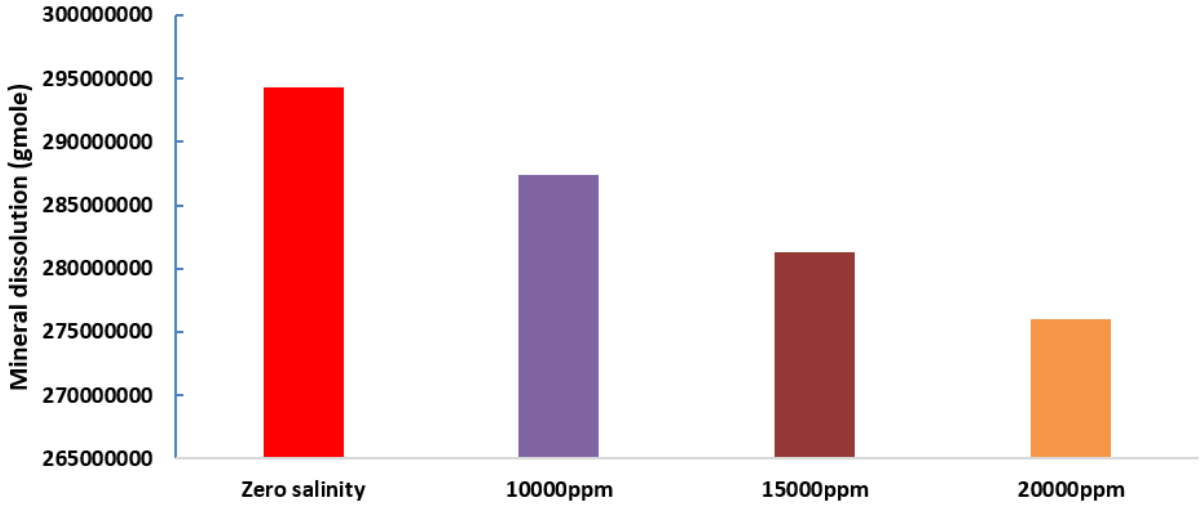

Figure 14. Mineral Dissolution Level

4. Conclusions

In this work, Numerical simulations were conducted using different salinity concentration and model outputs were compared to evaluate the affects of salinity concentrations on carbon dioxide sequestration by mineral trapping.

The following conclusions were drawn from the performed analysis:

i. The carbon dioxide dissolved in moles increases with duration of injection and decreases with increase in salinity.

ii. Increase in the salinity level with duration of injection decreases carbon dioxide conversion to aqueous ion.

iii. Increase in the level of salinity increases the mineral moles changes for Anorthite with time.

iv. Calcite precipitation rate decreases with increase in salinity level with time.

v. Kaolinite mineral moles changes decreases with increase in salinity level with duration of carbon dioxide injection.

References

Abas, N., and Khan, N. (2014). Carbon conundrum, climate change, CO_2 capture and consumptions. Journal of CO_2 Utility, 8, 39-48.

Al-Yaseri, A. Z., Lebedev, M., Barifcani, A., and Iglauer, S. (2016). Receding and advancing (CO_2 + brine + quartz) contact angles as a function of pressure, temperature, surface roughness, salt type and salinity. The Journal of Chemical Thermodynamics, 93, 416-423.

Al-khdheeawi, E.A.,Vialle, S.,Barifcani, A.,Sarmadivaleh,M.and Iglauer,S. (2017). Effect of brine salinity on CO_2 plume migration and trapping capacity in deep saline aquifers. APPEA J ,57,100-109.

Al-khdheeawi,E.A, Vialle, S.,Barifcani, A.,Sarmadivaleh,M., Zhang,Y.,and Iglauer,S. (2018).Impact of salinity on CO_2 containment security in highly heterogeneous reservoirs. Greenhouse Gases Sci Technol,8(1),93-105.

Arif, M., Al-Yaseri, A. Z., Barifcani, A., Lebedev, M., and Iglauer, S. (2016a). Impact of pressure and temperature on CO_2-brine-mica contact angles and CO_2-brine interfacial tension: implications for carbon geo-sequestration.

Journal of Colloid and Interface Science, 462, 208-215.

Bachu, S. (2016). Review of CO_2 Storage Efficiency in Deep Saline Aquifers. International Journal of Greenhouse Gas Control, 40, 188-202.

Gaus, I. (2010). Role and impact of CO_2-rock interactions during CO_2 storage in sedimentary rocks. International Journal of Greenhouse Gas Control, 4, 73-89.

Gunter, W. D., Bachu, S., and Benson, S. (2004). the role of hydrogeological and Geochemical trapping in sedimentary basins for secure geological storage of carbon dioxide. In: Geological Society of London, Special Publication, 233, 129-45.

Hesse, M., Orr, F., and Tchelepi, H. (2008). Gravity currents with residual trapping. Journal of Fluid Mechanics, 611(1), 35-60.

Iglauer, S., Al-Yaseri, A. Z., Rezaee, R., and Lebedev, M. (2015). CO_2 wettability of caprocks:Implications for structural storage capacity and containment security. Geophysical Research Letters, 42(21), 9279-9284.

Iglauer, S., Paluszny, A., Pentland, C. H., and Blunt, M. J. (2011). Residual CO_2 imaged with X- ray micro-tomography. Geophysical Research Letters, 38(21), 1-6.

Kolster, C., Agada, S., Mac Dowell, N., and Krevor, S. (2018). The impact of time-varying CO_2injection rate on large scale storage in the UK Bunter Sandstone. International Journal of Greenhouse Gas Control, 68, 77-85.

Krevor, S., Blunt, M. J., Benson, S. M., Pentland, C. H., Reynolds, C., Al-Menhali, A., and Niu, B. (2015). Capillary trapping for geologic carbon dioxide storage - from pore scale physics to field scale implications. International Journal of Greenhouse Gas Control, 40, 221-237.

Kumar, A., Noh, M. H., Ozah, R. C., Pope, G. A., Bryant, S. L., Sepehrnoori, K., and Lake, L.W. (2005). Reservoir simulation of CO_2 storage in aquifers. SPE Journal, 10(3), 336-348.

Kumar, R.,Campbell,S., Sonnenthal, E.,andCunningham,J.(2020). Effect of brine salinity on the geological sequestrationof CO_2 in a deep saline carbonate formation. Greenhouse Gas Sci Technol, 0,1-17.

Liu, B., Fu, X., and Li, Z. (2018). Impacts of CO_2-brine-rock interaction on sealingefficiency of sand caprock: a case study of Shihezi formation in Ordos basin. Advances in Geo-Energy Research, 2, 380-392.

Naylor, M., Wilkinson, M., and Haszeldine, R. (2011). Calculation of CO_2 column heights in depleted gas fields from known pre-production gas column heights. Marine Petroleum Geology, 28(5), 1083-1093.

Olajire, A. A. (2018). Recent progress on the nanoparticles-assisted greenhouse carbon dioxide conversion processes. Journal of CO_2 Utility, 24, 522-547.

Pentland, C. H., El-Maghraby, R., Iglauer, S., and Blunt, M. J. (2011). Measurements of the capillary trapping of super-critical carbon dioxide in Berea sandstone. Geophysical Research Letters, 38(6), 1-4 .

Pruess, K., Xu, T., Apps, J., and Garcia, J. (2003). Numerical modelling of aquifer disposal of CO_2. SPE Journal, 8(1), 49-60.

Rahman, T., Lebedev, M., Barifcani, A., and Iglauer, S. (2016). Residual trapping of supercritical CO_2 in oil-wet sandstone. Journal of Colloid and Interface Science, 469, 63- 68.

Saraji, S., Piri, M., and Goual, L. (2014). The effects of SO_2 contamination, brine salinity,pressure, and temperature on dynamic contact angles and interfacial tension of supercritical CO_2/ brine/quartz systems. International Journal of Greenhouse Gas Control, 28, 147-155.

Singh, H. (2018). Impact of four different CO_2injection schemes on extent of reservoir pressure and saturation. Advances in Geo-Energy Research, 2, 305-318.

Spycher, N., Pruess, K., and Ennis-King, J. (2003). CO_2-H_2O mixtures in the geological sequestration of CO_2. Assessment and calculation of mutual solubilities from 12 to 100 °C and up to 600bar. Geochimica et Cosmochimica Acta, 67(16), 3015-3031.

Venkatraman, V., and Alsberg, B. K. (2017). Predicting CO_2 capture of ionic liquids using machine learning. Journal of CO_2 Utility, 21, 162-168.

Xu, T., Apps, J. A., and Pruess, K. (2003). Reactive geochemical transport simulation to study mineral trapping for CO_2 disposal in deep arenaceous formations. Journal of Geophysical Research: Solid Earth, 108(B2), 1-13.

Xu, T., Apps, J. A., and Pruess, K. (2004). Numerical simulation of CO_2 disposal by mineral trapping in deep aquifers. Applied Geochemistry, 19(6), 917-936.

Xu, T., Apps, J. A., and Pruess, K. (2005). Mineral sequestration of carbon dioxide in a sandstone-shale system. Chemical Geology, 217(3), 295-318.

Zhang, Y., Lebedev, M., Sarmadivaleh, M., Barifcani, A., and Iglauer, S. (2016). Swelling-induced changes in coal microstructure due to supercritical CO_2 injection. Geophysical Research Letter 43(17), 9077-9083.

JOURNAL OF GAS TECHNOLOGY

Volume 9 /Issue 1 / Summer 2024 / Pages 19-33

Journal Home page: http://jgt.irangi.org

Improving Acidizing Fluid Selection in Oil Production: A Comprehensive Analysis with Expert Systems

Mohamad Norouzi Delaviz[1], Ahmad Rigi[1], Saman Jahanbakhshi[2*]

1. M.Sc. of Petroleum Engineering, Abdal Industrial Projects Management Co., MAPSA Technology Center, Tehran, Iran
2. Assistant Professor, School of Mining Engineering, College of Engineering, University of Tehran, Tehran, Iran

ARTICLE INFO

ORIGINAL RESEARCH ARTICLE

Article History:
Received: 12 February 2024
Revised: 08 March 2024
Accepted: 13 March 2024

Keywords:
Matrix acidizing
Candidate fluid selection
Formation damage
Expert systems
Improved oil recovery

ABSTRACT

Matrix acidizing plays an important role in improving oil recovery by decreasing reservoir damage. However, the complexity of selecting the most suitable acidizing fluid, given diverse reservoir conditions, poses a significant challenge. This article explores the utilization of expert systems in improving the acidizing fluid selection process. By examining the role, components and merits of expert systems, along with real-world case studies, the article highlights how these systems contribute to more efficient and informed decision-making. In this investigation, eight instances of damage have been selected for analysis using the proposed expert system. Following a thorough assessment, selecting a fluid for damage elimination, demonstrates the effectiveness of the expert system. The incorporation of expert systems in modeling and inference under conditions of high uncertainty and precision plays a key role in increasing productivity, declining errors, predicting events and refining decision-making processes. These systems utilize advanced algorithms and mathematical models for simulation and predicting implications across various applications, thereby aiding in expedited decision-making.

DOR: 20.1001.1/JGT.2024.2022791.1035

How to cite this article
M. Norouzi Delaviz,A. Rigi, S. Jahanbakhshi, Improving Acidizing Fluid Selection in Oil Production: A Comprehensive Analysis with Expert Systems. Journal of Gas Technology. 2024; 9(1): 19 -33. (https://jgt.irangi.org/article_711917.html)

* Corresponding author.
E-mail address: jahanbakhshi@ut.ac.ir, (S. Jahanbakhshi).

Available online 10 September 2024

1. Introduction

Reservoir damage is a critical major concern within the oil and gas industry that has the potential to have a significant impact on reducing reservoir productivity (Abdulmutalibov et al. 2023). In the scope of reservoir stimulation, matrix acidizing stands out as a crucial technique employed to improve the productivity of oil and gas wells (Alvarez et al. 2023). One of the key factors that considerably influences the success of acidizing matrix operations is the careful selection of treatment fluids. The choice of acidizing fluids can make the difference between a non-optimal treatment and a highly effective well stimulation. This article explores into the critical aspects of fluid selection in the matrix acidizing process, introducing the concept of an acidizing fluids selection (McLeod 1984, Mouedden et al. 2022). The acidizing fluid selection serves as a guide, enabling engineers and operators to make informed decisions about the type of acids and additives that will yield optimal results for a specific reservoir (Sumotarto 1995, Santos et al. 2022). Navigating through the complexities of matrix acidizing, one will explore the factors influencing fluid selection, the commonly used types of acids and the role of additives in tailoring the treatment to the unique characteristics of each well.

Dargi et al. (2023) demonstrated that machine learning models successfully predicted post-acidizing permeability changes in oil and gas wells, with genetic programming outperforming other models. The study underscores the potential of genetic programming and machine learning for accurate post-acidizing permeability forecasting, aiding in design and improving production rates. Sidaoui et al. (2018) used a machine learning model based on rock and HCl properties to predict optimum injection rates in matrix stimulation with 90% accuracy. This streamlined approach improves acid job design for production engineers and minimizes the demand for extensive laboratory experiments. Chavanne and Perthuis (1992) presented a novel expert system for fluid selection in matrix treatments, employing a chemistry-driven two-step reasoning process and providing multiple ranked solutions. Tested for conformity, the system offers safe recommendations, improving field practices and contributing a noteworthy addition to the literature on fluid selection advisors in well stimulation. Domelon et al. (1992) introduced the development of Acid Expert, a PC-based matrix acidizing expert system, utilized for designing damage removal treatments in sandstone formations. The system improves consistency in recommendations globally, facilitates timely technology transfer and considers technical, economic and product availability aspects for cost-saving benefits. Blackburn et al. (1990) discussed the development of acidman, an expert system for designing matrix acid treatments in oil wells, with anticipated benefits including rised treatment success rates and improved cost-effectiveness.

Chiu et al. (1993) explored the challenges of designing fluid systems for well completion, proposing expert systems as efficient tools for advising engineers on selecting base fluids and additives. It emphasized the necessity of knowledge representation, inference methods and user interface in system implementation. Using Acid Expert as an example, the study highlights the significance of knowledge acquisition and user interaction for excellent product recommendations, ultimately leading to cost savings and enhanced service quality in the oil industry. Xue et al. (2012)introduced a neural network method to predict acidizing fluid selection and dosages for oilfield applications, highlighting the complexity of conventional methods and the demand for a more efficient solution. Through successful training and testing, the study illustrates the network's ability to forecast optimal fluid systems based on diverse input parameters, aiming to foster systematization and intelligence in the oil industry.

The aim of this study is to develop an expert advisory system that accurately and quickly identifies the suitable acidizing fluid for acidizing operations, addressing well damages effectively. This system intends to utilize acidizing fluids and various acidizing stages to mitigate damages, ultimately bridging the gap between artificial intelligence and acidizing. By the end of this article, readers will gain invaluable insights into the importance of a well-informed fluid selection strategy and the tools available to make such decisions in the field of acidizing matrix.

2. Methodology

2.1. Diverting Agents

A diverter in well acidizing is a type of material or equipment used to control and prevent the uneven flow of acid or other fluids within the well. The purpose of employing a diverting agent in this process is to achieve a uniform distribution of acid in the reservoir structure and prevent pressure drop due to undesired acid diversion. Types of diverting agents include: 1) Gels: gel-forming materials are added to acid to create a gel that controls the flow of acid; 2) Polymers: polymers are additives, which added to acid for increasing viscosity and improving acid distribution in the reservoir; 3) Foams: foams are formed by adding gas to acid and can enhance the direction and distribution of acid; 4) Particulate diverters: particles such as carbonates or silica are combined with acid to act as barriers, diverting the acid flow to specific points. Diverters are typically used when the reservoir treatment interval is greater than 20 ft and the reservoir temperature is less than 300°F. As seen in (Figure 1), there are six types of diverters, which are explained below.

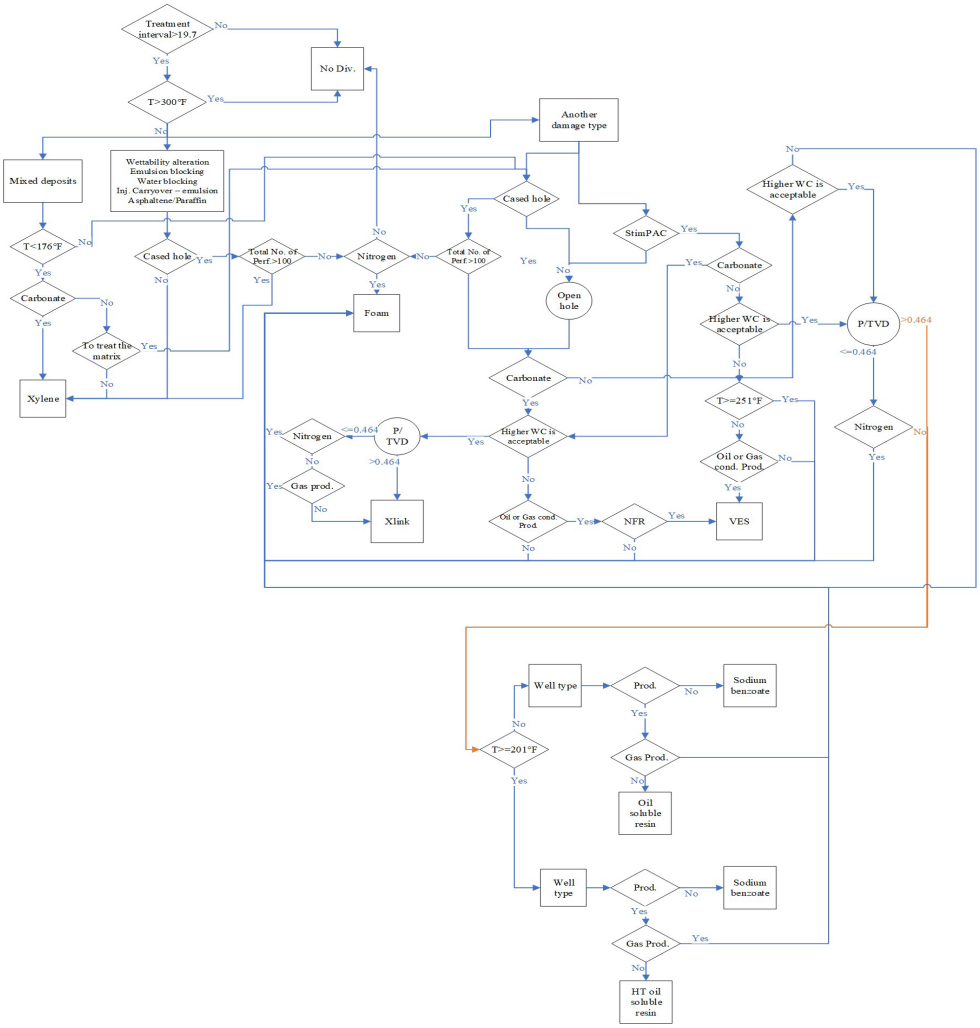

Figure 1. Detection of Diverting Agents Fluid

2.1.1. Xylene Foam Diverter

In the case of encountering damages such as mixed deposit, wettability alteration, emulsion blocking, water blocking, injection carryover-emulsion, asphaltene and paraffin in the reservoir, xylene can be used. Xylene is employed for reducing mixed deposit damage when the reservoir temperature is below 176°F and in situations where the target of acid injection is to treat the wellbore, perforation, or gravel pack solely in the sandstone reservoir. Otherwise, other diverting agents are utilized.

2.1.2. Temporary Xlink Acid Diverter

In the case of acidizing on a carbonate reservoir, if there is a need for a diverting agent, xlink should be used. The condition for using this type of diverting agent includes high water cut in the well or performing operations near the water-producing zone, along with the non-acceptance of water and avoiding the use of nitrogen. If it is not possible to use a foam diverter, xlink can be used instead.

2.1.3. Viscoelastic Surfactant (VES) Diverter

Completion type with stimPAC (stimPAC is a type of well completion method used to increase oil and gas production from oil wells) in an oil or gas condensate production well can be implemented when the reservoir temperature is below 250°F and there is a low water cut in the well. It can also be utilized when operations are conducted near the water-producing zone along with the non-acceptance of higher water cut values.

In addition, VES diverter can be utilized when the completion type is either an open hole or a cased hole in a carbonate reservoir with natural fractures and high water cut in the well, or operations are conducted near the water-producing zone along with the non-acceptance of higher water cut values.

2.1.4. High Temperature Oil Soluble in Resin/ Oil Soluble in Resin

In the reservoir, when the well produces oil or gas condensate at temperatures higher than 200 °F, high temperature oil soluble in resin diverter is utilized to address damage. This diverter is used in states with low water cut in the well and the absence of operations near the water-producing zone, along with either the non-acceptance or acceptance of higher water cut values and the avoidance of using nitrogen. Regarding reservoirs with temperatures below 200 °F, oil soluble in resin diverter is used.

2.1.5. Sodium Benzoate

In an injection well, if nitrogen is not used and there is a high water cut in the well, along with the absence of operations near the water-producing zone and either the non-acceptance or acceptance of higher water cut values, sodium benzoate diverter can be used.

2.1.6. Foam

In the case of performing various operations near the water-producing zone or observing a high water cut in the well, when using nitrogen in the wellbore treatment fluid, base foam diverters should be used. In the absence of nitrogen, only in the case of gas-producing wells, this type of diverter can be used. If a low water cut is observed in the well in sandstone formations, only base foam diverters are employed. In carbonate formations with gas-producing wells it can be used, however in other wells when there is no natural fracture in formation, foam diverters are used.

2.2. Main Fluid, Over Flush and Pre-Flush

2.2.1. Clay Swelling

For the selection of the main fluid, pre-flush and over-flush in clay swelling damage, mineralogy needs to be examined, which can be divided into two categories based on the amounts of calcite and dolomite: between 20-40% and less than 20%. If the amounts of calcite and dolomite are between 20-40% and with the absence of glauconite, chlorite and zeolite in the formation minerals, the selection of the

acidizing fluid depends on the temperature. If the temperature is below 200°F, the recommended main fluid is HCl 28% and for temperatures between 200-300 °F, the suggested main fluid is HCl 15%. If the temperature is higher than 300°F, the recommended main fluid is HCl 10%.

In the next state, where the content of calcite and dolomite is less than 20%, the mineral's presence in the formation, significantly impacts the injected acidizing fluid, as illustrated in (Figure 3). In a situation where only quartz, calcite and dolomite minerals are presented in the formation and there is no cement in the formation, the selection of the fluid depends on the reservoir permeability and the injected or produced fluids. Specifically, if the permeability is less than 20 mD and the produced fluid is oil or injection fluid, the pre-flush, main fluid and over-flush will be HCl 7.5%, mud acid 6/1.5 and HCl 7.5%, respectively. For permeability between 20-100 mD, if the produced fluid is oil or injection fluid, the pre-flush and over-flush fluids will be HCl 10% and the main fluid will be mud acid 8/2. However, as long as the produced fluid is gas, the pre-flush and over-flush fluids will be gas well acid 10% and the main fluid will be gas well mud acid. For gas condensate fluids, the pre-flush and over-flush fluids will be alcoholic acid 10% and the main fluid will be alcoholic mud acid 8/2.

Finally, providing that the permeability of the formation is greater than 100 mD, for oil and injection fluids, the pre-flush and over-flush fluids will be HCl 15% and the main fluid will be mud acid 12/3. In the case of gas produced fluids, the pre-flush and over-flush fluids will be gas well acid 15% and the main fluid will be gas well mud acid. For gas condensate fluids, the pre-flush and over-flush fluids will be alcoholic acid 15% and the main fluid will be alcoholic mud acid 12/3.

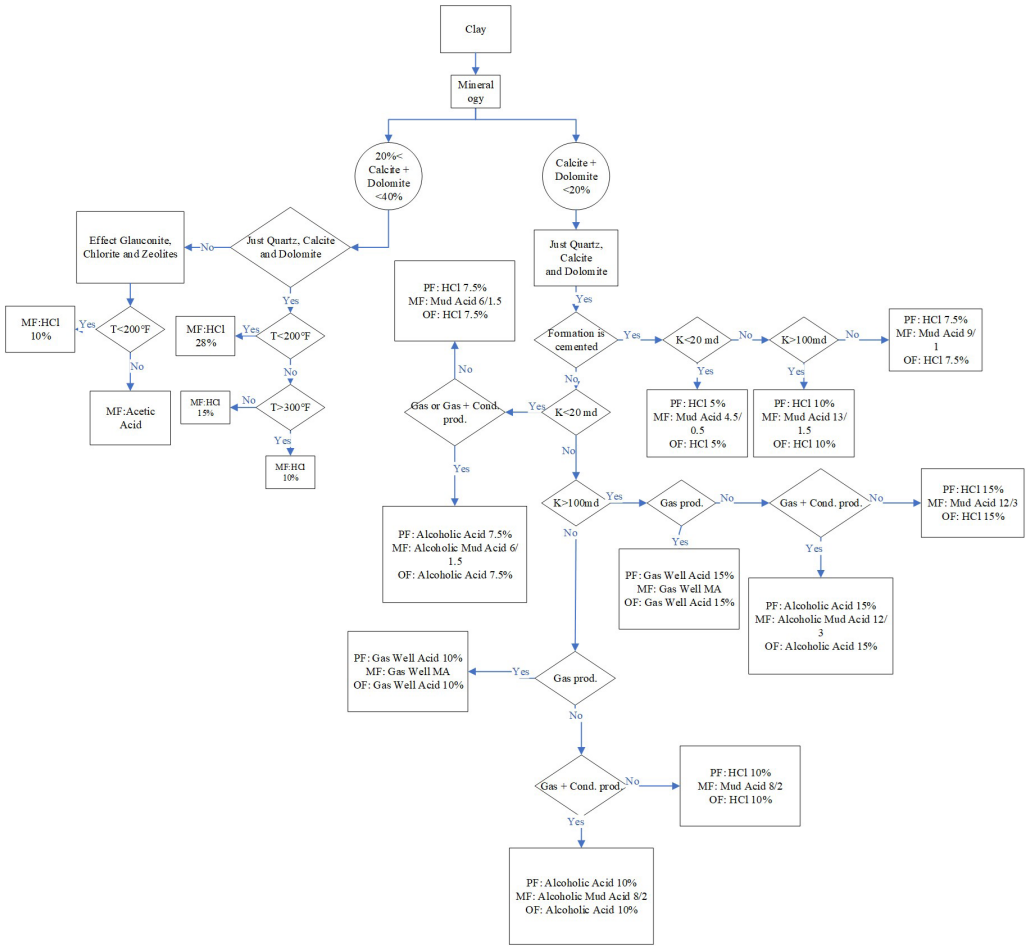

Figure 2. Detection of Main Fluid, Over-flush and Pre-flush in Clay Swelling Damage for Sandstone Reservoir

2.2.1.1. Mineralogy Effect

So long as there are other minerals except quartz, calcite and dolomite in the formation, the acid fluid injection depends on temperature, permeability and produced fluid.

If the amounts of calcite and dolomite is between 20-40% and the formation includes minerals such as glauconite, chlorite and zeolite, the acidizing fluid selection is as follows: if the temperature is lower than 200°F, the main fluid is HCl 10%, while for temperatures higher than 200 °F, main fluid is acetic acid.

In a state where the amounts of calcite and dolomite in the formation is less than 20% and with the presence of minerals such as Illite, kaolinite, smectite and mixed layer exceeds 30%, or minerals like chlorite, glauconite higher than 6.1%, or the presence of zeolite is more than 2.1%, the recommended pre-flush and over-flush fluid is acetic acid and the main fluid is organic fluoboric. If other minerals are in the formation with the percentage of 3-6% of chlorite and glauconite, also mica, K-feldspar and Na-feldspar are greater than 10%, with permeability less than 20 mD, the suggested pre-flush and over-flush are HCl/acetic 5/5 and the main fluid is mud acid/acetic 6/1/5. In formations with permeability greater than 20 mD, the pre-flush and over-flush are the same as in formations with less than 20 mD, but the main fluid is mud acid/acetic 9/1.5/5.

Another state is in addition to quartz, calcite and dolomite, the formation also contains 3-6% of the mineral's chlorite and glauconite. For formation with permeability less than 20 mD, the recommended pre-flush and over-flush are HCl/acetic 7.5/5 and the main fluid is mud acid/acetic 6/1.5/5. When formation permeability is greater than 20 mD, the pre-flush and over-flush are same as permeability in formations with less than 20 mD, but the main fluid is mud acid/acetic 8/2/5. In the next state, when the illite, kaolinite, smectite and mixed layer are between 10-30%, or mica, K-Feldspar and Na-Feldspar are greater than 10%, in formations with permeability less than 20 mD, the recommended pre-flush and over-flush for oil-producing formation is HCl 5% and the main fluid is mud acid 6/1. For gas and gas condensate producing formations, the pre-flush and over-flush are alcoholic acid 5% and the main fluid is alcoholic mud acid 6/1. In formations with permeability between 20-100 mD, for oil-producing formations, the pre-flush and over-flush is HCl 7.5% and the main fluid is mud acid 9/1.5. For gas-producing formations, the pre-flush and over-flush fluid are gas well acid 7.5% and the main fluid is gas well mud acid. If the produced fluid is gas condensate, the pre-flush and over-flush are alcoholic acid 7.5% and the main fluid is alcoholic mud acid 9/1.5.

In the final state, when the impact of zeolite content is greater than 2.1%, the effect of permeability is as follows: For formation with permeability less than 20 mD, the recommended pre-flush and over-flush are HCl/acetic 7.5/5 and the main fluid is mud acid/acetic 6/1.5/5. In formation with permeability between 20-100 mD, the suggested pre-flush and over-flush are HCl/acetic 10/5 and the main fluid is mud acid/acetic 8/2/5. For formations with permeability greater than 100 mD, the pre-flush and over-flush are HCl/acetic 15/5 and the main fluid is mud acid/acetic 12/3/5.

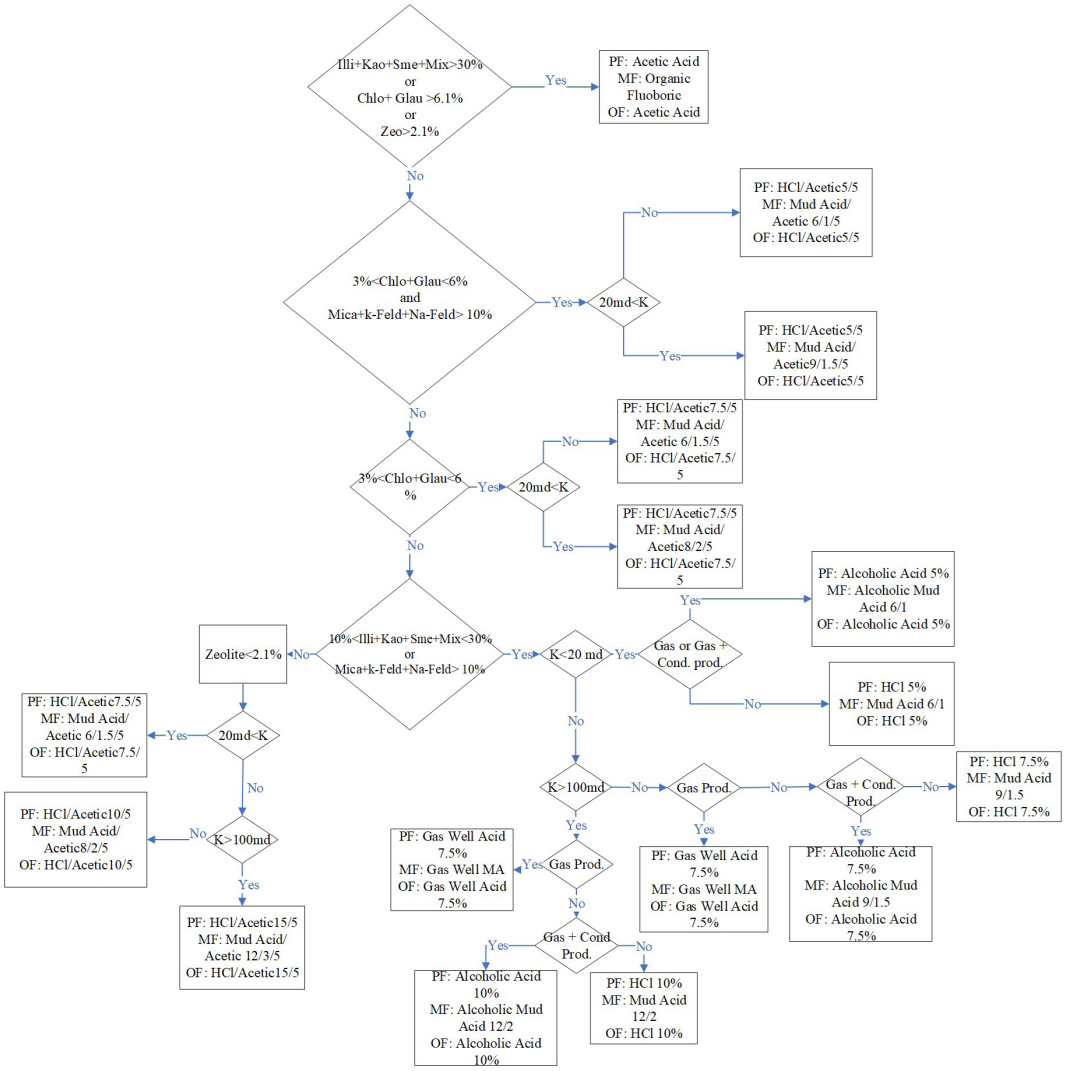

Figure 3. Mineralogy Effect in Acidizing Fluid Selection

2.2.1.2. Cement Effect

The effect of cementation is important, when the dolomite and calcite content is less than 20%. In a state that the formation includes minerals quartz, calcite, dolomite and cement, the recommended fluid is different from the situation in which cement is absent in the formation. The selection of fluid in this case depends on the permeability of the formation. For permeabilities below 20 mD, both pre-flush and over-flush are suggested to be with HCl 5%, accompanied by mud acid 4.5/0.5, as the main fluid. In cases with permeability between 20-100 mD, the recommended fluid for pre-flush and over-flush is HCl 7.5% and the main fluid is mud acid 9/1. Finally, for permeabilities greater than 100 mD, the recommended fluid for both pre-flush and over-flush is HCl 10% and the main fluid is mud acid 13/1.5.

In the formation, if the proportion of minerals such as glauconite and chlorite constituting is less than 6.1%, or zeolite is higher than 2.1%the recommended fluid for pre-flush and over-flush is acetic acid. In formations with permeability below 20 mD, the main fluid is mud acid/ acetic 4.5/0.5/10, while for permeabilities higher than 20 mD, mud acid/acetic 9/1/10 is suggested. When the formation contains glauconite and chlorite in the range of 3-6%, the proposed pre-flush and over-flush are HCl/ acetic 5/5. For permeability below 20 mD, the main fluid is mud acid/acetic 4.5/0.5/10 and for permeability higher than 20 mD, mud acid/

acetic 9/1/5, is recommended. However, if the zeolite content is less than 2.1%, the choice of fluid is similar to the state where the formation includes glauconite and chlorite in the range of 3-6%, while for permeabilities higher than 100 mD, a different fluid is suggested, with HCl/acetic10/5, for pre-flush and over-flush and mud acid/acetic13.5/1/5, as the main fluid. In the final state, if the formation contains glauconite and chlorite between 3-6%, along with mica, K-Feldspar and Na-Feldspar greater than10%, the injection acidizing fluid is similar to the state when glauconite and chlorite are between 3-6%, but the distinction in recommending mud acid/acetic 5/4.5/0.5, as the main fluid for permeabilities below 20 mD.

For carbonate reservoirs, if the calculated maximum pump rate is greater than zero and the anticipated pump rate is less than the maximum pump rate, then the main fluid can be selected from the available fluids (Nguyen et al. 2021, Novikov et al. 2022).

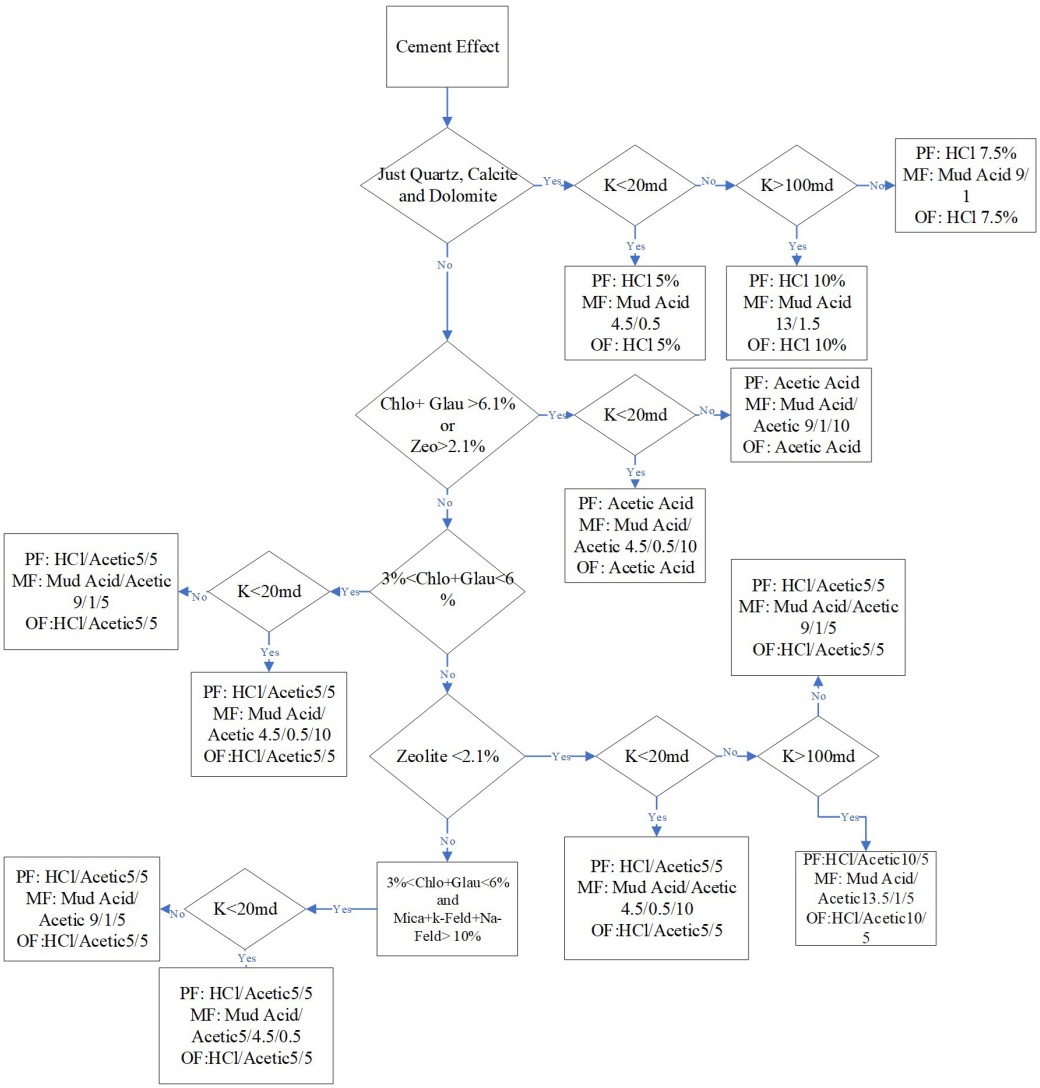

Figure 4. Cement Effect in Acidizing Fluid Selection

2.2.2. Emulsion Blocking

In this damage type, if emulsion blocking occurs without any secondary damage, the recommended fluid to eliminate this damage is a multifunctional solvent. If the emulsion phase is oil outside phase, it is type I and if it is water outside phase, it is type III.

If wettability alteration occurs along with emulsion blocking damage in the formation,

priority is given to addressing the wettability alteration damage as a secondary damage. If wettability alteration is the primary damage, the fluid selection is the same Irrespective of whether the secondary damage is emulsion blocking. In the first stage, the well state should be assessed to eliminate this damage. If the well is newly completed or suspected, the recommended main fluid is the multifunctional solvent. For another well state, if drilling mud is water base, the recommended main fluid is the multifunctional solvent and for oil-based drilling mud, the recommended main fluid is the oil mud removal system.

If solids-completion, workover, stim. fluids damage occurs as a secondary damage along with emulsion blocking damage in the formation, to address these damages, in addition to the fluids mentioned in the clay swelling damage section, a multifunctional solvent pre-flush should be used.

Another secondary damage types that can occur along with emulsion blocking damage is solids - mud (not filter cake) damage. In the case of using oil-based drilling mud, to address this damage along with emulsion blocking damage, a multifunctional solvent pre-flush and an oil mud removal system main fluid should be used. If water-based drilling mud is used and the mud loss is more than 5 gal/ft and the formation consists of calcite and dolomite is between 20-40%, the recommended pre-flush and main fluids are multifunctional solvents and mud dispersant system, respectively. If the formation contains less than 20% of dolomite and calcite, the recommended fluids are similar to when dealing with clay swelling damage, with the difference that the suggested main fluid is mud dispersant. If the water-based mud with mud loss less than 5 gal/ft, is used, the recommended fluids are similar to address clay swelling damage, with the difference that the suggested main fluid is a multifunctional solvent.

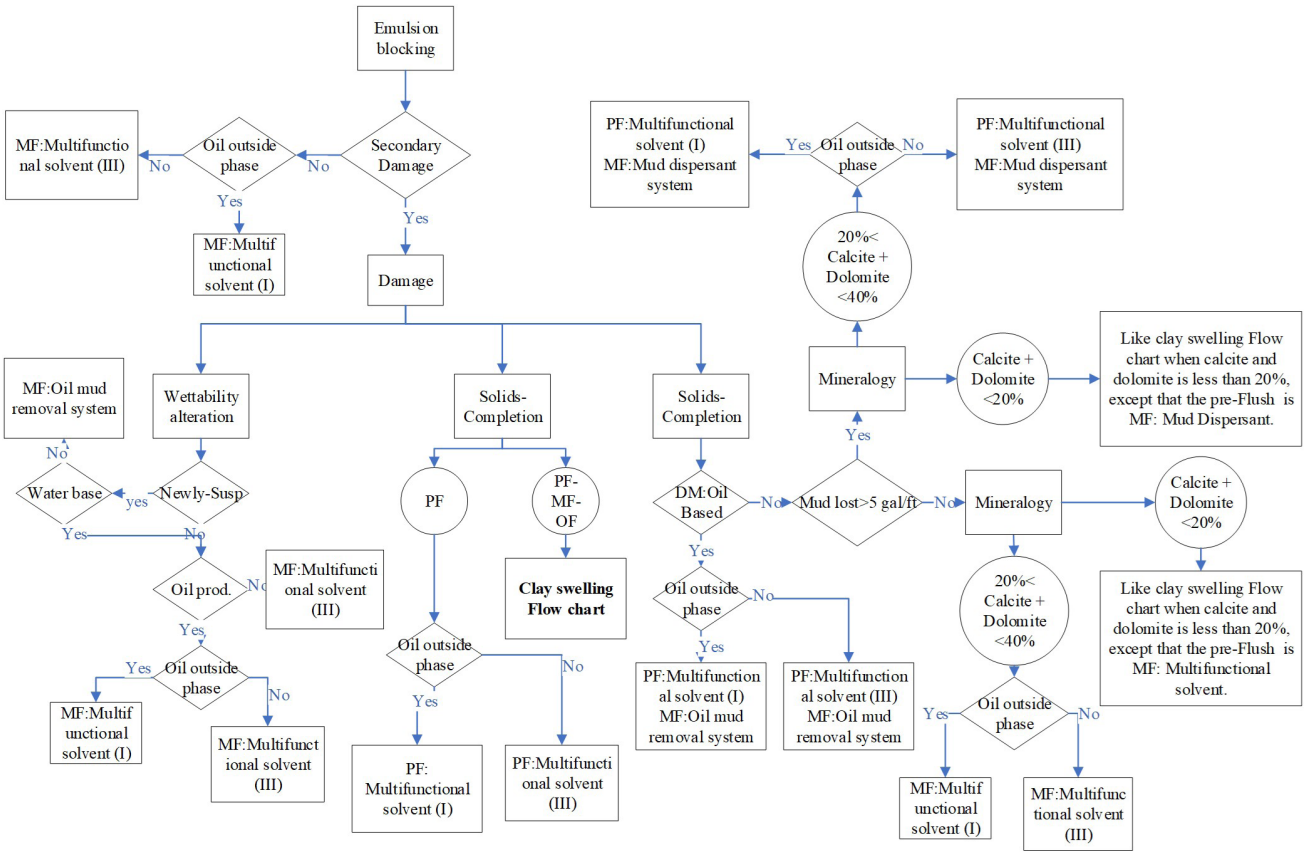

Figure 5. Detection of Main, Over Flush and Pre Flush Fluid In Emulsion Blocking Damage

2.2.3. Other Damage Types

with regard to (Figure 6), if damage other than clay swelling has occurred in the formation or well, the fluid selection is carried out as follows:

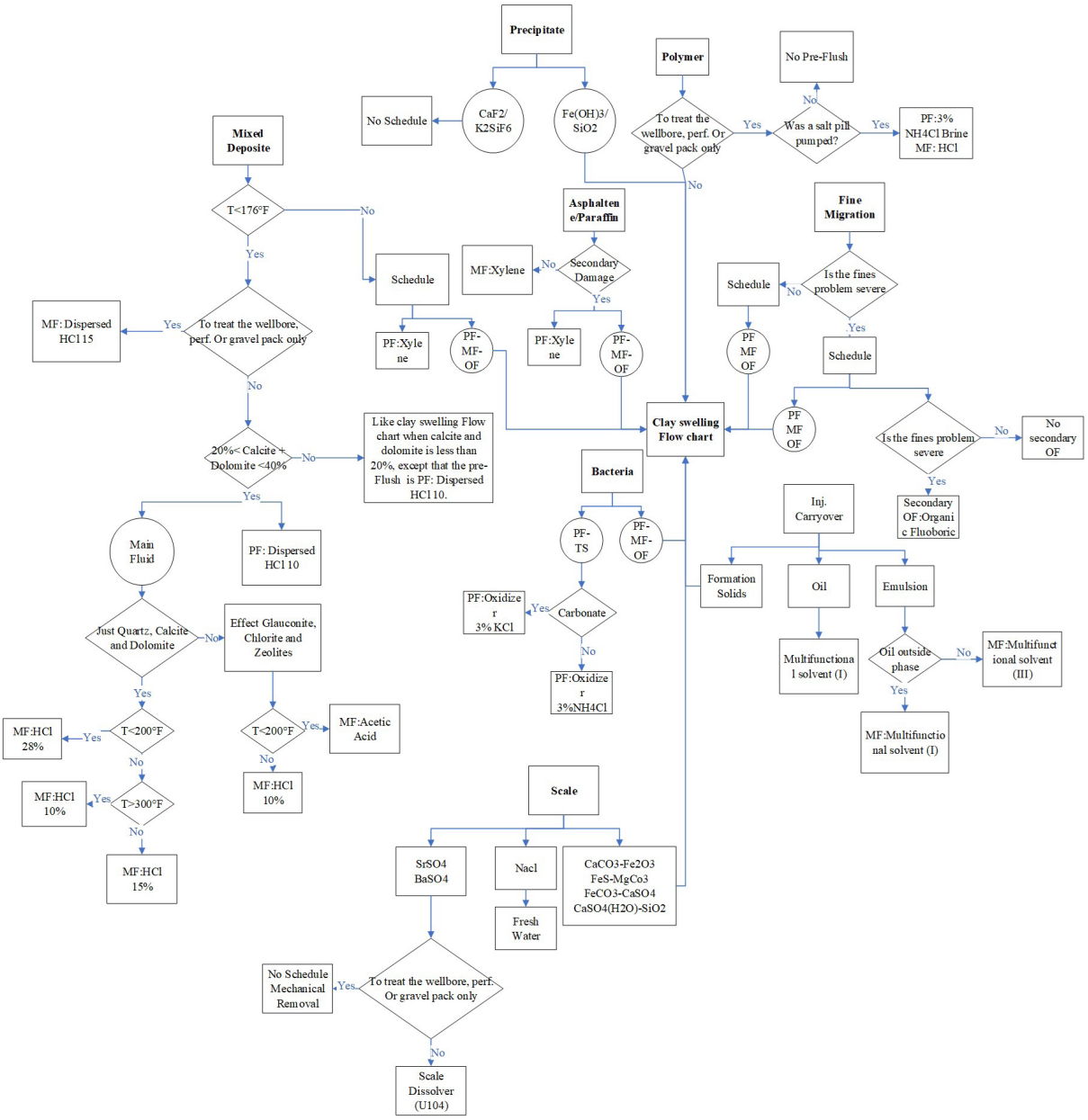

Figure 6. Detection of Main, Over Flush and Pre Flush Fluid in another Damage Types

2.2.3.1. Fine Migration

The selection of fluid for eliminating fine migration damage, such as clay swelling damage, is recommended in the previous section. However, if the fine problem is severe, it is recommended to use a secondary over-flush such as organic fluoboric to eliminate this damage completely. Fines migration is not typically observed in carbonate formation.

2.2.3.2. Polymer

If the reservoir is affected by polymer damage and the target of acidizing fluid injection is to treat the wellbore, perforation, or gravel pack, in addition to the fluids recommended for clay swelling damage recommended a pre-flush fluid of 3% NH_4Cl for sandstone reservoir and 2% KCl for carbonate reservoir are recommended. However, if the purpose of acid fluid injection is to treat the

matrix, the selected fluid, as recommended for clay swelling damage, should be used.

2.2.3.3. Mixed Deposition

If the reservoir suffers from mixed deposition damage, to eliminate this damage if the formation temperature is higher than 176 °F, a pre-flush fluid of xylene is recommended in addition to the fluids mentioned for clay swelling damage. However, if the temperature is lower than 176 °F and the target of injection is to treat the wellbore, perforation and gravel pack only, the recommended pre-flush is dispersed HCl 15%, while if the target of injection is to treat the matrix, an acidizing fluid injection similar to clay swelling damage is recommended, with the difference that the pre-flush in this case is dispersed HCl 10%.

2.2.3.4. Scale and Precipitate Damage

If scale damage is $BrSO_4$ or $SrSO_4$ and the aim is to treat the wellbore, perforation, or gravel pack only, an injection schedule is not recommended. However, if the injection objective is to treat the matrix, the only recommended fluid is the main fluid scale dissolver (U104). If the scale damage is because of the NaCl, using fresh water can potentially eliminate this damage. If the scale damage is other than the states mentioned, the recommended fluids in the clay swelling damage section can be used.

The selection of fluid for eliminating precipitate damage, if caused by CaF_2 or K_2SiF_6, does not recommend any injection fluid. However, if the damage is because of the $Fe(OH)_3$ or SiO_2 the recommended fluid for addressing the damage is similar to the one suggested for clay swelling damage.

2.2.3.5. Bacteria

In oil and gas wells, bacteria can enter through the water or chemicals injected into the well. These bacteria can thrive in the well environment and on the equipment. Some of these bacteria can cause damage to the well, such as producing acid or forming deposits. Therefore, bacterial damage in oil and gas wells occurs when bacteria infiltrate the well and their activities, which leads to various problems and damage to the well structure. However, for removing the bacteria damage, the recommended fluid for pre-flush, over-flush and main fluid is similar to the fluids used for clay swelling damage. However, to eliminate this damage completely, other fluids such as oxidizer for pre-flush and tubing spacer including 3% KCl for carbonate and 3% NH_4Cl for sandstone are also recommendedi

2.2.3.6. Asphaltene/Paraffin

If asphaltene or paraffin damage occurs alone, xylene is injected into the reservoir as the main fluid to address this damage. However, if asphaltene or paraffin damage occurs along with other damage, xylene is used as the pre-flush fluid along with other selected fluids, similar to the clay swelling damage and injected into the reservoir.

2.2.3.7. Injection Carryover

If the injection carryover damage is of the emulsion type, the selection of an acidizing fluid is similar to the case where emulsion blocking damage has occurred alone. Specifically, if the emulsion phase is oil outside phase the main fluid is multifunctional solvent I and if the emulsion phase is water outside phase, the main fluid is multifunctional solvent III. However, if the damage is of the oil type, it can only be eliminated with the main fluid multifunctional solvent I. The injection carryover-formation solids damage is different from the previous two cases. In this case, the selection of the fluid is similar to the clay swelling damage.

2.2.3.8. Water Blocking

Water blocking damage is different from other damages. for mitigating this damage in any conditions, only the main fluid Multifunctional solvent III can be used.

3. Results and Discussion

An expert system criterion for selecting acidizing fluid and eliminating reservoir damage was randomly applied to eight damages that may occur in the formation. Among these eight damages, five damages are related to sandstone reservoirs and three damages in carbonate reservoirs have been identified. Damages related to sandstone formations include three damages associated with calcite and dolomite less than 20% and two damages associated with calcite and dolomite between 20-40%. As can be seen in (Table 1), for selecting acidizing fluid to eliminate the specified damages in sandstone formations, actions have been taken based on parameters such as treatment objective, treatment interval, permeability, temperature, well type, water cut, nitrogen, emulsion phase and fines problem. When bacteria damage occurs in the sandstone formation, if the treatment interval is greater than 20 ft, a diverter should be injected. Here, due to the use of nitrogen, the diverter is foam. In addition to the main fluid, a secondary pre-flush and tubing spacer should also be injected in the case of bacterial damage occurrence. When emulsion blocking occurs as the primary damage and solid-mud as secondary damage in the sandstone formation composed of cement, if the loss of water-based drilling mud is higher than five and the well type is gas-injected and nitrogen is used, the injection fluids to remedy these damages include initial pre-flush, secondary pre-flush, main fluid, over-flush and diverters. In this situation, the emulsion phase parameter also affects the initial pre-flush. The next examined sample is mixed deposition damage that occurs in the sandstone formation when the amount of calcite and dolomite is less than 20% and minerals such as smectite, illite and glauconite present in the formation. To treat the wellbore, with a permeability of 45 mD and a formation temperature of 120°F, the injection fluids are in order, the main fluid and the diverter. The next examined damage is swelling damage accompanied by paraffin, which occurs in the sandstone formation. In this case, due to a treatment interval of less than 20 ft, a diverting agent will not be used. Therefore, considering the permeability and temperature of the formation, pre-flush fluid and main injection fluid are used. The last case for investigation is fine migration damage along with asphaltene damage, which occurs during gas production in the formation. To remedy these damages, pre-flush, main fluid, diverter and over-flush are used and xylene is used in this case to eliminate asphaltene damage, while over-flush injection is performed due to fine problem. In the carbonate formation, considering the entered parameters and the calculated maximum pump rate, If the maximum pump rate is suitable, it can determine the injected fluid in the formation. The damages of polymer, bacteria, clay swelling and paraffin that have occurred in the carbonate formation have been examined. The influential parameters on the selected fluid are reservoir information, treatment interval, pump rate and treatment fluid. The injection schedule is presented in (Table 2). In the case of clay swelling and paraffin damage occurrences, the maximum pump rate is less than zero. Therefore, a fluid for injection is not recommended. Based on the compiled information in the (Tables 1) and (Tables 2), it has been confirmed by the expert system that the damage is removed in the formation.

Table 1. Results of Expert System for Sandstone Formation

Primary Damage	Bacteria	Emulsion Blocking	Mixed Deposition	Clay Swelling	Fine Migration
Secondary Damage	None	Solid-mud	None	Paraffin	Asphaltene
Well State	-	-	-	-	-
Drilling Mud	-	Water Base Mud Lost > 5gal/ft	-	-	-
Mineralogy	Quartz: 83% Calcite: 7% Dolomite: 6% Glauconite: 4% No Cement	Quartz: 67% Calcite: 4% Dolomite: 5% k-Feldspar: 12% Kaolinite: 12% Cement	Quartz: 72% Calcite: 4% Dolomite: 5% Smectite: 6% Illite: 6% Glauconite: 2%	Quartz: 67% Calcite: 16% Dolomite: 15% Zeolites: 2% No Cement	Quartz: 72% Calcite: 12% Dolomite: 14% Glauconite: 2% No Cement
Treatment Objective	-	-	To Treat the Well-bore, Perforation, ...	-	-
Treatment Interval	20 ft	20 ft	20 ft	19 ft	20 ft
Permeability	75 md	105 md	45 md	15 md	7 md
Temperature	250 degF	190 degF	120 degF	170 degF	220 degF
Well Type	Oil Producing	Gas Injection	-	-	Gas Production
Is Higher Water Cut Acceptable?	Yes	Yes	-	-	No
Nitrogen	Yes	Yes	-	-	-
Emulsion Phase	-	Oil Out Phase	-	-	
Fines Problem	-	-	-	-	Yes
Schedule	PF: Oxidizer System TS:3%NH4Cl Brine PF: HCl/Acetic7.5/5 MF: Mud Acid/Acetic8/2/5 OF: HCl/Acetic7.5/5 FO: Foam Diverter	PF: Multifunctional Solvent PF: HCl 10% MF: Mud Dispersant OF: HCl 10% FO: Foam Diverter	MF: Dispersed HCl 15 FO: Xylene Foam Diverter	PF: Xylene MF: HCl 10%	PF: Xylene MF: Acetic Acid FO: Foam Diverter OF: Fluoboric Acid System

Table 2. Result of Expert System for Carbonate Formation

Primary Damage	Polymer	Bacteria	Clay Swelling
Secondary Damage	-	-	Paraffin
Mineralogy	Quartz: 55% Calcite: 45%	Quartz: 48% Calcite: 52%	Quartz: 50% Calcite: 50%
Reservoir Information	Permeability = 50md TVD = 1000ft Pressure = 500psi Temperature = 250degF Porosity = 30% Wellbore Radius = 3in Fracture Gradient = 0.7Psi/ft	Permeability =200md TVD =1500ft Pressure =200psi Temperature =160degF Porosity= 50% Wellbore Radius = 3in Fracture Gradient = 1Psi/ft	Permeability = 20md TVD = 1500ft Pressure = 1500psi Temperature = 200degF Porosity = 7% Wellbore Radius = 3in Fracture Gradient = 0.9Psi/ft
Treatment Interval	20 ft	20 ft	20 ft
Anticipated Pump Rate Maximum Pump Rate	0.1bbl/min 0.4bbl/min	5bbl/min 7.7bbl/min	- -0.2bbl/min
Treatment Fluid Dissolution	HFc Face Dissolution	HAc Wormhole	- -
Schedule	PF: 2%KCl MF: Formic Acid SD: Temporary Xlink Acid Diverter	PF: Oxidizer System TS: 3%KCl MF: Acetic Acid FO: Foam Diverter	Maximum pump rate must be higher than zero and anticipated pump rate must be less than maximum pump rate.

4. Conclusion

Determining the appropriate fluid to eliminate existing damages in a formation is a challenging process. This complexity persists when multiple damages are identified in the formation and the task involves selecting the best fluid for mitigating formation damages. Identifying the fluid for damage remediation requires a complete understanding of the formation and the damages occurring within it. In this study, our aim was to establish an expert system capable of fluid selection for damage remediation and well improvement. The results obtained in fluid selection for eliminate formation damages have been promising. Furthermore, in future research, our objective is to enhance these investigations by developing a fuzzy logic-based system for more precise fluid selection.

References

Abdulmutalibov, T., Y. Shmoncheva and G. Jabbarova (2023). Advancements in Applications of Machine Learning for Formation Damage Predictions. SPE Annual Caspian Technical Conference, SPE.

Alvarez, J., X. Alarcon and J. Tellez (2023). Implementing a Novel Organic Acid Matrix Stimulation to Successfully Remove Formation Damage: Case Studies, Iraq and Ecuador Oilfields. SPE Middle East Oil and Gas Show and Conference, SPE.

Blackburn, C., J. Abel and R. Day (1990). "An expert system to design and evaluate matrix acidizing." SPE Computer Applications 2(06): 15-17.

Chavanne, C. and H. Perthuis (1992). A fluid selection expert system for matrix treatments. SPE Europec featured at EAGE Conference and Exhibition?, SPE.

Chiu, T.-J., E. Caudell and F.-L. Wu (1993). "Development of an expert system to assist with complex fluid design." SPE Computer Applications 5(01): 18-20.

Dargi, M., E. Khamehchi and J. Mahdavi Kalatehno (2023). "Optimizing acidizing design and effectiveness assessment with machine learning for predicting post-acidizing permeability." Scientific Reports 13(1): 11851.

Domelon, M., W. Ford and T. Chiu (1992). An expert system for matrix acidizing treatment design. Paper No. SPE 24779. 67th SPE Annual Technical Conference and Exhibition, Washington, DC, October.

McLeod, H. O. (1984). "Matrix acidizing." Journal of Petroleum Technology 36(12): 2055-2069.

Mouedden, N., A. Laalam, M. Rabiei, A. Merzoug, H. Ouadi, A. Boualam, S. Djezzar and M. Mahmoud (2022). A Screening Methodology Using Fuzzy Logic to Improve the Well Stimulation Candidate Selection. ARMA US Rock Mechanics/Geomechanics Symposium, ARMA.

Nguyen, M. C., M. Dejam, M. Fazelalavi, Y. Zhang, G. W. Gay, D. W. Bowen, L. H. Spangler, W. Zaluski and P. H. Stauffer (2021). "Skin factor and potential formation damage from chemical and mechanical processes in a naturally fractured carbonate aquifer with implications to CO_2 sequestration." International Journal of Greenhouse Gas Control 108: 103326.

Novikov, V. A., D. A. Martyushev, Y. Li and Y. Yang (2022). "A new approach for the demonstration of acidizing parameters of carbonates: experimental and field studies." Journal of Petroleum Science and Engineering 213: 110363.

Santos, S., A. Salazar Munive, E. Hernandez Del Angel, O. Villaseñor, J. L. Guzman Almazo, D. Hernandez Vulpes, A. M. Beuterbaugh, E. A. Reyes, S. Squires and K. Campos (2022). Acidizing Treatment Design Assessment Based on Dolomitic Field Core Testing. SPE International Conference and Exhibition on Formation Damage Control, SPE.

Sidaoui, Z., A. Abdulraheem and M. Abbad (2018). Prediction of optimum injection rate for carbonate acidizing using machine learning. SPE Kingdom of Saudi Arabia Annual Technical Symposium and Exhibition, OnePetro.

Sumotarto, U. (1995). Sandstone acidizing simulation: development of an expert system, The University of Texas at Austin.

Xue, H., P. L. Liu, N. Y. Li, Z. F. Luo and L. Q. Zhao (2012). "Expert System for Acidizing Based on BP Neural Network." Advanced Materials Research 548: 438-443.

JOURNAL OF GAS TECHNOLOGY

Volume 9 /Issue 1 / Summer 2024 / Pages 34-49

Journal Home page: http://jgt.irangi.org

Comparative Study of Biotreated Leachate Before and After Using AOPs Treatment for Removing COD, BOD and Color

Sadegh Motaghed[1], Amir Hessam Hassni[2*], Seyed Alireza Hajiseyed Mirzahosseini[3], Seyed Masoud Monavari[2], Nabiollah Mansouri[2]

1. Ph.D. Student, Department of Environmental Engineering, Faculty of Natural Resources and Environment, Science and Research Branch, Islamic Azad University, Tehran, Iran
2. Professor, Department of Environmental Engineering, Science and Research Branch, Islamic Azad University, Tehran, Iran
3. Associate Professor, Department of Environmental Engineering, Science and Research Branch, Islamic Azad University, Tehran, Iran

ARTICLE INFO

ORIGINAL RESEARCH ARTICLE

Article History:
Received: 02 May 2024
Revised: 18 July 2024
Accepted: 20 August 2024

Keywords:
Decomposition
Leachate waste
Biotreatment
AOPs

ABSTRACT

In this research, a comparative study of the treatment the biotreated (UASB-AERATED LAGOON) leachate effluent before and after using advanced oxidation processes The combined application of biotreated processes (UASB + aerated lagoon) and advanced oxidation processes (AOPs) for treating leachate effluent offers significant advantages. This integrated approach allows for efficient decolorization, outperforming the use of biotreated leachate alone. The UV/H_2O_2 process also yielded significant pollutant removal rates in biologically treated effluent, achieving up to 74% COD, 71% BOD and 52% color reduction. Among the AOPs studied, UV/H_2O_2 showed the highest decolorization efficiency, reaching up to 98%. Ozonation was particularly effective as a pretreatment for raw, untreated leachate, achieving substantial reductions 93% in color, 88% in BOD and 77% in COD. Additionally, ozonation of the initial leachate provided superior results in terms of decolorization, COD removal and BOD removal compared to other AOPs. The Photo-Fenton process emerged as the most effective AOP, delivering the highest removal efficiencies across all parameters, especially for COD (82%) and color (92%). Its efficacy is attributed to the synergy between UV light and the Fenton reaction, which generates abundant hydroxyl radicals. Notably, the photo-Fenton treatment achieved the highest BOD removal efficiency. The order of COD removal efficacy across AOPs was UV/H_2O_2 > UV > ozone > photo-Fenton. Although ozone proved highly effective for COD and color removal in the initial leachate, the performance of UV/H_2O_2 may have been influenced by the low pH level used. However, combining UV or H_2O_2 with ozone further enhanced decolorization rates. Overall, UV/H_2O_2 emerged as the most efficient AOP for both COD and color removal. Applying UV and H_2O_2 to biotreated leachate shows strong potential for industrial use. In conclusion, this study proposes combining biological processes with tailored AOPs for efficient landfill leachate treatment. Initial ozonation prepares raw leachate, while UV-based AOPs and the photo-Fenton process excel in later stages. Customizing AOPs based on leachate properties like pH and organic content boosts pollutant removal, reduces environmental risks and meets discharge standards, offering a scalable solution for leachate management.

DOR: 20.1001.1/jgt.2024.2036910.1044

How to cite this article
S. Motaghed, A.H. Hassni, S.A. Hajiseyed Mirzahosseini, S.Masoud Monavari, N. Mansouri, Comparative Study of Biotreated Leachate before and After Using AOPs Treatment for Removing COD, BOD and Color. Journal of Gas Technology. 2024; 9(1): 34-49. (https://.jgt.irangi.org/article_719336.html)

* Corresponding author.
E-mail address: ahhassani@srb.iau.ir, (A.H. Hassni).

Available online 10 September 2024

1. Introduction

Human life is inevitably associated with the generation of substantial amounts of waste and wastewater. Various methods, including dumping, incineration, recycling and sanitary burial, are employed in different regions to manage waste and effluents based on the volume of waste and available technologies. Open dumpsites, which are the oldest and most prevalent solid waste landfills globally, can significantly impact the environment and human health in negative ways. One of the contributors to this pollution is leachate, a highly contaminated wastewater produced during waste disposal. Leachate results from rainwater infiltration and the decomposition of organic matter within solid waste (Faridun et al., 2019). The characteristics and quantity of leachate depend on several factors, such as waste composition, dumpsite lifespan, waste material stabilization, compaction level, initial moisture content, rainwater infiltration rate, regional climate, season, temperature, evaporation, transpiration and on-site management practices (Costa et. al, 2019; Salem et al., 2019). Leachate typically contains significant quantities of both organic and inorganic pollutants, ammonium, heavy metals, hazardous organic compounds, pathogenic microorganisms and toxic substances. Leachate is a critical factor in water source pollution (Shu, J et al., 2019). Leachate is one of the important factors that pollute water sources (Fallah et al., 2021; Rezaei et al., 2009).

Landfill leachate contamination is recognized as one of the major environmental health challenges in many developing countries, primarily due to the lack of cost-effective treatment technologies and regulatory standards for waste disposal (Alzamora BR et al., 2020). This contamination is driven by the rapid increase in municipal solid waste (MSW) generation globally, resulting in an estimated production of 2.2 billion tons of MSW per year (Cetrulo TB et al., 2018). Unlike specialized waste disposal facilities, such as incinerators and recycling plants, engineered landfills are often seen as the most feasible solution for managing large volumes of MSW, as they can contain waste while reducing risks of groundwater, surface water and air pollution (Yatsunthea T et al., 2020).

Consequently, a significant number of countries, particularly China (0.1%) and members of the European Union, utilize landfills as their primary method for MSW disposal (Ozbay G et al., 2020). However, leachate can escape due to damage or chemical degradation of protective liners, such as high-density polyethylene (HDPE) geomembranes (Sauve G et al., 2020). The leachate produced in landfills poses substantial environmental and public health hazards due to the release of toxic substances, harmful microorganisms and noxious gases into groundwater and the atmosphere. Leachate is a dark, complex liquid containing various toxic organic and inorganic compounds, including microbial contaminants (Amoatey P et al., 2021). Common pollutants in leachate include dissolved organic compounds, trace ions, xenobiotic organics, ammonia and coliform bacteria (Ankit ShL et al., 2021). Additionally, leachate can release persistent organic pollutants, heavy metals and emerging contaminants into the environment (Nika MC et al., 2021).

In many developing countries, unsustainable production and consumption patterns have led to increased MSW generation, a rise in landfill sites and thus more frequent leachate contamination events (Siddiqi SA et al., 2021).

This poses a severe environmental and health risk, especially in regions lacking engineered landfill infrastructure (Baawain MS et al., 2020). Studies have shown elevated levels of lead (Pb), cadmium (Cd) and chromium (Cr) in groundwater samples, exceeding critical

thresholds and posing cancer risks due to leachate contamination (Teng C et al., 2021). Research by (Propp VR et al., 2021) also revealed high concentrations of heavy metals, such as nickel (Ni), cadmium (Cd) and manganese (Mn), in crops irrigated with leachate-contaminated surface water, which highlights a potential carcinogenic risk to humans and animals (Abiriga D et al., 2021).

To mitigate the environmental impact of leachate, efficient and affordable treatment methods are crucial (Parvin F et al., 2021). Given the complexity of leachate as a pollutant, preliminary treatments-such as coagulation-flocculation, air stripping and chemical oxidation-are necessary to reduce COD, total dissolved solids and overall toxicity (Iravanian A et al., 2020). For many years, conventional biological treatments and classical physico - chemical methods have been considered the most appropriate technologies for manipulation and management of high strength effluents like landfill leachates. There are many advantages of destructive technologies for the treatment of nonbiodegradable pollutants. The AOPs generate free radicals, which act as strong oxidants to destroy the organic pollutants. In AOPs, oxidant agents such as H_2O_2, O_3, UV and ultrasound Fenton, are used alone or in a combination (Sarria et al., 2002).

Latest investigations on the degradation of organic pollutants are focused on the combination of biological and physical-chemical treatments. This saves a considerable amount of energy in comparison with what is needed to achieve the full mineralization of the pollutants by chemical oxidation. Torres et al. (2003) and Marco et al. (1997) reported the degradation of generated chlorophenol from bleaching process during paper production by sequential biological-AOP using T.versicolor and UV/TiO_2/Ru_xSe_y obtaining a 99% chlorophenol removal after 96 h and 20 min with a 97% reduction in chemical oxygen demand. A biological treatment does not prove to be so effective in color removal from treated leachate within permissible limits. Therefore, post treatment seems to be essential to bring anaerobically treated effluent to the recommended quality. In addition to these systems, advanced oxidation processes (AOPs) are the emerging post treatment options. The main advantages of AOPs include a lack of byproducts of environmental concern, high process rate and efficiency (Pedroza et al., 2007). These treatment processes are considered very promising methods for the remediation of pollutants containing non-biodegradable organic (Kos et al., 2008). Post treatment involves the application of UV and AOPs a schematic of chemical oxidation experimental set-up is presented in (Figure 2) in color and COD removal and disinfection of leachate. Post treatment is accomplished by UV and AOPs, including O_3, H_2O_2, UV/H_2O_2, Fe^{+2}/H_2O_2. According to Yasar et al. (2006), all processes show good performance for the removal of color and COD from the combined industrial biotreated (UASB) effluent. These systems are feasible to quickly remove both the parameters. AOPs (O_3, H_2O_2/UV and UV/H_2O_2/Fe^{+2}) result in over 90% and 80% removal for color and COD, respectively, UV and Fe^{+2}/H_2O_2 results in slightly less color removal of 76% and 68%, respectively and COD removal 57% and 60%, respectively. Overall it can be said that the photo-Fenton process appears to be the most effective technology, whereas ozonation appears to be similar with proper optimal conditions for pH and temperature. In a study, advanced oxidation processes (AOPs) such as Fenton, ultraviolet light (UV), hydrogen peroxide (UV/H_2O_2) and photo-Fenton processes were investigated in laboratory scale experiments as an effective alternative for leachate treatment (Tikhe et al., 2014). The other study showed that the photo-Fenton process was the most effective treatment process under acidic conditions at pH 2.5 - 3.5 and produced a higher percentage of COD removal and color

removal. Although these techniques are not economically acceptable for the treatment of large-scale effluents, the combination of AOPs with a biological process could significantly decrease the overall cost of leachate treatment (Neyens et al., 2006). Fang and colleagues used an up flow anaerobic sludge blanket (UASB) reactor at 37 ℃ to treat landfill leachate. The process achieved COD removal ranging from 66% to 90% within a 6-day hydraulic retention time. The UASB effluent, containing 1500 mg/L COD, was then subjected to Fenton coagulation. By adjusting the initial pH to between 4-6 and using a hydrogen peroxide concentration of 300 mg/L, they achieved 99.3% COD removal in just 30 minutes (Fang et al., 2005). Literature review revealed that though the sequential biological and advanced oxidation techniques have been studied, there is no available literature on using UASB+Aareated Lagoon as the pretreatment step followed by AOP ($UV/H_2O_2/O_3$) process. The objective of this study was to compare the effects of AOPs on biotreated leachate performance in reduction (COD, BOD and TOC) and comparison conclusions with before using AOPs. In this work the sequential biological degradation-advanced oxidation process for leachate was evaluated. Biological degradation was carried out using laboratory scale (UASB-AREATED LAGOON) process and AOP in a batch recycle photochemical reactor.

2. Material and Methods

Samples were collected at specific time intervals from the reaction vessel and transferred into 5 ml glass vials. These vials were filled completely to avoid any headspace and then sealed using Teflon-lined silicon septa and screw caps. Immediate analysis was conducted on the samples to prevent any further reactions. The concentration changes of phenol were determined using a spectrophotometer (DR 2500, HACH) following established methods (Cortez et al., 2011). The initial and biotreated solutions were also analyzed using the standard methods procedure, (Primo et al., 2008) pH measurements were carried out using a pH meter (Shu et al., 2006). To adjust the pH, 250 mL of leachate sample was mixed with H_2SO_4 to achieve pH values of 2.5, 3 and 3.5. The mixture was stirred for 15 minutes using a magnetic stirrer and pH testing occurred every 5 minutes. Once the pH stabilized, the sample was settled for 1 hour and supernatant samples were taken for COD measurements.

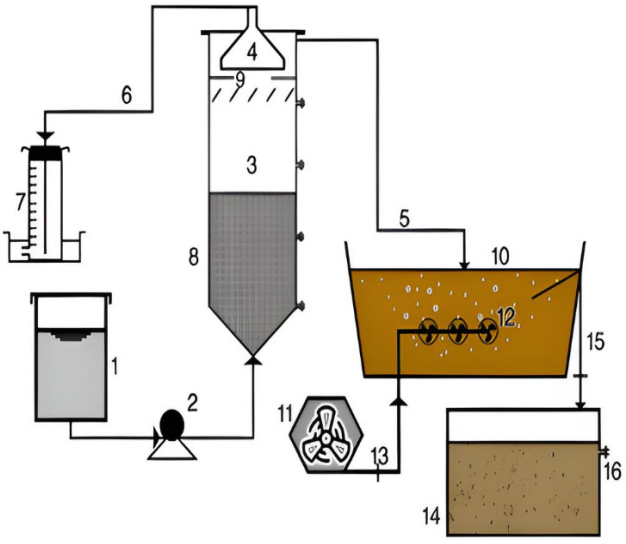

1. INLET TANK
2. Peristaltic pump
3. UASB reactor
4. Gas seperator
5. Effluent outlet
6. Gas outlet
7. Gas collection system
8. Sludge blanket
9. Deflector baffles
10. Areated lagoon
11. Air blower
12. Air nozel
13. Air flow
14. Sedimentation tank
15. Lagoon outlet
16. Ultimate outlet

Figure 1. Schematic view of the UASB Reactor, Aerated Lagoon and Sedimentation Tank

2.1. Experimental Setup

The schematic diagram of the experimental setup for biodegradation using an Upflow Anaerobic Sludge Blanket (UASB) reactor and an aerated lagoon is shown in (Figure 1). The UASB reactor, constructed from PVC material, has a cylindrical shape with a diameter of 15 cm and a height of 170 cm. Sampling valves are strategically placed at 20 cm intervals along the

vessel and the top of the cylinder serves as the gas outlet.

To initiate the reactor, approximately 4 liters of sludge obtained from activated sludge, which had been stored in a sealed container for one month, was used as inoculum material. This sludge was mixed with 7 liters of leachate diluted to a chemical oxygen demand (COD) of 1000 mg/L to provide necessary nutrients. The UASB reactor was also equipped with a peristaltic pump (KT-20, Model PDP-B-V, Italy).

Further details, including system specifications and operational information, please given in (Table 1).

Table 1. Characteristics of Bio Treated (UASB- AREATED LAGOON) Leachate

Leachate Parameter	Bio treated (UASB- AREATED LAGOON)
pH	7.6-8.3
Color (PtCo)	980
BOD_5 (mg/L)	1960
COD (mg/L)	960

In the initial stage, diluted leachate with a COD concentration of 2000 mg/L entered the reactor from the bottom to the top, with a volumetric loading of 1 g/L/d. The hydraulic retention time (HRT) was 1 day. The organic loading of the system varied between 1 and 20 kg/m^3/d of COD. The reactor pH ranged from 7 to 8, which is optimal for anaerobic microorganisms. We measured pH, COD, temperature and BOD. Due to faster results than BOD, COD measurements served as the daily indicator of pollution load in biological treatment. COD was determined using the digestion method with the HACH spectrometer DR-5000 (USA product). An aerated lagoon supplemented the anaerobic treatment system. The pilot study used a tank with dimensions of 0.5 × 0.5 × 0.5 m^3, equipped with a barrier to prevent short-circuiting. Lagoon ventilation was achieved by installing a diffuser at the tank bottom, maintaining dissolved oxygen levels at 2-3 mg/L. The aerated lagoon's effluent was directed to a sedimentation unit (0.2 × 0.5 × 0.5 m^3) with a retention time of 6 hours. (Figure 1) illustrates the UASB reactor, aerated lagoon and sedimentation tank. To establish the aerated lagoon, we introduced 10 liters of fresh brown sludge from a sewage treatment plant with an active sludge system. To prevent organic shock, we gradually replaced the leachate with twice the pollution every 5 days until the COD reached 3000 mg/L. The aerated lagoon's mixed liquor suspended solids (MLSS) concentration was 3500 mg/L, suitable for aerobic treatment (Tchobanglous et al., 2019).

We investigated retention times of 2, 4, 6, 8, 10 and 12 hours by adjusting the flow rate to optimize organic compound removal. Dissolved oxygen levels in the lagoon were maintained above 3 mg/L. Total nitrogen (TN) and total phosphorus (TP) concentrations were determined using persulfate digestion and persulfate UV oxidation methods with the HACH spectrometer DRB-5000 (USA product). Portable meters (Partech 740 monitor and soli-tech 10 sensors) measured total suspended solids. Volatile fatty acids (VFA) were quantified following standard methods (5560 C) (APHA, AWWA et al., 1998). To calculate filtered Chemical Oxygen Demand (CODF), samples were filtered using Whatman GF/C glass microfiber filters.

(Figure 2) depicts the experimental setup for advanced oxidation. The cylindrical reactor (250 mL volume) was made of quartz glass. A 125W UV lamp immersed in the glass tube provided irradiation. The lamp included a cooling water space within the reactor vessel. The reaction mixture filled the chamber between the reactor walls and UV lamp system, with an air bubbler ensuring suspension of the photocatalyst.

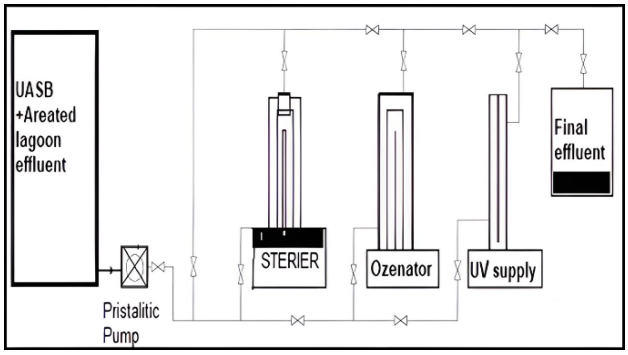

Figure 2. AOP Unit Used in the Experimentation

2.2. AOPS Setup

Ozonation was performed in a bubble column reactor made of plexiglass. The internal diameter and height of the reactor were 3.5 cm and 35.5 cm, respectively. Ozone was introduced at a rate of 100 mg/hr through a diffuser at the bottom of the reactor using an ozone generator (Enalay HGOZ 1000). Ozonation time varied from 5 to 25 minutes for solo experiments. For combined O_3/H_2O_2experiments, 112 mg/L of H_2O_2 was added to the sample, followed by varying ozonation times. A hydrogen peroxide reactor consisted of a graduated Pyrex glass cylinder with a magnetic stirring setup. Analytical-grade hydrogen peroxide (35% w/w) from Merck was used and the H_2O_2 dose ranged from 112 to 373 mg/L. Additionally, peracetic acid was prepared in different concentrations (1%, 5% and 15%) following standard methods (Cortez et al., 2011). For each concentration, a fixed dose of 1 ml/L was used. UV irradiation, both alone and in combination with H_2O_2 (H_2O_2/UV), took place in a cylindrical reactor with an internal diameter of 3.5 cm and a volume of 330 ml. To enhance UV absorbance, the reactor was wrapped with aluminum foil (Figure 2).

A low-pressure mercury UV lamp (Pen ray 3SC9 Upland, CA USA) with radiation intensity of 5 m W/cm^2 (at the surface of the lamp) and wavelength of 254 nm was used. The UV lamp was placed at the center of the reactor to ensure uniform distribution of UV irradiation and no lamp cooling was provided. All the experiments were performed in batch mode and at ambient temperature. UV irradiation time was varied from 5 to 25 min for UV solo experiment and for H_2O_2/UV. 112 mg/L of H_2O_2 was added to the sample and then UV irradiation time was varied from 10 to 60 sec. Disinfection by solar radiation was undertaken using a rectangular (40×5×5 cm) reactor made of Plexiglas. (Table 1) show the characteristics of (UASB+ Aerated Lagoon) treated leachate.

2.3. Ozone

Ozone has proved to be a powerful oxidizing agent and its oxidizing ability is owed to nascent oxygen atoms and hydroxyl radicals. It reacts, directly or indirectly, with complex compounds, breaking them into simpler and smaller molecules. The ozonation process minimally generates toxic byproducts and its prior application to wastes also enhances their biodegradation (Sevimlim et al., 2004). Consequently, no additional disposal problems are associated with the ozone treatment technique. However, process conditions like pH, temperature, initial leachate concentration, ozone dose and exposure time influence the performance of the ozonation process (Arslan et al., 2001, WU et al., 2001).

According to (Yasar et al., 2007), ozonation shows best results for post treatment of anaerobically (UASB, AREATED LAGOON) treated effluent for color and COD removal as compared to the pretreatment of combined industrial wastewater of the same nature. However, the efficiency of the ozonation process increases at elevated pH while temperature shows an adverse effect on removal efficiency as an increase in temperature (>30°C) results in continuous decrease of color and COD degradation. The effect of ozone on COD and biodegradability of leachate is also dictated by reaction time. Many studies (Tizaoui et al., 2007) reported an overall increase in COD removal as the reaction time of oxidation increased. This is because of

higher ozone doses. For instance, COD removal increased from 4% at 5 min reaction time to 10% at 60 minutes at an inlet ozone concentration of 63 mg/L (normal temperature and pressure) (Cortez et al., 2011) COD removal was observed when leachate was treated for 60% instead of 20 minutes.

2.4. UV Light

Ultraviolet (UV) light plays a crucial role in breaking chemical bonds by providing the necessary energy. When UV irradiation interacts with molecules, it can cleave chemical bonds, resulting in fragmented by-products. These by-products may either degrade further or become excited and prone to oxidation. Even strong bonds, such as the double oxygen bond (O=O) in molecular oxygen (O_2) or the double carbon-oxygen bond (C=O) in carbon dioxide (CO_2), can dissociate due to UV exposure. High-efficiency UV lamps are essential for delivering the required energy in applications like leachate treatment processes. However, selecting the appropriate UV lamp pressure and radiation intensity involves balancing cost and efficiency requirements. The duration of exposure to UV light has a direct effect on the removal of color and COD (chemical oxygen demand) from leachate. Notably, the reduction in color depends on the initial concentration of leachate. Even when using a high-intensity UV lamp, significant improvements in color removal may not be achieved if the leachate concentrations are already high. UV systems offer several advantages, as highlighted in numerous studies. These benefits include compact design, ease of operation, low maintenance requirements, rapid treatment and the absence of disinfection byproducts. However, it's essential to recognize that UV disinfection alone does not provide residual protection and bacteria can become reactivated after a few days of treatment (ZHOU et al., 2002).

2.5. UV/H_2O_2

The use of ultraviolet light in combination with hydrogen peroxide enhances the rate of generation of free radicals $OH^{\bullet}$ significantly. This occurs because UV light supplies energy required for the dissociation of H_2O_2 into hydroxyl radicals. Photolysis of aqueous hydrogen peroxide has been investigated by many researchers (Yasar et al., 2007). In the UV/H_2O_2 process, photon energy is high enough to break the chemical bonds of the organic compounds which enables the process to treat leachates that contains different organic contaminations. A low concentration of H_2O_2 did not generate enough $OH^{\bullet}$ in solution. Addition of H_2O_2 above optimum will lead to decrease in hydroxyl radical concentration due to free radical scavenging by the excess H_2O_2 (Chen et al., 1997).

UV/H_2O_2 process is efficient in mineralizing organic pollutants. A disadvantage of this process is that it cannot utilize solar light as the source of UV light due to the fact that the required UV energy for the photolysis of the oxidizer is not available in the solar spectrum (Neyens et al., 2003). Moreover, H_2O_2 has poor UV absorption characteristics and if the water matrix absorbs a lot of UV light energy, then most of the light input to the reactor will be wasted. Finally, special reactors designed for UV illumination are required, while residual H_2O_2 should be addressed (Crittenden et al., 2005). The major factors affecting this process are the initial concentration of the target compound, the amount of H_2O_2 used, leachate pH, presence of bicarbonate and reaction time. Specifically, the kinetic rate constant for the degradation process is inversely proportional to the initial concentration of the pollutant. As a result, leachate dilution should be done at an optimum level (Gogate et al., 2004). Moreover, there is an optimum concentration for H_2O_2. Beyond this limit, the presence of H_2O_2 is detrimental to the degradation reaction due to scavenging action.

2.6. Fenton and Photo-Fenton Processes

Fenton and photo-Fenton oxidation processes are effective for treating bio-treated leachate. The photo-catalytic treatment process efficiency is significantly higher than the simple Fenton process for bio-treated leachate as photo-Fenton provides almost complete color removal and significant COD reduction (BALCIOGLU I.A. et.al, 1999). The mechanism of Fenton's oxidation is based on the generation of hydroxyl radicals by the catalytic decomposition of the H_2O_2 in acidic media (Barusinski et al., 2000, Malato et al., 2007). Photo-Fenton process combining with aerobic biological processes have been successfully used for the treatment of saline industrial wastewater containing almost 0.6 g/l α-methyl phenylglycine (Mosteo et al., 2008). In that study, the optimal conditions were observed when 6 ml of H_2O_2 (70%) and 1 ml of $FeSO_4$ (0.5 M) were added to 50 ml of OMWW (reaction time = 6 days, pH = 4.2) (El-Gohary et al., 2008). In another study, Dias et al. (2000) investigated the use of Fenton process for the pretreatment of OMWW. COD removal up to 83% was achieved, at pH values ranging from 2 to 3 (initial COD = 23400 mg/L, reaction time = 90 min, H_2O_2/Fe^{2+} = 10). Fenton's oxidation has been applied for the pretreatment of landfill leachate. Petruzzelli et al. (2007) reported that under optimal conditions (initial COD = 10915 mg/L -1, reaction time = 120 min, H_2O_2/Fe^{2+} = 13 w/w, pH = 3.2) almost 50% COD removal was observed.

2.7. Application of Combined Systems

The mechanism of action of combined AOPs is not so straightforward. The application of an O_3/UV system enhances the disinfecting characteristics of ozone significantly (Benitez et al., 1996). However, it is desirable that UV irradiation should follow ozonation because simultaneous application of UV and ozone retards the efficacy of ozone due to the decomposition of ozone to molecular oxygen.

During the treatment of effluent by an H_2O_2/UV system, UV irradiation followed by H_2O_2 produces two hydroxyl radicals that react with organic contaminants or undergo an H_2O_2 decomposition-formation cycle. This decomposition formation cycle helps maintain nearly constant concentration of H_2O_2 during the treatment process (Zhouh et al., 2002). However, an excessive H_2O_2 dose may hinder the penetration of hydroxyl radicals because of its character to scavenge hydroxyl radicals (Glaze et al., 1987).

3. Results and Discussion

3.1. Ozonation

Ozone is commonly employed for leachate treatment due to its potent oxidative properties resulting from the decomposition of O_3 into nascent oxygen (O^-) and hydroxyl radicals (Camel et al., 1998). Ozone effectively reduces pollutants (such as Aeromonas salmonicida, Aeromonas liquidfaciens Pseudomonas fluorescens and Yersinia ruckeri) by up to 99%, even in systems containing suspended and dissolved particles. In a study, the impact of ozonation time on the removal of COD, color and BOD (biochemical oxygen demand) was investigated using 99.5% pure oxygen fed into the ozone generator. Initially, COD, color and BOD removal increased with ozonation exposure time, up to 25 minutes and then stabilized. This behavior can be attributed to variations in the susceptibility of different organic compounds to oxidation (Azbar et al., 2004).

Despite ozone being a highly oxidizing agent, pH values significantly influence COD removal, with higher pH values enhancing removal efficiency (Fallah et al., 2021).

Results suggest that initial leachate decolorization can be achieved efficiently at a constant pH of 6.2 through ozonation, achieving 62% removal within 25 minutes (Figure 3). Additionally, ozonation experiments on biotreated leachate effluent (from

UASB and Aerated Lagoon processes) were conducted at a constant pH of 6.2, using 5% ozone concentration and a pure oxygen supply of 1.5 l/min. These experiments yielded promising results: 93% color removal, 88% BOD reduction and 77% COD removal within 25 minutes (see Figures. 3, 4 and 5). Notably, the color removal initially increased with ozone dosage but reached a plateau, likely due to the prior reduction in leachate intensity through biotreatment.

The reactivity of ozone and its efficiency in leachate treatment depend on the nature and concentration of compounds present (Frontistis et al., 2008).

The higher COD values correspond to greater concentrations of oxidizable pollutants. Therefore, initial COD concentration plays a crucial role in ozonation effectiveness. Emphasize the Photo-Fenton process's potential for effective leachate treatment (Shu et al., 2005).

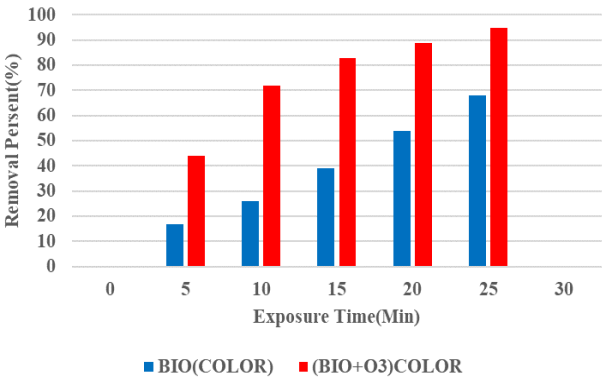

Figure 3. Removal of Color versus O_3 Exposure Time

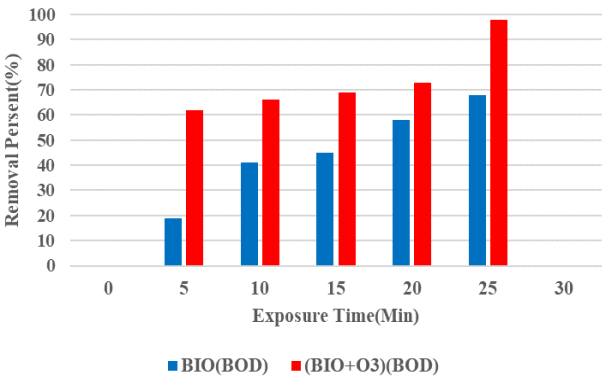

Figure 4. Removal of BOD versus O_3 Exposure Time

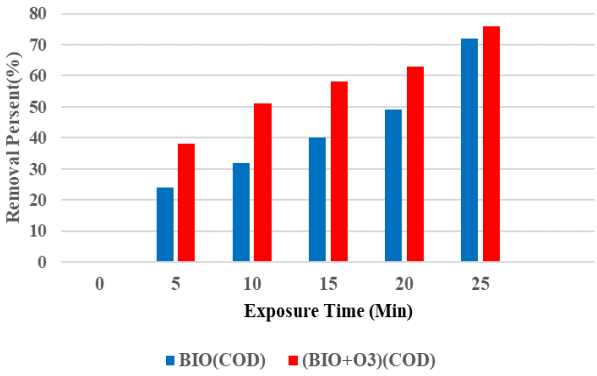

Figure 5. Removal of COD versus O_3 Exposure time

3.2. UV Radiation in Landfill Leachate Treatment

UV radiation has become a well-established method for treating landfill leachate, often paired with advanced oxidation processes (AOPs) to improve treatment outcomes. Leachate is a complex wastewater, typically containing various organic and inorganic pollutants, including colorants, that absorb UV light. This absorption can diminish the overall UV intensity and reduce treatment efficiency, especially in untreated leachate with high color intensity. Despite these challenges, UV irradiation has been effectively used for decades, particularly for disinfecting leachate effluents.

In one study, untreated landfill leachate was exposed to UV radiation alone, aiming to reduce levels of COD, color and BOD. The results showed that after 20 minutes of exposure, the highest removal efficiencies were observed: COD, color and BOD were reduced by approximately 32%, 28% and 37%, respectively (see Figures 6 and 7). Beyond the 25 minutes mark, however, the removal rates declined. This reduction in effectiveness may be due to the intense color of the untreated leachate, which absorbs UV light and interferes with the irradiation process. Generally, UV-supported treatments perform best with aqueous wastes that have lower color intensities, as high color levels can shield pollutants from UV exposure.

The study also explored the effect of UV radiation on leachate that had been pre-treated biologically through an upflow anaerobic sludge blanket (UASB) reactor and an aerated lagoon system. Applying UV radiation to this biotreated effluent produced significantly better results, especially in terms of color removal, with 82% decolorization, as well as strong reductions 84%, 71% in COD and BOD levels (see Figure 6). The improved effectiveness is likely due to the lower initial color intensity of the biotreated effluent, which allowed the UV light to penetrate more effectively and treat remaining contaminants. This finding highlights the importance of integrating UV radiation with pre-treatment steps for highly colored leachate, as it can enhance the overall efficiency of the treatment process.

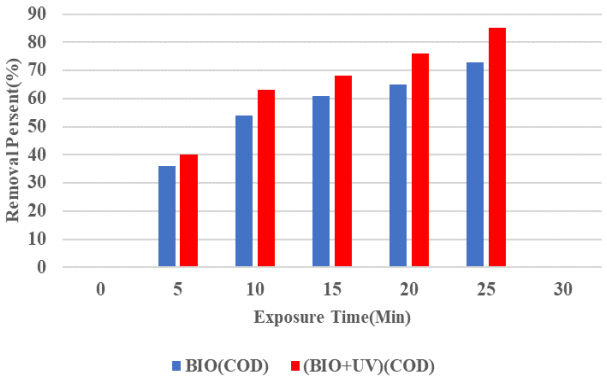

Figure 6. Removal of COD versus UV Exposure Time

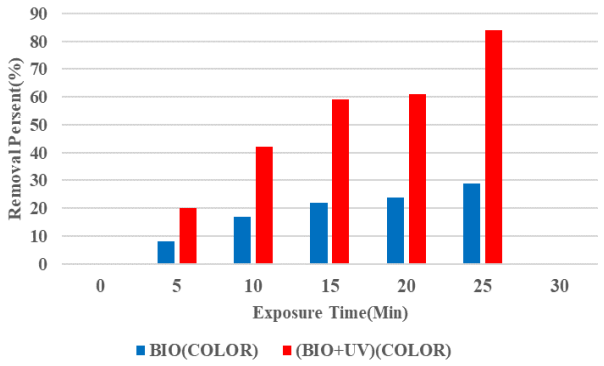

Figure 7. Percentage Removal of COLOR Exposure Time UV

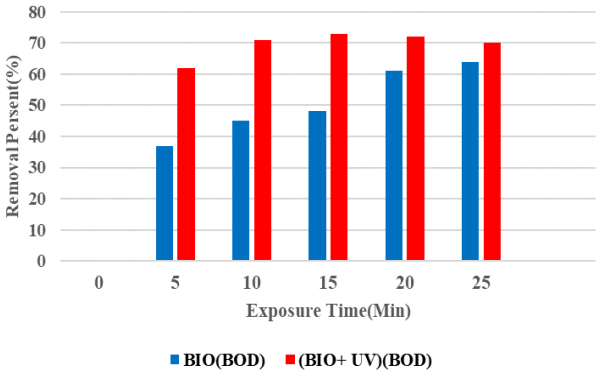

Figure 8. Removal of BOD versus UV Exposure Time

3.3. UV/H_2O_2

The utilization of the UV/H_2O_2 process for treating biotreated leachate yielded significant removal efficiencies for various pollutants. Specifically, the process achieved the following removal percentages:

- (COD): A remarkable 74% removal (as depicted in Figure 10).
- Color: An impressive 52% removal (as illustrated in Figure 11).
- (BOD): A substantial 71% removal (as shown in Figure 9).

The overall contaminant removal efficiency did not meet initial expectations, which may be attributed to the pH-dependent modulation of hydroxyl radical generation. This effect suggests that the production and availability of hydroxyl radicals, essential for effective UV-mediated decolorization, are influenced by solution pH. Enhancing decolorization performance may involve increasing the concentration of H_2O_2 or optimizing the operational parameters of the UV/H_2O_2 system to improve radical generation and sustainability of the oxidation process.

Interestingly, when applying this process to biotreated effluent leachate (from UASB+ Aerated Lagoon), the results diverged. After 20 minutes of exposure, color increased by 93% (see Figure 11) and after 25 minutes, an impressive 98% of color was removed (see Figure 11). However, the reduction in COD was

not linear over time. Initially, it rapidly decreased to 98% (within the first 20 minutes), but then it gradually declined to 95% (between 20 and 25 minutes, as shown in (Figure 10). This suggests that UASB-ARETED LAGOON-treated effluents may contain compounds that necessitate a more potent oxidizing system. Additionally, the BOD removal was 95% after 20 minutes (Figure 9) and decreased to 93% after 25 minutes (Figure 9). These findings underscore the necessity of tailoring AOP configurations to the unique characteristics of leachate, especially when dealing with effluents that may harbor complex, partially oxidized intermediates resistant to conventional treatment approaches. This nuanced approach to process design can significantly enhance the effectiveness of AOPs in handling variable effluent compositions.

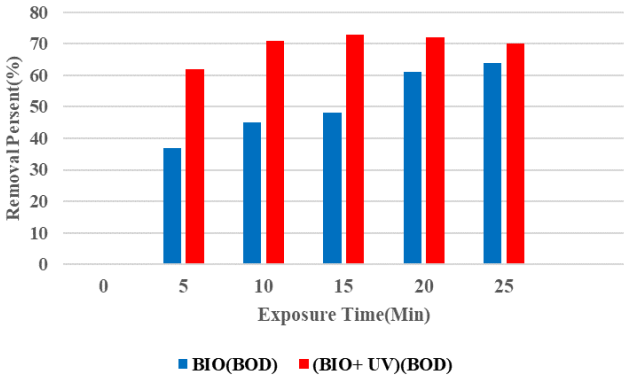

Figure 9. Removal of BOD versus UV/H_2O Exposure Time

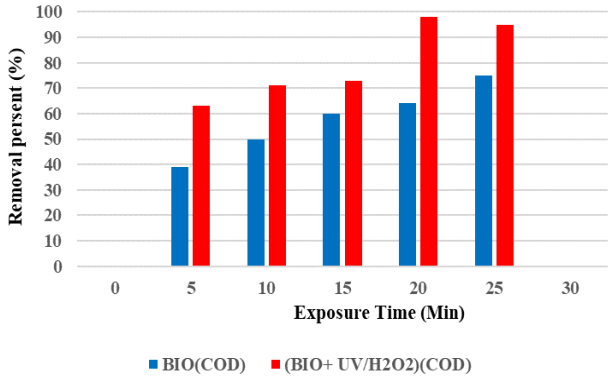

Figure 10. Removal of COD versus UV/H_2O_2 Exposure Time

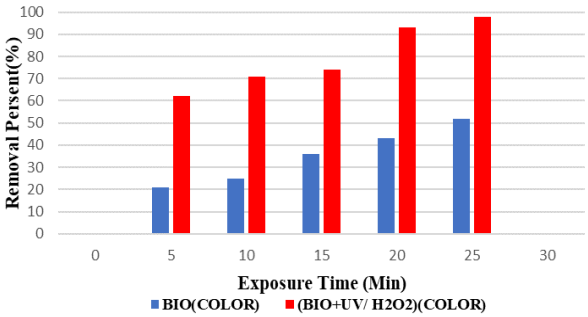

Figure 11. Removal of COLOR versus UV/H_2O_2 Exposure Time

3.4. Photo-Fenton Process

The Photo-Fenton process represents a significant advancement in oxidation technologies. In this process, various tests were conducted using a $FeSO_4$ concentration of 10 mg/L and a UV exposure time of 30 minutes. The results are:

Color Removal: In the treatment of biotreated leachate using the Photo-Fenton process, optimal color removal was observed after 25 minutes of UV irradiation. At this stage, color removal efficiency reached 49% (as shown in Figure 14), indicating a significant reduction in color intensity, which is a primary indicator of effective treatment.

(COD): The Photo-Fenton process also demonstrated high effectiveness in reducing COD levels. After 25 minutes of UV exposure, COD removal efficiency reached an impressive 63% (refer to Figure 13), underscoring the method's capability in breaking down organic compounds and reducing overall chemical pollution load.

(BOD): The treatment's impact on BOD levels was equally notable. Following 25minutes of exposure, the process achieved 77% BOD removal (see Figure 12). This substantial reduction in BOD reflects the process's ability to degrade biodegradable organic matter effectively.

However, an intriguing phenomenon was observed when the Photo-Fenton process was applied to effluent leachate pretreated with (UASB) and Aerated Lagoon systems. The UV spectrum between 200-300 nm was found to

primarily disrupt biological substances, signifying the selection of an appropriate wavelength range for optimal degradation. After 25 minutes of UV irradiation, the percentage removal rates for color, COD and BOD were recorded as follows:

COD: 82% (Figure 13), Color: 92% (Figure 14) Beyond this point, no removal efficiency was observed. These findings emphasize the Photo-Fenton process's potential for effective leachate treatment.

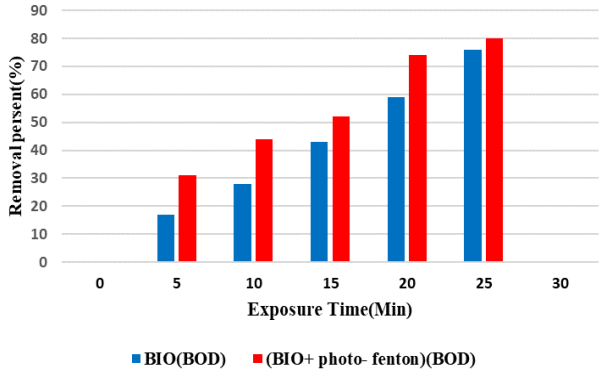

Figure 12. Removal of BOD versus Photo-Fenton Exposure Time

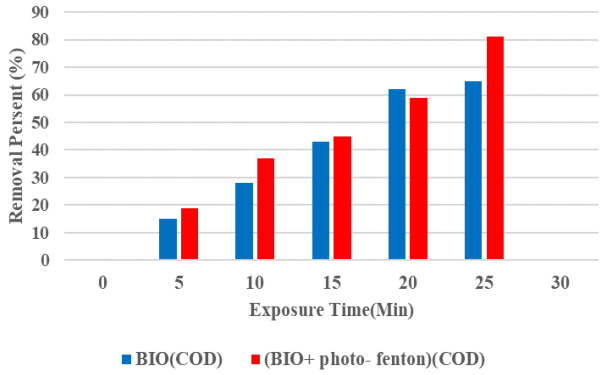

Fig. 13. Removal of COD versus Photo-Fenton Exposure Time

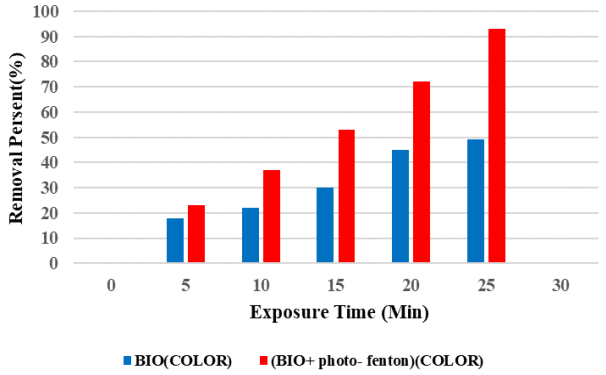

Figure 14. Removal of COLOR versus Photo-Fenton Exposure Time

4. Conclusion

The combined application of biotreated (UASB + Aerated lagoon) and advanced oxidation processes (AOPs) for treating leachate effluent offers significant advantages. This integrated approach allows for efficient decolorization, surpassing the effectiveness of using biotreated leachate alone.

Ozonation was particularly effective as a pretreatment for raw, untreated leachate, achieving substantial reductions-93% in color, 88% in BOD and 77% in COD.

UV irradiation alone showed limited effectiveness on untreated leachate due to its high color intensity, which impedes UV light penetration. However, when applied to biologically pretreated effluent, UV irradiation achieved notable improvements, including up to 82% color removal and substantial reductions in COD and BOD.

The UV/H_2O_2 process also yielded significant pollutant removal rates in biologically treated effluent, achieving up to 74% COD, 71% BOD and 52% color reduction. The Photo-Fenton process emerged as the most effective AOP, delivering the highest removal efficiencies across all parameters, especially for COD (82%) and color (92%). Its efficacy is attributed to the synergy between UV light and the Fenton reaction, which generates abundant hydroxyl radicals.

The combined application of biotreated (UASB + Aerated lagoon) and advanced oxidation processes (AOPs) for treating leachate effluent offers significant advantages. This integrated approach allows for efficient decolorization, surpassing the effectiveness of using biotreated leachate alone. Among the AOPs studied, UV/H_2O_2 demonstrated the highest decolorization efficiency, reaching up to 98%. Additionally, ozonation of initial leachate resulted in superior decolorization, COD removal and BOD removal compared to

other AOPs. Notably, photo-Fenton treatment achieved the highest percentage removal of BOD. The order of COD removal across AOPs was UV/H_2O_2 > UV > O_3 > photo-Fenton. While ozone proved effective as a strong oxidizing agent, particularly for COD and color removal in initial leachate, UV/H_2O_2's performance may have been impacted by the pH used (6.4). However, combining UV or H_2O_2 with ozone enhanced the decolorization rate. Overall, UV/HO_2 emerged as the most efficient AOP for both COD and color removal. Simultaneously applying UV and H_2O_2 to biotreated leachate holds promise for industrial implementation.

References

Agrawal L.K., Ohashi Y., Mochida E., Okui H., Ueki Y., Harada H., Ohashi A. (1997),"Treatment of raw sewage in a temperate climate using a UASB reactor and the Hanging Sponge Cubes processes", Water Science and Technology. 36, (6-7), 433.

Alzamora BR, Barros RTV. (2020)," Review of municipal waste management charging methods in different countries. Waste Manage.115:47-55.

Amoatey P, Izady A, Al-Maktoumi A, Chen M, Al-Harthy I, Al-Jabri K, et al. A critical review of environmental and public health impacts from the activities of evaporation ponds. Sci Total Environ.

Ankit ShL, Kumar V, Tiwari J, Sweta RS, et al., (2021),"Electronic waste and their leachates impact on human health and environment: Global ecological threat and management. Environ Technol Innovation.102049.

APHA, AWWA and WPCF. (1998)," Standard Methods for the Examination of Water and Wastewater Washington, DC", American Public Health Association.

Arsalan I., Balcioglu I., (2001),"Advanced oxidation of raw and bio-treated textile industry wastewater with O_3, H_2O_2/UV and their sequential application", J. Chem. Tech. Biotech. 76, 53.

Azbar, N., Yonar, T. and Kestioglu, K., (2004), "Comparison of Various Advanced Oxidation Processes and Chemical Treatment Methods for COD and Color Removal from a Polyester and Acetate Fiber Dyeing Effluent", Chemosphere, 55: 35-43.

Baawain MS, Al-Mamun A, Omidvarborna H, Al-Sabti A, Choudri B., (2020),"Public perceptions of reusing treated wastewater for urban and industrial applications: challenges and opportunities. Environ Dev Sustain.22:1859-71.

Balcioglu I.A., Arsalan I., (1999),"Treatment of textile industry wastewater by enhanced photocatalytic oxidation reaction", J. Adv. Oxid. Technol. 4, (2), 189.

Barbusinski K., Filipek K., (2000),"Aerobic Sludge Digestion in the Presence of Chemical Oxidizing Agents Part II. Fenton's Reagent", Polish Journal of Environmental Studies. 9, (3), 145.

Benitez E.J., Beltrn-Heredia J., Acero R.L., Gonnzalez T., (1996),"Degradation of protocatechuic acid by two advanced oxidation processes, ozone/UV radiation and H_2O_2/UV radiation",Water Res. 30, 1597.

Camel, V. and Bermond, A., (1998), "The Use of Ozone and Associated Oxidation Processes in Drinking Water Treatment", Water Research, 32, 3208-3222.

Cetrulo TB, Marques RC, Cetrulo NM, Pinto FS, Moreira RM, Mendiz´abal- Cort´es AD, et al., (2018), "Effectiveness of solid waste policies in developing countries: a case study in Brazil. J Cleaner Prod.205:179-87.

Chen J., Rulkens W.H., Bruning H., (1997),"Photochemical elimination of phenols and COD in industrial wastewaters", Water Science and Technology. 35, (4), 231.

Comninellis C., Kapalka A., Malatos., Parsons S., Poulios I., (2008),"Mantezavinos D. Advanced oxidation processes for water treatment:

advances and trends for R&D Journal of Chemical Tech & Biotech. 83, (6), 769.

Cortez, Teixeira P, Oliveira R, Mota M., (2011), "Evaluation of Fenton and ozone-based advanced oxidation processes as mature landfill leachate pre-treatments", Journal of Environ- mental Management, vol. 92, no. 3, pp. 749-755.

Cortez S., Teixeira P., Oliveira R., Mota M., (2011)," Mature landfill leachate treatment by denitrification and ozonation", Process Biochemistry, 46, 148-153.

Costa, A. M. Alfaia, R. G. D. S. M. & Campos, J. C., (2019)," Landfill leachate treatment in Brazil An overview", Journal of environmental management, 232, 110-116.

Crittenden J.C., Trussell R.R., Hand D.W., Howe K.J. and Tchobanoglous G., (2005)," Water treatment", Principles and Design, second ed., Wiley, New Jersey.

Dias M E., Law S.E., Frank J.S., (2000),"Control of pathogenic microorganisms and turbidity in poultry-processing chiller water using UV-enhanced ozonation", Ozone, Science and Engineering. 23, (6), 65.

El-Gohary F.A., Badawy M.I., El-Khateeb M.A. and El-Kalliny A.S., (2008)," Integrated treatment of olive mill wastewater (OMW) by the combination of Fenton's reaction and anaerobic treatment", J. Hazard. Mater. (In press, doi: 10.1016/j.hazmat.2008.06.098).

Fallah, N. and Johri, i. and Tusi Jamali, M. and follow, m., (2021), " Recycling of used catalysts of Klaus unit above natural gas plants and using them for the synthesis of poly pyrrole coated composite sides in order to remove lead from aqueous solution", Environmental Science and Technology, 322 (Reference 94), 99-109.

Fang H. H. P. I., Lau W. C. and Wang P., (2005), "Water Sci. Techno"l52 (10-11), 41.

Faridun, F., Javadi Sharif P., (2019)," the effect of Arak landfill leachate on the quality of groundwater in Amanabad Arak plain in terms of heavy metals", Scientific Research Journal of Natural Environment Hazards, 9th Volume, 26th Issue, Winter 2019.

Frontistis Z., Xekoukoulotakis N.P., Diamadopoulos E., Mantzavinos D., (2008)," Ozonation of Landfill Leachates: Treatment Optimization by Factorial Design", Journal of Advanced Oxidation Technology, 11, 370-376.

Glaze W.H., Kang J.W., Chapin D.H. (1987),"The chemistry of water treatment processes involving ozone, hydrogen peroxide and ultraviolet radiation", Ozone Science and Engineering. 9, (4), 335.

Gogate P.R. and Pandit A.B., (2004b)," A review of imperative technologies for wastewater treatment II: hybrid methods, Adv", Environ. Res., 8, 553-597.

Iravanian A, Ravari SO. (2020)," Types of contamination in landfills and effects on the environment: a review study. IOP Conf Ser Earth Environ Sci .614:012083.

Kurniawan T. A., Wai-hung L., (2009)," Removal of refractory compounds from stabilized landfill leachate using an integrated H_2O_2 oxidation and granular activated carbon (GAC) adsorption treatment",Water Research, 43, 4079 - 4091.

Kakai, K. and Riahi Bakhtiari, A., (2018), "Investigating the effect of Hamadan waste landfill on underground water and soil", Water and soil sciences (agricultural sciences and techniques and natural resources): 22(1) 2008-2018.

Kos L., Percowski J., (2003)," Decolorization of Real Textile Wastewater with Advanced oxidation processes", Fibres & Textiles in Eastern Europe. 11, (4), 43.

Malato S. Blanco J., Maldonado M.I., Oller I., Gernjak W. and Perz-Estrada L., (2007)," Coupling solar photo-Fenton and biotreatment at industrial scale: main results of a demonstration plant, J. Hazard. Mater", 146, 440-446.

Marco A., Esplugas S., Saum G., (1997), "How and why combine chemical and biological processes for wastewater treatment", Water Sci. Technol. 35, 321-327.

Marttinen SK, Kettunen RH, Sormunen KM, Soimasuo RM, Rintala JA., (2002)," Screening of physical-chemical methods for removal of organic material, nitrogen and toxicity from low strength landfill leachates", Chemosphere;46:851-8.

Mosteo R., Sarasa J., Ormad M.P. and Ovelleiro J.L., (2008)," Sequential solar photo-Fentonbiological system for the treatment of winery wastewater", J. Agric. Food Chem., 56, 7333-7338.

Neyens, Baeyens J., (2006),"A review of classic Fenton's peroxidation as an advanced oxidation technique", Journal of Hazardous Materials, vol. 98, no.1-3, pp.33-50.

Neyens E. and Baeyens J., (2003)," A review of classic Fenton's peroxidation as an advanced oxidation technique", J. Hazar. Mater., B98, 33-58.

Nika MC, Ntaiou K, Elytis K, Thomaidi VS, Gatidou G, Kalantzi OI, et al. (2020)," Wide-scope target analysis of emerging contaminants in landfill leachates and risk assessment using Risk Quotient methodology. J Hazard Mater. 394:122493.

Ozbay G, Jones M, Gadde M, Isah S, Attarwala T. (2021),"Design and operation of effective landfills with minimal effects on the environment and human health. J Environ Public Health. 6921607.

Parra S., Sarria V., Malato S., Péringer P., Pulgarin C., (2000),"Photochemical versus coupled photochemical-biological flow system for the treatment of two biorecalcitrant herbicides: metobromuron and isoproturon, Appl. Catal", B 27: 153-168.

Parvin F, Tareq SM. (2021)," Impact of landfill leachate contamination on surface and groundwater of Bangladesh: a systematic review and possible public health risks assessment. Appl Water Sci, 11:100.

Parvin F, Tareq SM. (2021)," Impact of landfill leachate contamination on surface and groundwater of Bangladesh: a systematic review and possible public health risks assessment. Appl Water Sci. 11:100.

Pedroza A.M., Mosqueda R., Alonso-Vante N., Rodríguez-Vázquez R. (2007), "Sequential treatment via Trametes versicolor and UV/TiO2/RuxSey to reduce contaminants in waste water resulting from the bleaching process during paper production", Chemosphere 67, 793-801.

Petruzzelli D., Boghetich G., Petrella M., Dell'Erba A., L'Abbate P., Sanarica S. and Miraglia M., (2007)," Pre-treatment of industrial landfill leachate by Fenton's oxidation", Global NEST Journal, 9, 51-56.

Primo, Rivero M J, Ortiz I, (2008),"Photo-Fenton process as an e cient alternative to the treatment of landfill leachates", Journal of Hazardous Materials, vol. 153, no. 1-2, pp. 834-842.

Propp VR, De Silva AO, Spencer C, Brown SJ, Catingan SD, Smith JE, et al. (2021)," Organic contaminants of emerging concern in leachate of historic municipal landfills. Environ Pollut. 276:116474.

Renou S, Givaudan JG, Poulain S, Dirassouyan F, Moulin P., (2008), "Landfill leachate treatment: review and opportunity", J Hazard Mater;150:468-93.

Rezaei R., Maleki A., Safari M., Qavami A., (2009), "Assessment of chemical contamination of underground water sources in the downstream areas of Sanandaj landfill", Scientific journal of Kurdistan University of Medical Sciences. 15 (3) 89-98.

Salem, Z., Hamouri, K., Djemaa, R., & Allia, K., (2019), "Evaluation of landfill leachate pollution and treatment", Desalination, 220(1-3), 108-114.

Sauve G, Van Acker K. The environmental impacts

of municipal solid waste landfills in Europe: a life cycle assessment of proper reference cases to support decision making. (2020)," J Environ Manage. 261:110216.

Sevimli M.F., Sarikaya H.Z., (2004)," Effect of some operational zparameters on the declorization of textile effluents and dye solutions by ozonation", Environmental Technology. 26, 135.

Shu, H. Y. and Chang, M. C., (2005)," Pre-Ozonation Coupled with UV/H_2O_2 Process for the Decolorization and Mineralization of Cotton Dyeing Effluent and Synthesized C.I. Direct Black 22 wastewater, J. of Hazardous Materials B121, 127-133.

Shu Y, Fan H J, Chang M C, Hsieh W P, (2006)," Treatment of MSW landfill leachate by a thin gap annular UV/ H_2O_2 photoreactor with multi-UV lamps", Journal of Hazardous Materials, vol. 129, no. 1-3, pp. 73-79.

Shu, J., Chen, M., Wu, H., Li, B., Wang, B., Li, B., ... & Liu, Z., (2019)," An innovative method for synergistic stabilization/solidification of Mn+, NH+-N, POST- and F- in electrolytic manganese residue and ghesehegypsum", Journal of hazardous materials, 376, 212-222.

Siddiqi SA, Al-Mamun A, Baawain MS, Sana A. (2021)," Groundwater contamination in the Gulf Cooperation Council (GCC) countries: a review. Environ Sci Pollut Res. 1-22.

Tandukar M., Ohashib A., Harada. H., (2007),"Performance comparison of a pilot-scale UASB and DHS system and activated sludge process for the treatment of municipal wastewater", Water Res. 41, 2697.

Tchobanglous, G. and Burton, F., (2019)," Wastewater Engineering Treatment, disposal and reuse", 4th Ed., McGraw-Hill, Metcalf and Eddy Inc., New York.

Teng C, Zhou K, Peng C, Chen W. (2021)," Characterization and treatment of landfill leachate: a review. Water Res. 203:117525.

Tikhe A, Gidde M R, "Decolourization of Nigrosine WS (AB2), (2014),"Dye by Solar Photo-Fenton Process", the international journal of science and technology, 2(5), 2014, 68-73.

Tizaoui C., Bouselmi L., Mansouri L., Ghrabi A., (2007),"Landfill leachate treatment with ozone and 316- ozone/hydrogen peroxide systems" Journal of Hazardous Materials, 140,324.

Torres R., Sarria V., Peringer P., Pulgarin C., (2003),"Electrochemical treatment of industrial wastewater containing 5-amino-6-methyl-2 benzimidazole: toward an electrochemical-biological coupling, Water Res. 37: 3118-3.

V. Sarria, S. Parra, N. Adler, P. Péringer, C. Pulgarin, (2002)," Recent developments in the coupling of photo assisted and aerobic biological processes for the treatment of biorecalcitrant compounds, Catal", Today 76: 301-315.

Wu J., Wang T., (2001)," Ozonation of aqueous azo dye in a semi batch reactor", Water Res. 34, 1093.

Yasar A., Ahmad N., Khan A. A. A., (2006),"Energy requirement of ultraviolet and AOPs for the post treatment of treated combined industrial effluent", Color Tech. 122, 201.

Yatsunthea T, Chaiyat N. A very small power plant - Municipal waste of the organic Rankine cycle and incinerator from medical and municipal wastes. Therm Sci Eng Progress 2020; 18:100555.

Yasar A., Ahamd N., Rehman M. S., Khan A. A. A., (2007b),"Ozone for color and COD removal of raw and anaerobically bio-treated combined industrial wastewater", Polish Journal of Environmental Studies. 16, (2), 289.

Yasar A., Ahmad N., Khan A. A. A.,Yousaf A., (2007b)," Decolourisation of Blue CL-BR dye by AOPs using bleach wastewater as source of H_2O_2", Journal of Environmental Sciences China. 19, 1183.

Zhou H., Smith D.W., (2002),"Advanced technologies in water and wastewater treatment", J. Environ. Eng. Sci. 1, (4).

JOURNAL OF GAS TECHNOLOGY

Volume 9 /Issue 1 / Summer 2024 / Pages 50-66

Journal Home page: http://jgt.irangi.org

Numerical Simulation of Natural Gas Pipeline in Dense and Hybrid Phases

Moslem Abrofarakh[1], Mortaza Zivdar[2*], Davod Mohebbi-Kalhori[3]

1. Ph.D. Student, Department of Chemical Engineering, Faculty of Engineering, University of Sistan and Baluchestan, Zahedan, Iran
2. Professor, Department of Chemical Engineering, Faculty of Engineering, University of Sistan and Baluchestan, Zahedan, Iran
3. Associate Professor, Department of Chemical Engineering, Faculty of Engineering, University of Sistan and Baluchestan, Zahedan, Iran

ARTICLE INFO

ORIGINAL RESEARCH ARTICLE

Article History:
Received: 04 July 2023
Revised: 07 August 2023
Accepted: 20 August 2023

Keywords:
Dense phase
Hybrid mode
Pipeline
Natural gas

DOR: 20.1001.1/jgt.2024.2040645.1047

ABSTRACT

Transmission of natural gas via pipelines is predominantly employed due to its cost-effectiveness compared to other methods. Transportation of natural gas through pipelines faces several challenges, such as high energy consumption, significant pressure drops, and two-phase flow problems. In this study, the transmission of natural gas in dense, hybrid (regions of dense phase and near-dense phase), and vapor phases was investigated to address some of these limitations. Additionally, mathematical models of quadratic forms for the pressure drop in the dense phase and hybrid modes, in terms of the diameter, mass flow, and length of the pipeline, were proposed. According to the models, the pipeline diameter had a more significant effect on the pressure drop than the flow rate and pipeline length. Moreover, the results showed that the energy consumption of the heat exchanger for the hybrid mode was 35% less than the dense phase. On average, the densities in dense phase and hybrid modes were 2.5 times higher than the two-phase flow. The pressure drop and velocity in the dense phase and hybrid modes were 2.2 times less than the two-phase conditions. In the dense phase and hybrid modes, the capacity of the pipeline for natural gas transmission increased by 52% compared with two-phase gas transmission.

How to cite this article
M. Abrofarakh, M. Zivdar, D. Mohebbi-Kalhori, Numerical Simulation of Natural Gas Pipeline in Dense and Hybrid Phases. Journal of Gas Technology. 2024; 9(1): 50 -66. (https://jgt.irangi.org/article_718891.html)

* Corresponding author.
E-mail address: mzivdar@eng.usb.ac.ir, (M. Zivdar).

Available online 10 September 2024

1. Introduction

Natural gas is one of the most important sources of energy in the world. Natural gas is a hydrocarbon fuel that forms below the earth's surface (Chen et al., 2021; Dorao and Fernandino, 2011; Faramawy et al., 2016). Following the extraction and refining of natural gas, its transmission becomes the most critical phase. Several methods are used for transmitting natural gas, such as, liquefied natural gas, pipeline transport, converting gas to solid, gas to electricity, and gas to liquid (Thomas and Dawe, 2003). The optimal method depended on the volume and distance required for natural gas transmission. (Figure 1) illustrates the relationship between distance and the suitable volume for transmission using each method (Mokhatab et al., 2018). For example, if the distance is less than 2000 km, the pipeline method is acceptable. The most common method of transporting natural gas is the pipeline.

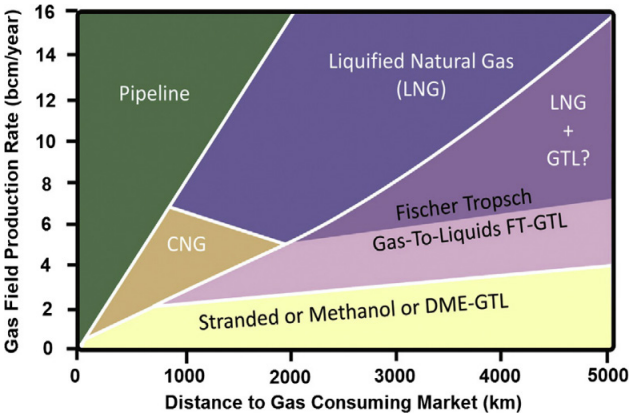

Figure 1. Gas Transmission Methods (Mokhatab et al., 2018)

Natural gas pipeline systems are crucial for advancing and transmitting natural gas due to their cost-effectiveness and reliability (Lanzano et al., 2013; Wei et al., 2023). The cost-effectiveness of natural gas transmission through pipelines has spurred substantial scholarly research in this field. Academic studies have focused extensively on improving pipeline performance, particularly concerning operational pressure and diameter characteristics in natural gas transmission pipelines.

Gregori et al. (Gregory et al., 1979) conducted mathematical modeling and simulation of a 12-inch diameter pipeline using ethane. Their study considered variations in physical properties, employing one-dimensional energy and mass balance equations. Results emphasized significant impacts of physical property changes on temperature and pressure profiles. Moore et al. (Moore et al., 1980) explored high-pressure pipeline design and modeling, focusing on natural gas hydrodynamics. They utilized energy and flow equations for modeling and employed the Benedict-Webb-Rubin (BWR) equation to calculate gas properties. Their study involved analyzing eleven natural gas samples and comparing model predictions with actual pipeline data, showing consistent alignment. Prittit and Toth (Peretti and Toth, 1982) optimized natural gas transmission pipelines by identifying ideal compressor combinations and outlet pressures from compressor stations for optimized fuel gas delivery. Shariati et al. (Shariati et al., 1999) investigated a two-phase natural gas transmission pipeline to assess the effect of different hexane plus percentages. Their focus was on understanding liquid content variations with decreasing temperatures along the pipeline, finding increased liquid content as temperature drops. Gato et al. (Gato and Henriques, 2005) explored dynamic behavior of high-pressure natural gas flow through mathematical modeling. Zhang et al. (2006) conducted an investigation into gas transmission within pipelines, with a focus on analyzing pressure drop under adiabatic and isothermal conditions. Their findings indicated that the variations in pressure drop between the two conditions were negligible. Tend et al. (Teng et al., 2016) investigated gas transmission and analyzed pressure drop under isothermal and adiabatic conditions, finding density

decreases along the pipeline and negligible pressure drop variations. Mokhatab (Mokhatab, 2007) developed an analytical method using momentum and continuity equations to calculate temperature and pressure in natural gas pipelines containing hydrogen sulfide gas, showing close agreement with literature data. Chaczykowski et al. (2012) conducted numerical simulations of fast and slow fluid transients in pipelines to evaluate velocity, pressure, and temperature profiles. Witkowski et al. (Witkowski et al., 2018) simulated natural gas pipelines incorporating hydrogen, focusing on safety concerns. Abd et al. (2020) explored the influence of impurities on the properties of natural gas. Their analysis revealed that these impurities significantly affect pressure drop, and physical properties. Cristello et al. (2023) analyzed the influence of hydrogen on natural gas pipelines, highlighting its effects on pressure and velocity.

Recently, the transmission of natural gas in dense phase has been investigated. Transmission of natural gas in dense phase leads to a decrease in pressure drop in the pipeline. To transfer natural gas in the dense phase state, the natural gas pressure must be greater than the cricondenbar, and its temperature should be between the critical temperature and the cricondentherm (Zivdar, 2021).

Researches on the transmission of natural gas through pipelines in the dense phase are limited. However, we have made an effort to review the most relevant studies on dense-phase pipeline modes. Botros (Botros, 2002) investigated an experimental work to determine the thermodynamic equation of state in the dense phase mode. The results showed that the Peng-Robinson equation of state was in good agreement with the experimental data. Vera et al. (Vargas-Vera et al., 2020) simulated an undersea pipeline in the dense phase mode and compared results with the two-phase mode. Results showed that in the dense phase mode the pressure drop was about 100% less than the Two-phase case. Zivdar and Abrofarakh (Zivdar, 2021) simulated a gas pipeline in the dense phase mode and compared results with a vapor phase. They showed that when natural gas was transported in the dense phase, the number of the compressor stations were reduced. Also, they showed that the cooling duty of dense phase was 563 MW. Almora et al. (Almara et al., 2023) examined the physical properties of natural gas in supercritical conditions. Their study indicated that the density behavior in supercritical phase resembles that of liquids, while its viscosity is similar to gases. Parsad et al. (Prasad et al., 2023) investigated the transportation of natural gas in supercritical conditions through mathematical modeling. Their findings showed that natural gas at a flow rate of 800 kilograms per second can be transported up to 4801 kilometers without compression.

Although the transmission of natural gas in dense phase mode has advantages, however, due to the low cricondentherm temperature of natural gas, this method requires extensive cooling of natural gas. Additionally, a comprehensive study and development of mathematical models are crucial to improve the understanding of pipelines in this phase. According to our review and to the best of our knowledge, there have been no studies investigating natural gas in combined dense and hybrid phases, along with the development of mathematical modeling for these phases. Therefore, this study proposes the transmission of natural gas in a hybrid phase (combining dense phase and near dense phase) to decrease the required cooling energy. Additionally, the results of the hybrid mode were compared with those of the dense phase and two-phase flow. Finally, quadratic models for the pressure drop in dense phase and hybrid modes were developed, considering pipeline diameter, mass flow, and length.

Table1. Mole Fraction of Components, Masjed Soleyman to Mahshahr Gas Pipeline (Mokhatab, 2007)

Components	Mole fraction (%)
H_2S	25.6
N_2	0.2
CO_2	9.9
C_1	62.9
C_2	0.7
C_3	0.2
iC_4	0.06
nC_4	0.09
iC_5	0.04
nC_5	0.05
C_7	0.26

2. Mathematical Modeling

2.1. Physical Model

The pipeline information of the Masjed Soleyman is shown in (Table 2). At two-phase (normal mode), the inlet pressure and temperature of the pipeline are 80.29 bar and 35 degrees Celsius, respectively. To transmit the natural gas of Masjed Soleyman in the dense phase, its pressure must be higher than 112 bar and its temperature between -27 to 19 degrees Celsius. Also, to transmit the natural gas in the hybrid mode, its pressure must be higher than 110 bar and its temperature between 17 to 35 degrees Celsius. (Table 3) shows specifications of inlet pipelines for the three cases.

Table 2. Pipeline specifications, Masjed Soleyman pipeline (Mokhatab, 2007)

Specification	Value
Length (km)	168
Diameter (cm)	48.26
Wall thickness (mm)	14
Mass flow (kg/s)	59.12
Inlet Pressure (bar)	80.29
Inlet Temperature (˚C)	35
Ambient temperature(˚C)	15
Permissible outlet pressure (bar)	55

Table 3. Specifications of Inlet Conditions for the Three Cases

State	Temperature (˚C)	Pressure (bar)
Two- phase flow	35	80.29
Dense phase	19	122
Hybrid	35	122

For simulating the pipeline, the system is modeled as steady-state, compressible, and one-dimensional. The steady-state assumption implies that the properties of the system, such as pressure, temperature, and velocity, do not change with time. The compressible flow of natural gas was considered because the density and volume of the gas can change with variations in pressure and temperature. Additionally, frictional losses within the pipeline were determined using the Darcy friction factor, which represents the flow resistance resulting from the interaction between the gas and the pipeline's internal surface. Physical properties such as density, viscosity, heat capacity, and thermal conductivity vary with temperature and pressure. Therefore, an equation of state for high-pressure natural gas mixtures is also required to describe the relationship between natural gas density, pressure, and temperature, and to calculate other thermodynamic properties accurately. In this study, the equation of state was employed to calculate thermophysical properties due to the presence of a hydrocarbon system and high-pressure conditions (Saffari and Zahedi, 2013).

Thermo-hydrodynamics modeling of natural gas requires equations of continuity, momentum, and energy. These equations are as follows (Helgaker and Ytrehus, 2012):

$$\nabla.(\rho u) = 0 \text{ (continuity)} \quad (1)$$

$$0 = -\nabla p - f_D \frac{\rho}{2D} u|u| = 0 \textbf{ (momentum)} \quad (2)$$

$$\rho A C_P u.\nabla T = \nabla.(Ak\nabla T) + f_D \frac{\rho A}{2D}|u|^3 + Q_W \textbf{ (energy)} \quad (3)$$

$$\rho = f(T,p) \quad (4)$$

Where A, ρ, u, p, f_D, D, C_P, T, k and Q_W are area, density, velocity, pressure, Darcy friction factor, diameter, heat capacity, temperature, thermal conductivity and heat exchange with the surroundings through the pipeline, respectively. The first and second terms on the right-hand side in Eq. (2) represents the gradian pressure and viscous pressure drop. both for turbulent and laminar flow regimes (Darcy friction factor), respectively. The term on the left side of Eq. (3) (energy) represents convection heat transfer. The first, second and third terms on the right side of Eq. (3) represent the conduction heat transfer, friction heat dissipation due to viscous and external heat exchange through the pipeline wall, respectively.

The expression of the Darcy friction factor in Eq. (2) is shown as follows (Haaland, 1983):

$$\frac{1}{\sqrt{f_D}} = -1.8\log_{10}\left(\frac{\frac{e}{D}}{3.7}\right)^{1.11} + \frac{69}{Re} \tag{5}$$

Where e and Re are pipe wall roughness and Reynolds number, respectively. The expression of the Reynolds number in Eq. (5) is shown as follows:

$$Re = \frac{\rho u D}{\mu} \tag{6}$$

The expression of Q_W in Eq. (3) is shown as follows (Haaland, 1983):

$$\mathrm{Q_W} = \mathrm{hZ(T_{env} - T)} \tag{7}$$

In this study, we consider a buried and insulated pipeline. The overall heat transfer coefficient includes contributions from internal film resistance, wall resistance and external film resistance (Figure.2), Eq. (8).

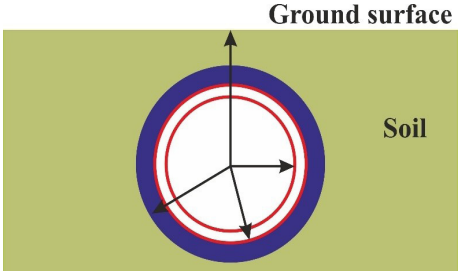

Figure 2. Cross-section of the Pipeline

$$hZ = \frac{1}{\frac{1}{r_i h_i} + \frac{\ln\left(\frac{r_o}{r_i}\right)}{2\pi k_{wall}} + \frac{\ln\left(\frac{r_{ins}}{r_o}\right)}{2\pi k_{ins}} + \frac{\ln\left(\frac{r_{soil}}{r_{ins}}\right)}{2\pi k_{soil}} + \frac{1}{r_{soil} h_o}} \tag{8}$$

Where r_i, r_o, r_{ins}, r_{soil}, k_{wall}, k_{ins}, k_{soil}, h_i, h_o are the inner radius, outer radius, insulation radius, soil radius, thermal conductivity of the pipeline, thermal conductivity of the insulation, thermal conductivity of the soil, internal heat transfer coefficient and external heat transfer coefficient respectively. Nusselt number inside of the pipeline is as follows (Haaland, 1983):

$$Nu_i = \frac{h_i D}{k} \tag{9}$$

$$Nu_i = \frac{\frac{f_D}{8}(Re - 1000)Pr}{1 + 12.7\sqrt{\frac{f_D}{8}}\left(Pr^{\frac{2}{3}} - 1\right)} \tag{10}$$

The expression for Pr in Eq. (9) is shown as follows.

$$Pr = \frac{C_P \mu}{k} \tag{11}$$

Nusselt number outside the pipeline is as follows:

$$Nu_o = 0.3 + \frac{0.62\sqrt{Re_{air} Pr_{air}^{\frac{1}{3}}}\left(1 + \left(\frac{Re_{air}}{282000}\right)^{\frac{5}{8}}\right)^{\frac{4}{5}}}{\left(1 + \left(\frac{0.4}{Pr_{air}}\right)^{\frac{2}{3}}\right)^{\frac{1}{4}}} \tag{12}$$

2.2. Physical Properties

Since the variations of the temperature and pressure in the pipeline are significant, the physical properties change along the pipeline. Duo to high pressure system, the behavior of natural gas is real gas. The density and heat capacity are calculated from Peng-Robinson equation. Botros (2002) showed that the Peng-Robinson equation is suitable for dense-phase natural gas; therefore, this study used this equation for density calculation. Also, Brokaw equations and kinetic theory were used to calculate viscosity and thermal conductivity of natural gas, respectively. Brokaw (1965) established the suitability of the

Brokaw equation for natural gas; therefore, this equation was used in this study for viscosity calculation. The density in Equations (1) to (3) is not constant. Therefore, Equations (1) to (4) are coupled. For example, the mixture density from Peng- Robinsons is as follow (Haaland, 1983):

$$Z^3_{mix} + MZ^2_{mix} + NZ_{mix} + r = 0 \quad (13)$$

$$M = B_{mix} - 1 \quad (14)$$

$$N = A_{mix} - 2B_{mix} - 3B^2_{mix} \quad (15)$$

$$r = B^3_{mix} + B^2_{mix} - A_{mix}B_{mix} \quad (16)$$

$$A_{mix} = \sum_{i=1}^{k}\sum_{j=1}^{k} x_i x_j A_{ij} \quad (17)$$

$$B_{mix} = \sum_{i=1}^{k} x_i B_i \quad (18)$$

$$A_{ii} = 0.45724 \left(\frac{\left(\frac{p}{p_c}\right)}{\left(\frac{T}{T_C}\right)^2} \right)_i \alpha_i \quad (19)$$

$$A_{ij} = (1 - K_{ij})\sqrt{A_{ii}A_{jj}} \quad (20)$$

$$\rho = \frac{pM_W}{RTZ_{mix}} \quad (21)$$

Where, Z_{mix} is compressibility factor of the gas mixture; k is the number of components; x is mole fraction; p is pressure; T is temperature; p_c is critical pressure; T_C is critical temperature. K is interaction parameter.

2.3. Boundary Conditions

Equations (1), (2) and (3) require boundary conditions for velocity (mass flow), pressure, and temperature. The boundary conditions in this study are as follows:

$$u|_{z=L} = u_{out} \quad (22)$$

$$u_{out} = \frac{m}{\rho A} \quad (23)$$

$$p|_{z=0} = p_{in} \quad (24)$$

$$T|_{z=0} = T_{in} \quad (25)$$

$$\nabla . q|_{z=L} = 0 \quad (26)$$

Where u_{out}, m, p_{in}, T_{in} and q are outlet velocity, mass flow rate, inlet pressure, inlet temperature and heat flux, respectively. For the inlet of the pipeline, the inlet pressure and temperature for each phase were considered. Additionally, for the outlet of the pipeline, the velocity was used. The reason for this choice is that the mass flow rate is constant due to the conservation of mass, and the velocity depends on the mass flow rate. Moreover, Eq.(26) is typically used for the outlet boundary of the energy equation because the temperature variation between the outlet node and its adjacent node is insignificant.

COMSOL Multiphysics version 6 was used to solve the continuity, momentum and energy equations. COMSOL Multiphysics solves a finite element discretization of the continuity, momentum and energy equations. Also, the Peng- Robinson equation of state was used to calculate the physical properties of the natural gas, simultaneously.

3. Results and Discussion

3.1. Simulation of the Pipeline

(Figure 3) illustrates the dense and hybrid regions within the phase envelope based on the Majed Soliman natural gas composition (Table 3). In this Figure, the pressure of the dense phase region was at least 112 bar and the temperature should be between -27 and 19 °C. Also, in this Figure, hybrid phase is also shown. The pressure of the hybrid phase was at least 100 bar and the temperature should be between 19 and 35°C. The phase envelope in (Figure 3) is plotted using Aspen Plus and the Peng-Robinson equation. (Figure 4) shows the process flow diagram of two- phase flow, dense phase and hybrid. In two-phase mode, the natural gas enters the pipeline at a given temperature and pressure, then the exited natural gas enters the separator and the liquid separate from the gas phase, then the natural gas flows into the compressor and the pressure reaches 80.29

bar. Finally, the natural gas enters the heat exchanger and its temperature reduced to 35 degrees Celsius. In the dense phase state, the compressor first increases the pressure to 122 bar and then the heat exchanger reduces the natural gas temperature to 19 ℃. In this state, the natural gas enters the dense phase region. In the hybrid mode, the compressor increases the pressure to 122 bar and then the heat exchanger reduces the natural gas temperature to 35 ℃. In this mode, the natural gas enters the hybrid region. The difference between dense phase and hybrid mode is the inlet temperature of the pipeline. The temperature of hybrid mode is higher than the dense phase mode. In this research, Aspen plus V12.1 and Peng-Robinson equation of state were used to calculate the duty of the heat exchangers and the compressors duties. Equations of continuity, momentum and energy were solved simultaneously using COMSOL Multiphysics and Peng-Robinson equation of state to determine pressure, velocity, physical properties and temperature of the pipeline.

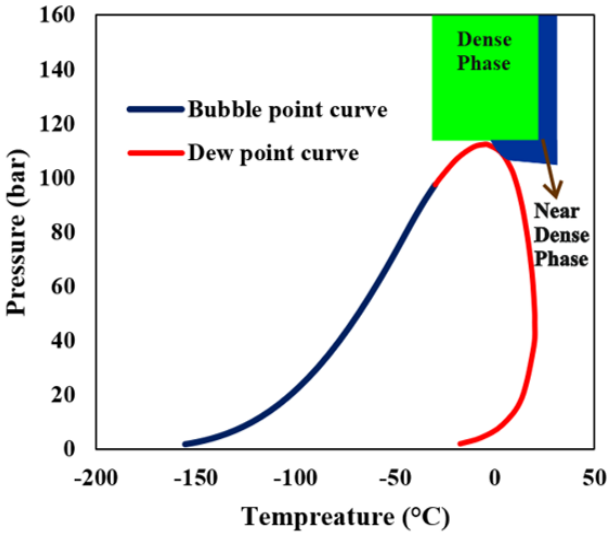

Figure 3. Masjed Soleyman Natural Gas Phase Envelope, Dense Phase Region, and Near Dense Phase Region

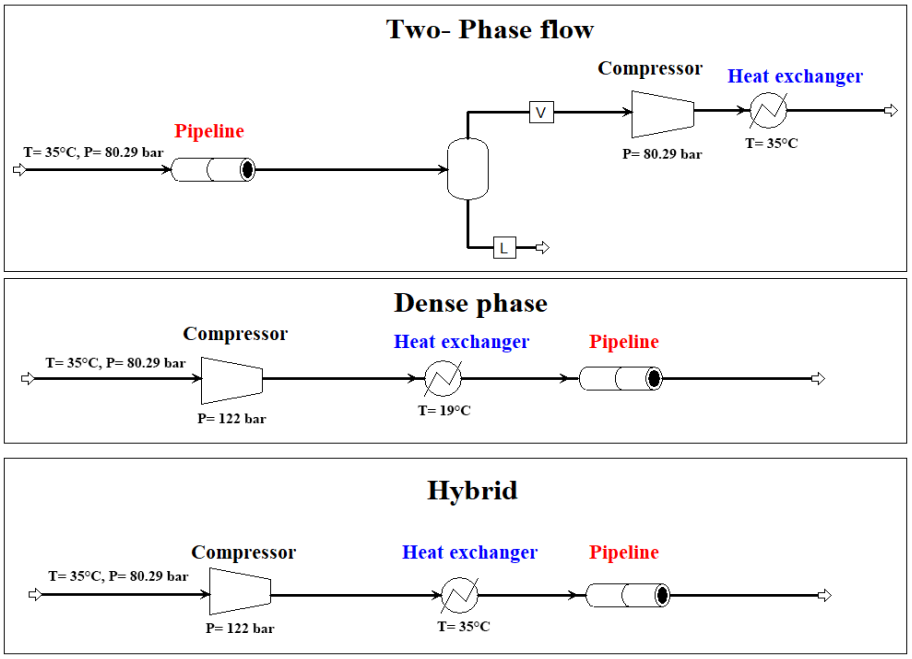

Figure 4. Process Flow Diagram of two- Phase Flow, Dense Phase and Hybrid Mode

(Table 4) shows the required compression power and the duty of the heat exchangers for both dense phase and hybrid mode. Due to the fact that the inlet temperature and pressure of the compressors are the same in both modes, the power of the compressors are also the same. Due to the fact that the inlet temperature of the pipeline for hybrid mode is higher than dense phase, the duty of hybrid mode is 35 % less than dense phase.

Table 4. Power of the Compressors and Duty of the Heat Exchangers

Mode	Power of compressor (MW)	Duty of heat exchanger (MW)
Dense phase	2.87	-9.71
Hybrid	2.87	-6.37

3.2. Density Effect

It is necessary to understand the density variations in the pipelines since it is related to volumetric flow and velocity. As density increases, the volumetric flow rate corresponding to a specific mass flow rate decrease, resulting in a reduction in fluid velocity. In this state, if the viscosity of the fluid is almost unchanged, according to the continuity and momentum equations, as the velocity reduced, the pressure drop is also reduced. (Figure 5) shows the density profiles along the pipeline. On average, the density in dense phase and hybrid modes is 2.5 times higher than the two-phase flow. The density profiles in the dense phase and hybrid modes are similar to liquids. The changes in density for the dense phase, hybrid mode, and two-phase mode are 8.7%, 11.1%, and 25%, respectively. Small variation of density in the pipeline causes small variation in volumetric flow, velocity, and pressure drop. Moreover, the variation in density in the hybrid mode differs from that in the dense phase and two-phase flow. This difference is attributed to the distinct temperature and pressure conditions in this phase. Compared to the dense phase, the variation in density in the hybrid mode is influenced by higher temperatures, while the variation in the hybrid mode differs from the two-phase flow due to higher pressure. Consequently, the higher temperature difference between the natural gas flow and the surrounding environment in the initial section of the pipeline leads to an increase in density (the temperature of the natural gas decreases with increasing pipeline length). After 100 kilometers, the density decreases due to the pressure drop, and the effect of temperature variation becomes less significant as the temperature difference between the natural gas and the environment decreases.

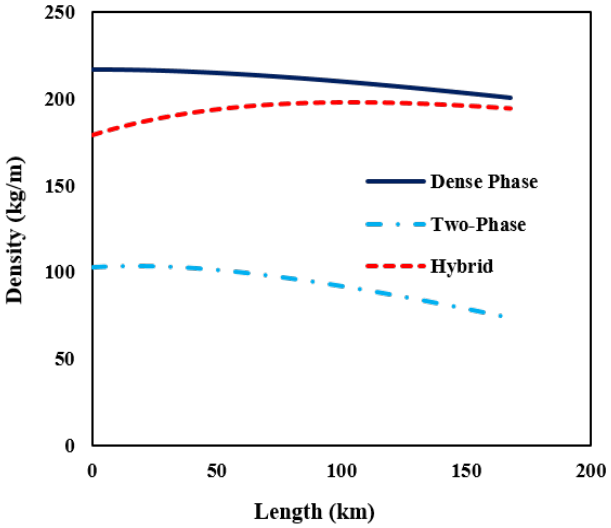

Figure 5. Density Profiles in Dense, Hybrid, and Two-phase Flow Modes

3.3. Viscosity Effect

(Figure 6) presents the viscosity profiles for the dense phase, hybrid, and two-phase flow modes. The viscosity variations in all three states are similar to gases. Moreover, the viscosities of the three phases are nearly identical, indicating that the frictional effects associated with viscosity are consistent across these phases. While the dense phase and hybrid state exhibit densities comparable to liquids and significantly higher than vapor, their viscosities remain similar to gases. Consequently, viscosity has a negligible impact on the comparative results, while density differences play a more critical role in influencing flow behavior.

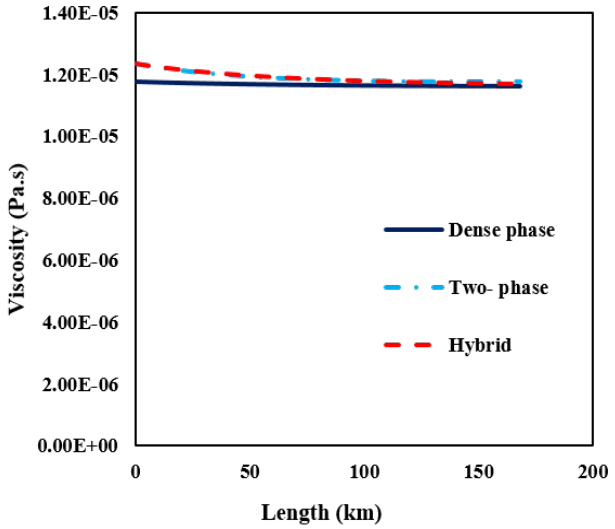

Figure 6. Viscosity Profiles in Dense Phase, Hybrid, and Two-phase Flow Modes

3.4. Pressure Drop

(Figure 7) shows the pressure-drop profiles of the pipeline for dense phase, hybrid, and two-phase flow modes. In the dense phase and hybrid modes, the pressure drop is lower compared to the two-phase mode, primarily due to differences in density. The higher density in the hybrid and dense phases, compared to the two-phase flow, is attributed to the higher pressure in these phases. Since the mass flow rate remains constant for all three phases, a higher density results in a lower volumetric flow rate and consequently a lower velocity of natural gas. Since the pressure drop is directly related to flow rate and frictional resistance within the pipeline, the decrease in velocity leads to a lower pressure drop in both the dense and hybrid phases. The lower velocity in the dense and hybrid modes results in reduced turbulence and friction compared with the two-phase flow.

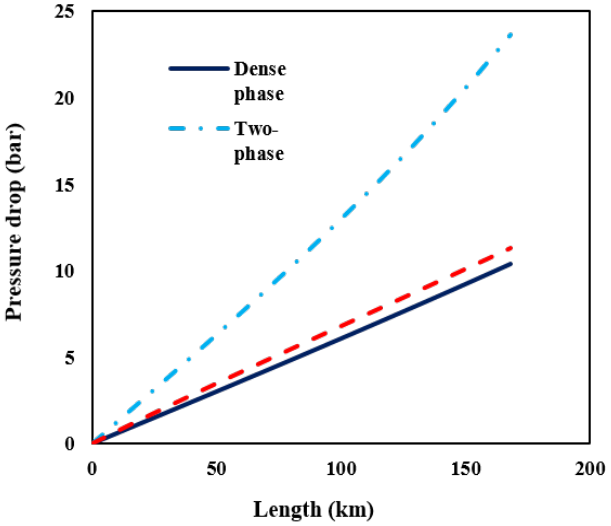

Figure 7. Pressure-drop Profiles in Dense, Two-phase, and Hybrid Modes

3.5. Effect of Phase

(Figure 8) illustrates the temperature and pressure profiles of the pipeline for dense phase, hybrid, and two-phase flow modes on the phase envelope. Additionally, the inlet and outlet conditions of the pipeline are depicted. As shown, the profile for the two-phase case enters the two-phase region, resulting in two-phase flow. This occurrence leads to issues such as high-pressure drop and potential damage to the pipeline. In contrast, the dense phase and hybrid profiles indicate only single-phase flow, thereby eliminating the problems associated with two-phase flow.

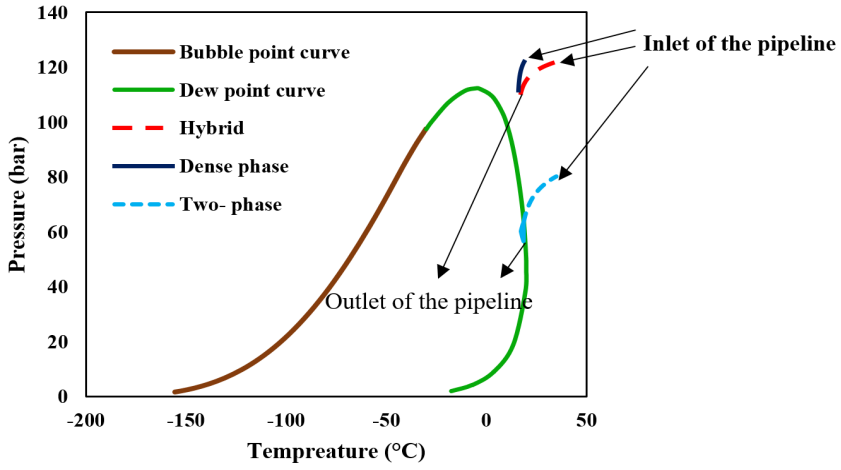

Figure 8. . Pressure and Temperature Profiles in Dense Phase, Hybrid, and Two- phase Flow Modes

3.6. Velocity

(Figure 9) shows the natural gas velocity profile in the pipeline for dense phase, hybrid, and two-phase flow modes. On average, the gas velocities in the dense phase and hybrid modes are 2.2 times smaller than the two-phase flow. Since the velocities in the dense phase and hybrid modes are lower than the two-phase flow, the possibility of pipeline erosion and associated problems is eliminated.

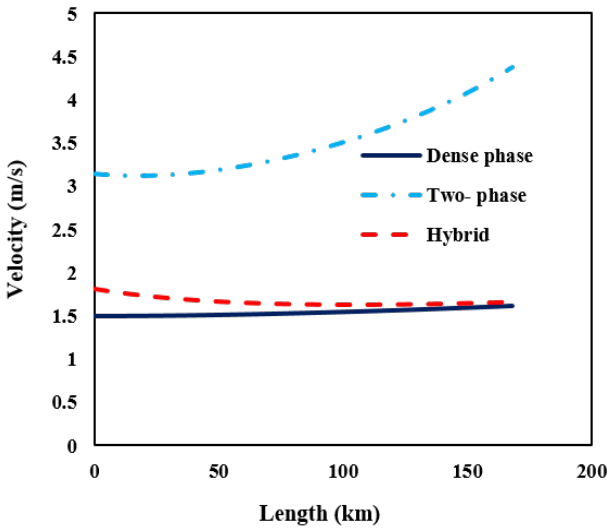

Figure 9. Velocity Profiles in Dense Phase, Two-phase and Hybrid Modes

3.7. Heat Transfer

(Figure 10A) shows the temperature profiles in the pipeline for dense phase, hybrid, and two-phase flow modes. The temperature variations are smaller in the dense phase because the difference between its inlet temperature and the environmental temperature is smaller. Additionally, the temperature profiles for the hybrid mode and two-phase flow are almost identical because the inlet temperatures for these phases are similar. Moreover, the temperature variation for all three phases decreases as the pipeline length increases because the temperature difference between the natural gas flow and the environment diminishes.

(Figure 10B) shows the heat loss profiles in the pipeline for dense phase, hybrid, and two-phase flow modes. The heat loss in the dense phase is lower than in the hybrid mode and two-phase flow because the temperature difference between the natural gas flow and the environment in this phase is smaller than in the other two modes. The maximum heat loss in the dense phase, hybrid, and two-phase modes are 12, 60, and 59.9 W/m, respectively.

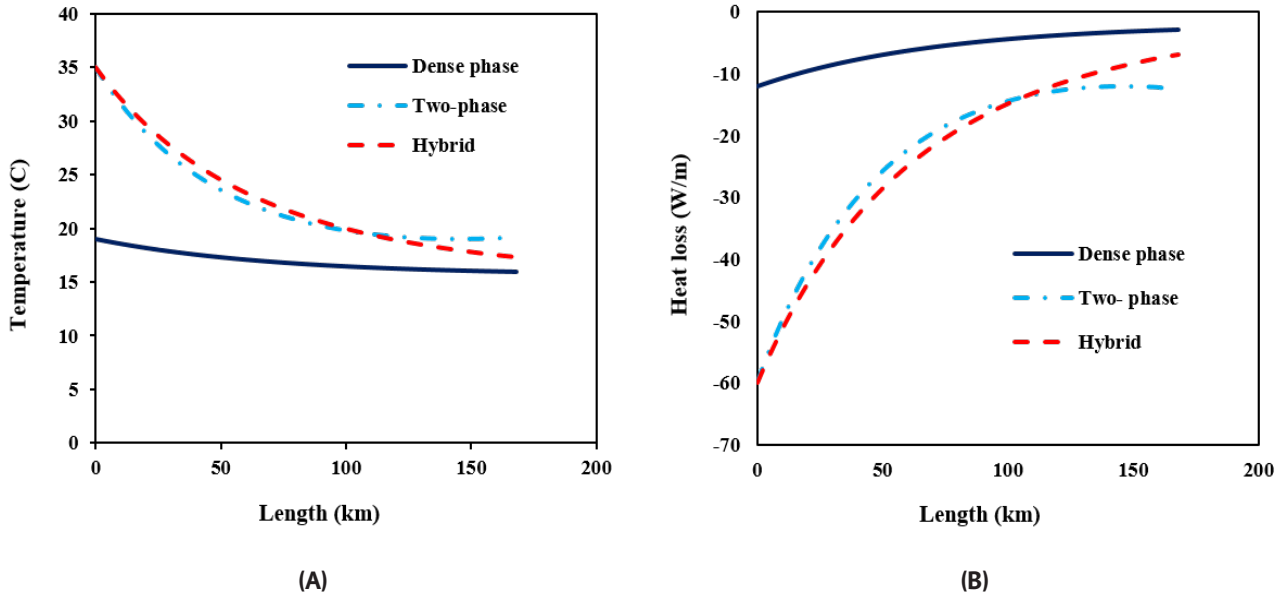

Figure10. Temperature (A) and Heat Loss (B) Profiles in Dense Phase, Two-phase, and Hybrid Modes

3.8. Transmission Capacity

One of the major advantages of natural gas transmission in dense phase or hybrid modes is the increase in gas transmission capacity. (Figure 11) shows the pressure drop versus gas mass flow rate. The capacity increase has been investigated in two cases with the limitation of two-phase flow formation. Therefore, the maximum amount of gas that can be transmitted in dense phase or hybrid mode is 90 kg/s, which is 52% higher compared to normal conditions. In this state, the pressure drops in dense phase and hybrid modes are 27 and 30 bar, respectively.

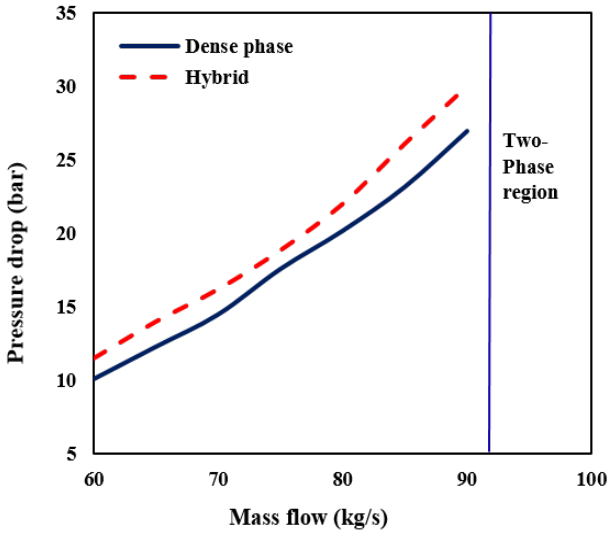

Figure 11. Variation of Pressure-drop versus to the Mass Flow Rate in Two Cases

3.9. Validation

Validation of simulation results is a crucial step to ensure confidence in the results. To achieve this, the results of Moreh et al. (Moore et al., 1980) were used for validation purposes. Detailed information on natural gas components and pipelines one to three were reported earlier (Moore et al., 1980). Pressure and temperature outputs from these pipelines were used to validate the simulation results. (Table 5) compares the simulated pressure and temperature outputs with the actual outputs from the three pipelines. The validation results indicate that the maximum error between the simulation results and Moreh et al.'s results is 4.55%. (Table 6) demonstrates the validation of the present model using experimental data for high-pressure natural gas. The study by Sletfjerding (1999) investigates the pressure drop at various mass flow rates. The maximum and average relative errors between the present model and the experimental data are 6.0% and 4.8%, respectively. Therefore, there is a good agreement between the simulation results and the pipeline outputs.

Table 5. Validation of outlet pressure (MPa) and temperature (K) from simulation results (Moore et al., 1980)

Pipeline	Outlet Pressure (Pipeline)	Outlet Pressure (Simulation)	Relative Error (%)	Outlet Temperature (Pipeline)	Outlet Temperature (Simulation)	Relative Error (%)
1	2.26	2.15	2.15	283.2	283.3	0.03
2	4.66	4.55	4.55	290.6	288.9	0.58
3	3.59	3.57	3.57	280.6	282.4	0.64

Table 6. Comparison of Pressure Drop Between the Present Model and Experimental Data (Sletfjerding, 1999)

Mass flow rate (kg/s)	Pressure (bar)	Temperature (°C)	ΔP (mbar): Experimental	ΔP (mbar): Present model
3.046	71.77	36.30	0.93	0.94
5.999	72.33	37.26	3.12	3.25
14.61	71.01	37.43	19.09	20.28
17.65	71.79	37.43	27.56	29.22
20.45	71.42	37.45	37.34	39.47
23.04	70.78	37.24	47.93	50.60
25.86	70.82	37.15	60.58	63.71
28.46	70.54	36.95	73.59	77.50
32.86	69.79	36.87	98.45	104.77

4. Statistical Analysis

The Response Surface Method can produce extensive data from a few trials and is powerful in distinguishing the interaction effects between factors on the results, along with determining the optimal conditions. However, in multivariable operations containing different effective factors, an initial screening design before optimization seems essential. Design-Expert software v13 was used to analyze the data and the regression coefficients (Bezerra et al., 2008; Said and Amin, 2015). A three-level Box-Behnken scheme was used to indicate the relative importance of the selected factors for the proposed models of the pressure drop in dense phase and hybrid modes using numerical trials. In this research, the factors are diameter, mass flow, and length of the pipeline. (Table 7) shows the factors and their ranges. Also, (Table 8) shows the levels of the factors and their corresponding results. Numerical trials (solving equations of continuity, momentum, and energy) were accomplished according to the shown trial plan (Table 8). The quadratic regression equations for the pressure drop in dense phase and hybrid modes in terms of diameter, mass flow, and length of the pipeline are given by Equations (27) and (28), respectively.

(Tables 9) and 10 present the p-values for each model and factor in the dense phase and hybrid mode, respectively. A p-value below 0.05 signifies a significant effect, whereas values above 0.05 indicate a negligible influence. For the pressure drop model in both modes, the quadratic effects of mass flow area (A^2) and length (C^2), as well as the interaction between mass flow rate and length (AC), have no significant impact on pressure drop. Other factors exhibit a significant effect on pressure drop, as their p-values are below 0.05.

(Figure 12A) and (Figure 12B) show the predicted pressure drop in dense phase and hybrid modes, respectively. According to the values of R^2, the predicted values are in good agreement with the actual values. According to the models and their coefficients, it is clear that the diameter has a significant effect on the pressure drop compared to the mass flow and length of the pipeline.

Table 7. Factors and Their Range

Factor	Low Level	High Level
m: mass flow (kg/s)	60	90
D: diamete (m)	0.45	0.75
L: Length (km)	100	200

Table 8. Factors and Their Corresponding Results

Run	m. (kg/s)	D (m)	L (km)	ΔP (bar) of the dense phase	ΔP (bar) of the hybrid
1	75	0.75	200	1.93	2.06
2	75	0.45	100	14.91	17.04
3	90	0.6	200	9.21	10.076
4	90	0.45	150	37.73	43.64
5	60	0.6	100	1.97	2.19
6	75	0.75	100	0.97	1.08
7	60	0.6	200	3.95	4.22
8	75	0.45	200	33.53	37.3
9	60	0.75	150	0.92	0.99
10	90	0.6	100	4.53	5.13
11	75	0.6	150	4.68	5.14
12	90	0.75	150	2.09	2.30
13	60	0.45	150	14.09	15.50

$$\Delta P(bar) = -91.73 + 3.38m - 354.70D + 1.02L - 2.49mD - 0.58DL + 459.69D^2 \quad (27)$$

$$\Delta P\,(bar) = -109.23 + 3.93m - 403.84D + 1.18L - 2.98mD - 0.64DL + 528.85D^2 \quad (28)$$

Table 9. The Analysis of Variance of Dense Phase Mode (Eq. 27)

Model Terms	Sum of Squares	Degree of Freedom	Mean Square	p-value (Significant)
Model	193.5700	9	193.5700	0.0061
A-m	188.6900	1	188.6900	0.0062
B-D	1112.7400	1	1112.7400	0.0011
C-L	141.4200	1	141.4200	0.0083
AB	126.2300	1	126.2300	0.0093
AC	18.7700	1	18.7700	0.0578
BC	77.9700	1	77.9700	0.0149
A^2	3.4600	1	3.4600	0.2297
B^2	213.9600	1	213.9600	0.0055
C^2	9.5800	1	9.5800	0.1047

Table 10. The Analysis of Variance of Hybrid Mode (Eq. 28)

Model Terms	Sum of Squares	Degree of Freedom	Mean Square	p-value (Significant)
Model	2265.4000	9	251.7100	0.0104
A-m	258.5900	1	258.5900	0.0100
B-D	1432.4600	1	1432.4600	0.0018
C-L	173.8500	1	173.8500	0.0148
AB	179.9600	1	179.9600	0.0143
AC	26.4400	1	26.4400	0.0867
BC	92.9300	1	92.9300	0.0271
A^2	4.1000	1	4.1000	0.3380
B^2	283.1800	1	283.1800	0.0092
C^2	14.2500	1	14.2500	0.1453

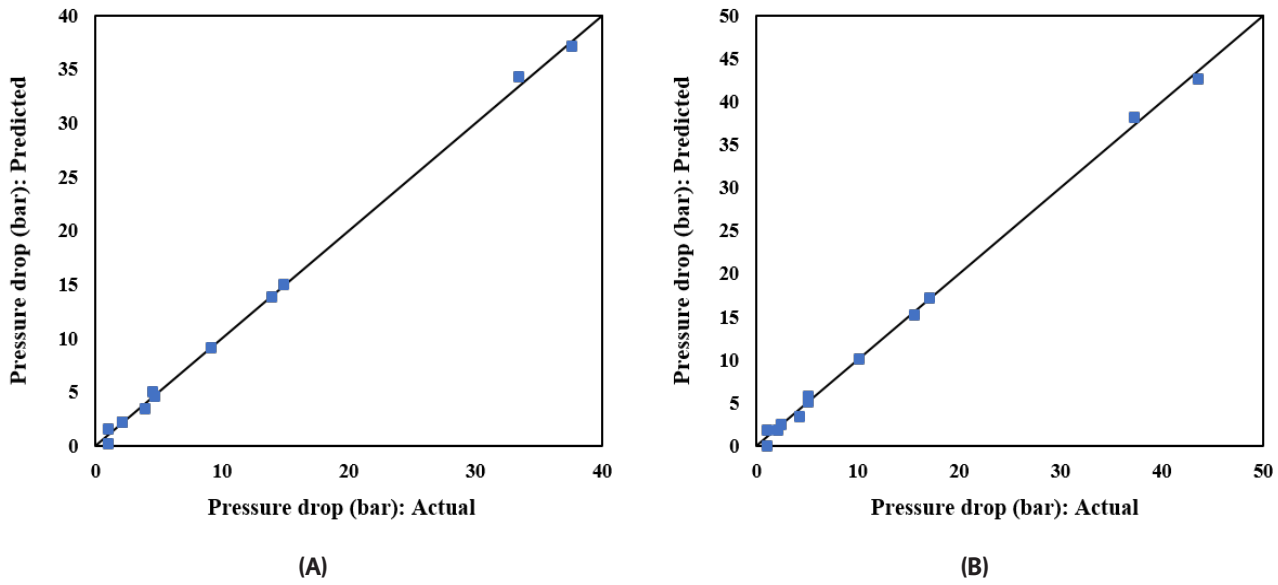

Figure 12. Comparison of Predicted and Actual Pressure Drop of the Dense Phase (A) and the Hybrid Mode (B)

5. Conclusion

In this study, the performance of natural gas pipelines in dense phase and hybrid modes was evaluated. These modes reduced issues such as high pressure drop, high velocity, low capacity,

and the formation of two-phase flow. The main findings are as follows:

- The pressure drops and velocities in the dense phase and hybrid modes were, on average, 2.2 times lower than in two-phase flow. This suggests that transporting natural gas in dense phase or hybrid mode is a suitable method to mitigate pressure drop concerns in pipelines.
- The densities in dense phase and hybrid modes were, on average, 2.5 times higher than in two-phase flow. Thus, increasing the density in these modes helps reduce velocity and pressure drop.
- The viscosities in dense phase and hybrid modes were similar to those of gases, indicating no significant concern about an increased pressure drop due to viscosity when transporting natural gas in these modes.
- The maximum gas flow rate that can be transmitted in dense phase or hybrid mode is 90 kg/s, which is 52% higher than under normal conditions. Therefore, if additional capacity is needed, using dense phase or hybrid mode can increase pipeline capacity.
- The duty of the hybrid mode was 35% lower than that of the dense phase mode. This suggests that the transmission of natural gas in hybrid mode is more suitable than in dense phase mode when the cricondentherm temperature (maximum temperature of the dew point curve) is low.
- Quadratic models for pressure drop in dense phase and hybrid modes, in terms of diameter, mass flow rate, and pipeline length, were proposed.
- Pipeline diameter had a greater impact on pressure drop compared to mass flow rate and pipeline length.

Nomenclature

A	Area (m^2)
C_P	Heat capacity ($J\ kg^{-1}K^{-1}$)
D	Diameter (m)
e	Surface roughness (m)
f_D	Darcy friction factor (-)
h	Overall heat transfer coefficient ($W\ m^{-2}\ K^{-1}$)
k	Thermal conductivity ($W\ m^{-1}\ K^{-1}$)
p	Pressure (Pa), Perimeter (m)
Pr	Prandtl number (-)
QW	Heat exchanged with the environment (Wm^{-1})
r	Outer radius of the pipeline (m)
Re	Reynolds number (-)
T	Temperature (°C)
u	Velocity (ms^{-1})

Subscripts	
in	inlet
out	outlet
env	environment
Greek Letters	
μ	Gas viscosity (Pa s)
ρ	Gas density (kgm^{-3})

References

Abd, A. A., Naji, S. Z., & Hashim, A. S. (2020). Effects of non-hydrocarbons impurities on the typical natural gas mixture flows through a pipeline. Journal of Natural Gas Science and Engineering, 76, 103218.

Almara, L.M., Wang, G.-X. and Prasad, V. 2023. Conditions and thermophysical properties for transport of hydrocarbons and natural gas at high pressures: Dense phase and anomalous supercritical state. Gas Science and Engineering 117, 205072.

Bezerra, M.A., Santelli, R.E., Oliveira, E.P., Villar, L.S. and Escaleira, L.A. 2008. Response surface methodology (RSM) as a tool for optimization in analytical chemistry. Talanta 76(5), 965-977.

Botros, K.K. 2002. Performance of five equations of state for the prediction of VLE and densities of natural gas mixtures in the dense phase region. Chemical Engineering Communications 189(2), 151-172.

Brokaw, R.S. 1965. Approximate formulas for the viscosity and thermal conductivity of gas mixtures. II. The Journal of Chemical Physics 42(4), 1140-1146.

Chaczykowski, M. and Osiadacz, A.J. 2012. Dynamic simulation of pipelines containing dense phase/supercritical CO_2-rich mixtures for carbon capture and storage. International Journal of Greenhouse Gas Control 9, 446-456.

Chen, C., Li, C., Reniers, G. and Yang, F. 2021. Safety and security of oil and gas pipeline transportation: A systematic analysis of research trends and future needs using WoS. Journal of Cleaner Production 279, 123583.

Cristello, J. B., Yang, J. M., Hugo, R., Lee, Y., & Park, S. S. (2023). Feasibility analysis of blending hydrogen into natural gas networks. International Journal of Hydrogen Energy, 48(46), 17605-17629.

Dorao, C. and Fernandino, M. 2011. Simulation of transients in natural gas pipelines. Journal of Natural Gas Science and Engineering 3(1), 349-355.

Faramawy, S., Zaki, T. and Sakr, A.-E. 2016. Natural gas origin, composition, and processing: A review. Journal of Natural Gas Science and Engineering 34, 34-54.

Gato, L. and Henriques, J. 2005. Dynamic behaviour of high-pressure natural-gas flow in pipelines. International Journal of Heat and fluid flow 26(5), 817-825.

Gregory, G., Aziz, K. and Moore, R. 1979. Computer Design of Dense-Phase Pipelines. Journal of Petroleum Technology 31(01), 40-50.

Haaland, S.E. 1983. Simple and explicit formulas for the friction factor in turbulent pipe flow.

Helgaker, J.F. and Ytrehus, T. 2012. Coupling between continuity/momentum and energy equation in 1D gas flow. Energy Procedia 26, 82-89.

Lanzano, G., Salzano, E., de Magistris, F.S. and Fabbrocino, G. 2013. Seismic vulnerability of natural gas pipelines. Reliability Engineering & System Safety 117, 73-80.

Mokhatab, S. 2007. Explicit method predicts temperature and pressure profiles of gas-condensate pipelines. Energy Sources, Part A 29(9), 781-789.

Mokhatab, S., Poe, W.A. and Mak, J.Y. (2018) Handbook of natural gas transmission and processing: principles and practices, Gulf professional publishing.

Moore, R., Bishnoi, P. and Donnelly, J. 1980. Rigorous design of high pressure natural gas pipelines using BWR equation of state. The Canadian Journal of Chemical Engineering 58(1), 103-112.

Peretti, A. and Toth, P. 1982. Optimization of

a pipe-line for the natural gas transportation. European journal of operational research 11(3), 247-254.

Prasad, V., Almara, L.M. and Wang, G.-X. 2023. Ultra-long-distance transport of supercritical natural gas (SNG) at very-high mass flow rates via pipelines through land, underground, water bodies, and ocean. Gas Science and Engineering 117, 205053.

Saffari, H. and Zahedi, A. 2013. A new alpha-function for the Peng-Robinson equation of state: application to natural gas. Chinese Journal of Chemical Engineering 21(10), 1155-1161.

Said, K.A.M. and Amin, M.A.M. 2015. Overview on the response surface methodology (RSM) in extraction processes. Journal of Applied Science & Process Engineering 2(1), 8-17.

Shariati, A., Moshfeghian, M. and Maddox, R. 1999. Effect of C6+ characterization on two-phase flow pipelines. International Journal of Modelling and Simulation 19(4), 352-356.

Sletfjerding, E. (1999). Friction factor in smooth and rough gas pipelines. An experimental study.

Teng, L., Zhang, D., Li, Y., Wang, W., Wang, L., Hu, Q., Ye, X., Bian, J. and Teng, W. 2016. Multiphase mixture model to predict temperature drop in highly choked conditions in CO_2 enhanced oil recovery. Applied Thermal Engineering 108, 670-679.

Thomas, S. and Dawe, R.A. 2003. Review of ways to transport natural gas energy from countries which do not need the gas for domestic use. Energy 28(14), 1461-1477.

Vargas-Vera, B.-H., Rada-Santiago, A.-M. and Cabarcas-Simancas, M.-E. 2020. Gas transport at dense phase conditions for the development of deepwater fields in the Colombian Caribbean sea. CT&F-Ciencia, Tecnología y Futuro 10(1), 17-32.

Wei, Q., Zhou, P. and Shi, X. 2023. The congestion cost of pipeline networks under third-party access in China's natural gas market. Energy 284, 128521.

Witkowski, A., Rusin, A., Majkut, M. and Stolecka, K. 2018. Analysis of compression and transport of the methane/hydrogen mixture in existing natural gas pipelines. International Journal of Pressure Vessels and Piping 166, 24-34.

Zhang, Z. Wang, G., Massarotto, P., & Rudolph, V. (2006). Optimization of pipeline transport for CO_2 sequestration. Energy Conversion and Management, 47(6), 702-715.

Zivdar, M. 2021. Natural gas transmission in dense phase mode. Journal of Gas Technology. JGT 6(2).

JOURNAL OF GAS TECHNOLOGY

Volume 9 / Issue 1 / Summer 2024 / Pages 67-75

Journal Home page: http://jgt.irangi.org

Application of Plant Extract as Barite Scale Inhibitor in Water Injection Operation

Amirhossein Maleki[1], Mastaneh Hajipour[2*], Sayed Jamal Sheikhzakariaee[2]

1. M.Sc. Student, Department of Petroleum Engineering, Science and Research Branch, Islamic Azad University, Tehran, Iran
2. Assistant Professor, Department of Petroleum Engineering, Science and Research Branch, Islamic Azad University, Tehran, Iran

ARTICLE INFO

ORIGINAL RESEARCH ARTICLE

Article History:
Received: 06 June 2024
Revised: 26 July 2024
Accepted: 23 August 2024

Keywords:
Formation damage
Inorganic scale
Green inhibitor
Plant extract

ABSTRACT

Water injection into oil reservoirs is a common method to compensate for the pressure drop due to oil production. Injection water is mainly seawater, which contains ions such as sulfate and carbonate. Formation water generally contains cations such as calcium, barium, strontium, etc. Therefore, mineral scales are formed as a result of mixing injection water with formation brine. One of the most important problems in water injection operation is the formation of mineral scales, which causes reservoir damage, loss of production, pressure reduction, depreciation of the wellhead equipment, and in more severe cases, well closure. Using scale inhibitors is an effective method to prevent scale formation. In this study, olive leaf extract was used as a green inhibitor to prevent and reduce barite scale formation. For this purpose, water samples were synthesized according to real ionic composition of formation brine and sea water, and mixed at different mixing ratios. The inhibition performance of olive leaf extract was explored at different concentrations. Characterization of the used extract was carried out using FTIR analysis. The highest amount of barium sulfate precipitation was observed 0.37 gr/l in the mixture containing 90% formation brine. Experimental results indicated that the most effective concentration of the inhibitor for reduction of scale formation is 20 ml/l. Moreover, the effect of pH value and salinity of injection water was investigated and the best performance of inhibitor was observed at 4100 ppm salinity and pH 7.7.

DOR: 20.1001.1/jgt.2024.2037729.1045

How to cite this article
A.H. Maleki, M. Hajipour, S.J. Sheikhzakariaee, Application of Plant Extract as Barite Scale Inhibitor in Water Injection Operation. Journal of Gas Technology. 2024; 9(1): 67 -75. (https://jgt.irangi.org/article_717198.html)

* Corresponding author.
E-mail address: m.hajipour@srbiau.ac.ir, (M. Hajipour).

Available online 10 September 2024

1. Introduction

Formation damage is one of the most important reasons for declining well injectivity as well as productivity in oil and gas reservoirs. Several mechanisms responsible for formation damage are reported in the literature including fines migration, clay swelling, fluid-fluid incompatibility, phase blocking, scale formation, dissolution and precipitation reactions, and wettability alteration. The formation of mineral scales in hydrocarbon reservoirs and oil field facilities is the main challenge in water injection operations (Asadollahi et al., 2021). Scale formation and deposition can occur during certain operations such as stimulation, production and transportation in petroleum industry. Carbonates, sulfates and sulfides are common scales in oil fields. Usually, these scales are caused by changes in temperature, pressure and mixing of incompatible waters in the reservoir (Merdhah and Yassin, 2007). Controlling and preventing the formation of scales as one of the most effective solutions has been the concern of both research and industry for many years. The most effective method to reduce mineral scales in water injection operations is the use of scale inhibitors, which requires a comprehensive study under different conditions. To select the best type and concentration of scale inhibitor, laboratory tests should be performed on formation brine and injection water. Scale inhibitors have different mechanisms of inhibition. A group of inhibitors can reduce the activities of the ions in the solution and consequently reduce the scale formation. Sum types of inhibitors affect the scale after the formation of the solid crystal core and prevent the crystal growth through adsorption to the active sites on the crystal surface. Another inhibition mechanism is the modification of the crystal structure, which often reduces the adhesion of scales on the solid surface. Another category of inhibitors reduces the deposition of scales by increasing the dispersion of solid crystals and reduces the accumulation and settling of suspended solid particles (Valadbeigian et. al., 2023).

For the best inhibitor performance, some factors should be investigated. The scale inhibitor (SI) must be stable against high temperature and salinity. In addition, since the chemistry and ionic composition of sea water and formation water vary at different regions, an effective SI should be compatible with these waters. Hence, a SI that performs well in a given oil field may not do so in another (Tantayakom et al., 2005; Viloria et al., 2010). Changes in environmental conditions such as pH value, temperature, fluid hydrodynamics, and presence of other chemicals can also influence the performance of a scale inhibitor. Factors such as brine supersaturation and the presence of divalent cations, such as Ca^{2+} and Mg^{2+} ions or even Zn^{2+} can lead to incompatibility between the brine system with the chemical, hence reducing its concentration in solution and its scale inhibition performance (Kan and Tomson, 2012).

Most commercial inhibitors used in oil fields are based on phosphonate and polyacrylate. Phosphonates are phosphorus-containing organic compounds that are not easily hydrolyzed due to the strong bond between phosphorus and carbon in their structure. Phosphorus and nitrogen compounds have been used effectively to prevent inorganic scale formation. Today, chemicals which are toxic and harmful to the environment are severely restricted. Therefore, it is important for the industry to develop alternative solutions, i.e., the use of green and environmentally friendly inhibitors to control the formation of mineral scales. Green chemicals are defined according to three criteria of non-toxicity, non-biological accumulation and possibility of biological degradation (Zojaji, 2020). Various natural products, especially from plants, contain generous amounts of polyphosphates, carboxylic acid groups, alcohol and aromatic amines, which are potential functionalities for adsorption or antiscaling effect of the chemical SIs. Research on

the use of plant materials as oilfield chemicals like drilling mud (Ghazali et al., 2015), biosurfactants (Silva et al., 2014) and corrosion inhibitors (Ituen et al., 2016; Ituen et al., 2017) is very active, but very little has been done to explore some plant materials as SIs. Extracts of natural plants are environmentally friendly, non-toxic, relatively less expensive, readily and sustainably available and also biodegradable. Nevertheless, this biodegradability limits the storage and long-term usage of plant extracts. Leaf extracts of Fig (Ficus carica L.) contains β-amyrine, umbelliferone, bergabten, psoralene, β-sitosterol, p-coumaric acid, lupeol and other organic compounds and have been used to inhibit calcium carbonate scales (Abdel-Gaber et al., 2008). Other plants materials reported as efficient scale inhibitors include sea weeds polysaccharides and soybean oil methyl ester (Miksic et al., 2005; Abdel-Gaber et al., 2011), and leaf extracts of Punicagranutum (Abdel-Gaber et al., 2017). There are also reports on products or compounds from plants and natural products such as humic acid, leucine, citric acid and xanthan used as scale inhibitors (Chaussemier et al., 2015). Recently, due to the limitations of the world community to protect the environment and also considering the fact that before using any scale inhibitor, laboratory studies of the inhibitor's performance under field conditions are required, environmentally friendly green inhibitors have received much attention by researchers (Zojaji, 2020).

In this research, an attempt was made to investigate the efficiency of olive leaf extract as a green inhibitor to control the formation of barite scales. To ensure the presence of functional groups such as hydroxyl and carboxyl in the olive leaf extract, a fourier transform infrared (FTIR) spectrometer was used for characterizing the extract. Brines compatibility experiments were conducted via standard jar test at reservoir temperature of 90 ℃ to explore the optimum inhibitor concentration. Furthermore, the effect of salinity and pH value of injected water on inhibition efficiency was also investigated.

2. Experimental Procedure

2.1. Brines Preparation

The formation brine and injection water samples were synthesized by dissolving a certain amount of high purity salts in distilled water. To prepare the injection water sample, 0.47 g sodium sulfate salt and 3.63 g sodium chloride salt were dissolved in 100 cc distilled water. The formation water sample was made by dissolving 0.26 g barium chloride and 14.98 g sodium chloride in 100 cc distilled water. All samples were passed through filter paper in order to remove any solid particles from the prepared solutions.

Olive leaf extract was prepared by two extraction methods using a Soxhlet apparatus and by boiling the powdered leaves in distilled water. In the first method, 100 g of dried olive leaves were ground into powder by grinding in a mortar. Then, 5 g of the powder was mixed with 100 cc distilled water and the extraction process was performed for 6 hours using a Soxhlet apparatus. Finally, the refluxed solution was filtered to remove any contamination and solid particles.

In the second method, 5 g of dried olive leaves that were ground into powder were mixed with 100 cc distilled water and placed on a heater stirrer. After boiling the mixture for 30 minutes, the mixture was filtered using a 0.45 µm cellulose acetate filter paper and stored in a closed bottle at ambient temperature. A fourier transform infrared (FTIR) spectrometer was used for characterizing the olive leaves extract.

2.2. Brines Compatibility Test

Static jar tests were performed to determine the amount of scale and the performance of olive leaf extract as scale inhibitor. To this end, formation and injection water samples were mixed in different volume ratios in different glass tubes. The glass tubes were kept at constant temperature and pressure

and their content was stirred every 15 minutes to complete the precipitation reaction. After complete mixing of brines, the electrical conductivity and turbidity of the solutions were measured. Finally, by passing each solution through 0.45 µm filter paper, the solid scale was separated, dried, and weighed using a digital balance.

The same procedure was repeated by adding the olive leaf extract at various concentrations (i.e., 20, 40, 50 and 100 ml/l) to the injection water and the amount of the formed scale was measured accurately. Using the experimental data, the percentage of scale inhibition was calculated.

The salinity of injection water is a key factor in designing low salinity water injection operations. In order to observe the effect of the salinity of injected water on the green inhibitor efficiency, 2, 5 and 10 times diluted seawater samples were prepared as shown in (Table 1) and compatibility tests were conducted at different salinities. In (Table 1), SW denotes seawater and SWXD indicated X times diluted seawater.

Table 1: Diluted Injection Water Composition

Concentration (ppm)	SW	SW2D	SW5D	SW10D
Na^+	13100	6550	2620	1310
Cl-	23800	11900	4760	2380
$SO4^{2-}$	3200	1600	640	320
TDS	40100	20050	8020	4010

One of the main parameters affecting the solubility of mineral scales is pH value. Therefore, the impact of injection water pH value on the amount of scale and inhibitor efficiency were explored in this study. To this end, the injection water samples were prepared at different pH values by adding a specified amount of Sodium Hydroxide. At each pH value, jar tests were performed at different inhibitor concentrations, and variations in the amount of scale was measured. (Figure 1) demonstrates the procedure of the experiments.

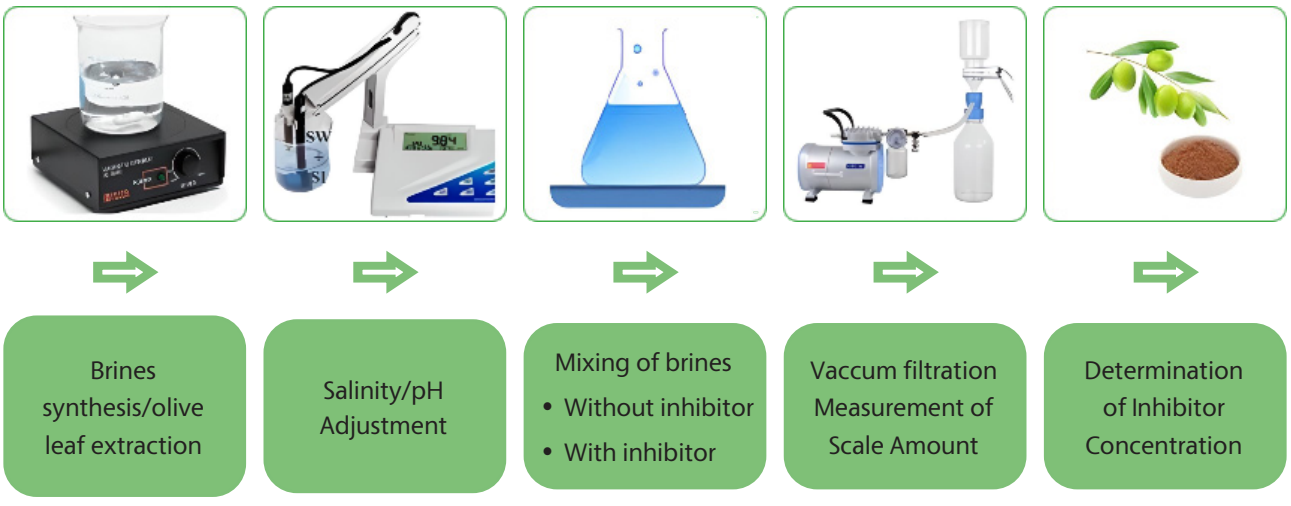

Figure 1. Schematic of the Experimental Procedure

3. Result and Discussion

(Figure 2) illustrates the FTIR spectrum of the olive leaf extract. The observed peak at wavenumber 3428.22 cm^{-1} can be attributed to the hydroxyl functional group, and the two peaks at 1730.98 and 1631.77 cm^{-1} are related to the C = O bond of the carboxylic group.

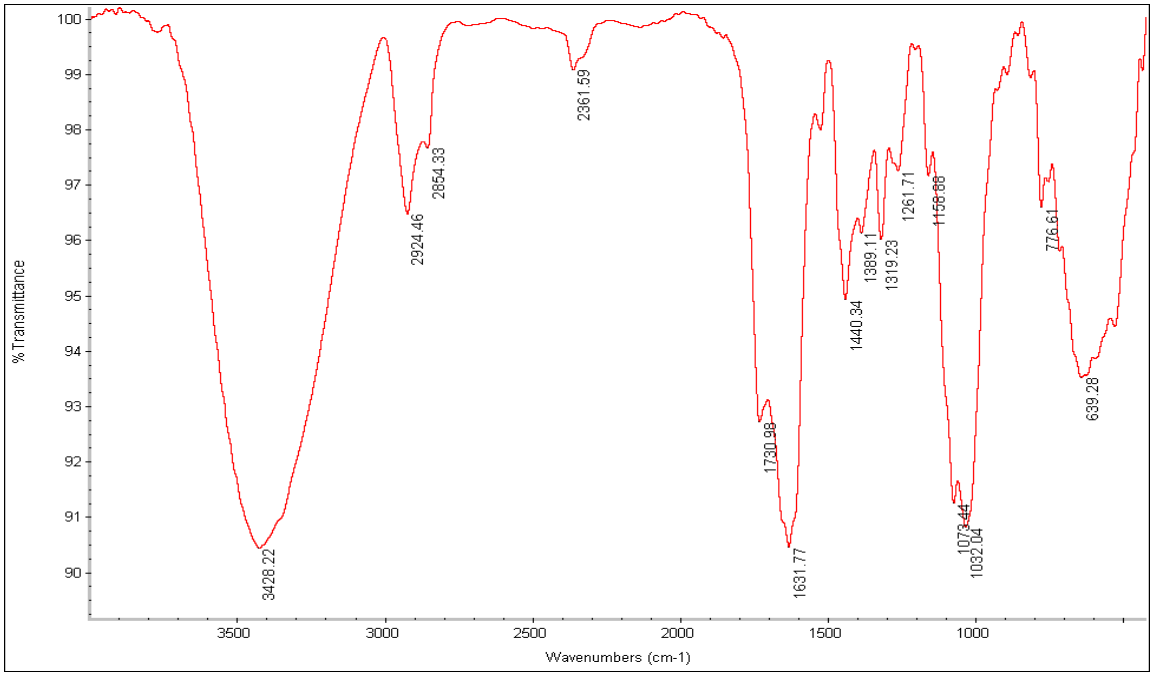

Figure 2. FTIR Spectrum of Olive Leaf Extract

3.1. Effect of Mixing Ratio

In the first set of static tests, the effect of the mixing ratio of formation brine to injection water was investigated. It was observed that with the increase in the volume of formation water more scale is formed due to the increase of barium ions concentration and more reaction with sulfate anions. As shown in (Figure 3), in the mixture containing 50% formation brine and 50% injection water, the amount of scale was measured 0.033 g, and in the solution including 90% formation brine, the amount of scale was detected 0.074 g. The highest amount of scale was observed in the mixture containing 90% formation water. In fact, with increasing the volume fraction of formation brine, the amount of barium ions in the solution increases, and therefore the chemical reaction of barium sulfate formation (i.e., Eq. 1) proceeds toward the formation of solid phase and the formation of solid crystals of scale.

$$Ba^{2+}\,(aq) + SO_4^{2-}\,(aq) \leftrightarrows BaSO^4\,(s) \qquad (1)$$

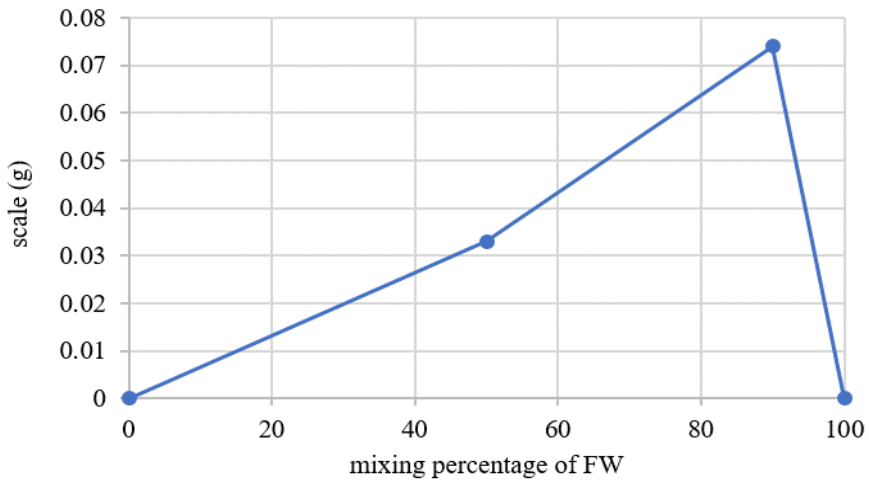

Figure 3. The Amount of Scale at Different Percentage of Formation Water

3.2. Inhibitor Performance Analysis

Static jar tests were performed at different inhibitor concentrations of 20, 40, 50 and 100 ml/liter of injected water. As can be seen in (Figure 4), the lowest amount of scale was formed at inhibitor concentration of 20 (ml/l). Increasing the concentration of inhibitor more than 20 (ml/l) leads to increase the scale amount. In fact, similar to chemical inhibitors, an optimum value for the concentration of green inhibitors should be determined to reach the highest inhibition efficiency. For olive leaf extraction using a Soxhlet apparatus, the best efficiency was observed at the concentration of 20 ml/l, and the amount of barite scale was decreased to 0.068 g.

For the second method of extraction in which the olive leaf extract was obtained by boiling the powdered leaves in distilled water, static jar tests were repeated. As shown in (Figure 5), the best inhibition efficiency was again detected when the inhibitor concentration was 20 (ml/l).

Figure 4. The Amount of Scale at Different Inhibitor Concentrations from Soxhlet Extraction

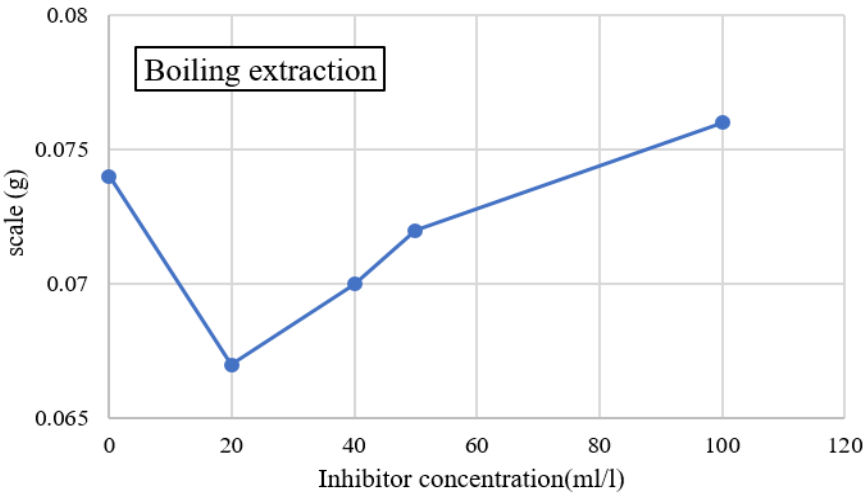

Figure 5. The Amount of Scale at Different Inhibitor Concentrations from Boiling Extraction

By comparing the obtained results of two different extraction methods, it can be concluded that the extracts obtained from both methods were equally effective in reducing the barite scale. Therefore, the boiling method which is simpler and done in less time can be used as an effective extraction method.

3.3. Effect of Salinity

The effect of injection water salinity on inhibitor performance was explored by diluting the injection water. The measurement of the electrical conductivity of brine mixture containing inhibitor at different salinities showed that the decrease in injection water salinity, decreases the electrical conductivity, which means that the dissolved ions in the solution are decreased. As can be seen in (Figure 6), with the decrease of injection water salinity and consequently the decrease of electrical conductivity, the amount of barite scale decreases.

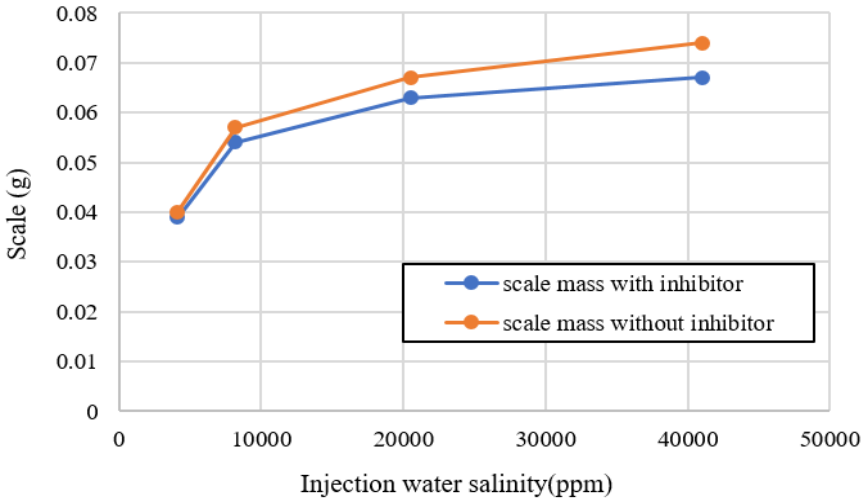

Figure 6. The Effect of Salinity on the Scale Amount

3.4. Effect of pH Value

As most mineral scales are soluble in acidic solvents, the pH value of injection water is an effective factor on inorganic scales. As shown in (Figure 7), pH value has no effect on barium sulfate precipitation in the absence of inhibitor and it can be stated that barium sulfate scale formation is independent of pH value. Similar results have been reported in the experiments of Tantayakom et al. (2005).

The effect of pH value on barite scale is different in the presence of inhibitor. It was found that with increasing the injection water pH value, the amount of scale increases slightly which is in accordance with the results of previous studies (Asadollahi et al., 2021; Merdhah and Yassin, 2007). The amount of scale formed at pH 8.7, 9.7, and 10.7 was measured 0.070, 0.074, and 0.080 g, respectively.

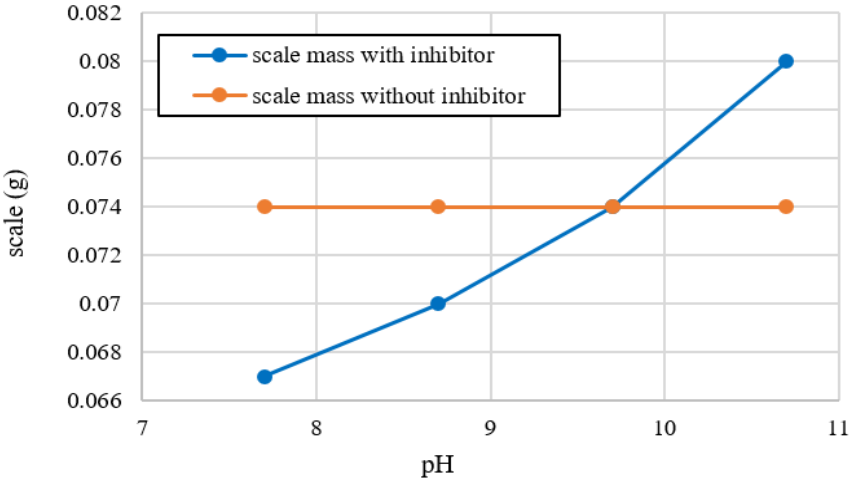

Figure 7. The Effect of pH Value on the Scale Amount

3. Conclusions

In this study, olive leaf extract was used as a novel green inhibitor to prevent and reduce barite scale formation. For this purpose, the brine samples were synthetized according to the ionic composition of formation brine and sea water, and static jar tests were conducted to investigate the efficiency of the proposed inhibitor. The effect of the volume ratio of formation brine to injection water, salinity and pH value of injection water was explored at different concentrations of inhibitor. FTIR analysis of olive leaf extract confirmed the presence of hydroxyl and carboxyl functional groups which are effective chelating agents.

Static compatibility tests showed that the highest amount of barium sulfate scale i.e., 0.37 (g/l) is formed in the mixture containing 90% formation water. By adding olive leaf extract to the brines mixture, first the amount of scale reduces and then increases. The minimum amount of scale was detected when the concentration of green inhibitor was 20 ml/ liter. Although in the absence of inhibitor no change in the amount of barium sulfate scale was observed by changing pH value, but the performance of green inhibitor was decreased at higher pH values. The results of experiments at different salinities of injection water indicated that that the green inhibitor has a good performance at high salinities. The findings of this study confirm that olive leaf extract can be considered as an alternative to chemical and toxic inhibitors of barite scale.

References

Abdel-Gaber, A.M., Abd-El-Nabey, B.A., Khamis, E., Abd-El-Khaled, D.E. (2008). "Investigation of fig leaf extract as a novel environmentally friendly antiscalent for $CaCO_3$ calcareous deposits" Desalination. 230: 314-328.

Abdel-Gaber, A.M., Abd-El-Nabey, B.A., Khamis, E., Abd-El-Khaled, D.E. (2011). "A natural extract as scale and corrosion inhibitor for steel surface in brine solution" Desalination 278: 337-342.

Abdel-Gaber, A.M., Abd-El-Nabey, B.A., Khamis, E., Abd-El-Rhmann, H., Aglan, H., Ludwick, A. (2012). "Green anti-scalant for cooling water systems" International Journal of Electrochemical Science. 7(12): 11930-11940.

Asadollahi A., Hajipour M., Biniaz Delijani E., Rajabi M.S. (2021). "Laboratory assessment of formation damage due to re-injection of production water into oil reservoirs" 5th International Conference on Global Studies in Technology and Engineering Sciences, Tehran.

Chaussemier, M., Pourmohtasham, E., Gelus, D., Pécoul, N., Perrot, H., Lédion, J., Cheap-Charpentier, H., Horner, O. (2015). "State of art of natural inhibitors of calcium carbonate scaling. A review article" Desalination. 356:47-55.

Ghazali, N. A., Jaih, M. Z. M., Mohd, T. A. T., Alias, N., Azizi, A., Yahya, E. (2015). "The Characteristic Study of Oil Palm Kernel Expeller as Lost Circulation Material in Water Based Drilling Mud (WBM)" Advanced Materials Research. 1113:648-653.

Ituen, E., Akaranta, O., James, A., Sun, S. (2017). "Green and sustainable local biomaterials for oilfield chemicals: Griffonia simplicifolia extract as steel corrosion inhibitor in hydrochloric acid" Sustainable Materials and Technologies.11, 12-18.

Ituen, E., James, A., Akaranta, O., Sun, S. (2016). "Eco-friendly corrosion inhibitor from Pennisetum purpureum biomass and synergistic intensifiers for mild steel" Chinese Journal of Chemical Engineering, 24(10), 1442-1447.

Kan, A., Tomson, M. (2012). "Scale prediction for oil and gas production" SPE Journal. 17(02):362-78.

Merdhah, A.B., Yassin, A.A. (2007). "Scale formation in oil reservoir during water injection at high-salinity formation water" Journal of Applied Sciences 7(21):3198-207.

Miksic, B.A., Kharshan, M.A., Furman, A.Y. (2005). "Vapor corrosion and scale inhibitors formulated from biodegradable and renewable raw materials" European Symposium on Corrosion Inhibitors (10 SEIC) Ferrara, Italy.

Silva, R. D. C. F., Almeida, D. G., Rufino, R. D., Luna, J. M., Santos, V. A., Sarubbo, L. A. (2014). "Applications of biosurfactants in the petroleum industry and the remediation of oil spills" International journal of molecular sciences, 15(7), 12523-12542.

Tantayakom V, Sreethawong T, Scott Fogler H, de Moraes FF, Chavadej S., (2005). "Scale inhibition study by turbidity measurement" Journal of Colloid and Interface Science 284: 57-65.

Tantayakom, V., Fogler, H.S., Charoensirithavorn, P., Chavadej, S. (2005). "Kinetic study of scale inhibitor precipitation in squeeze treatment" Crystal Growth and Design. 5(1):329-35.

Valadbeigian V., Hajipour, M., Behnood, M. (2023). "Static and dynamic evaluation of formation damage due to barium sulfate scale during water injection in carbonate reservoirs" Journal of Petroleum Exploration and Production Technology 13(8), 1819-1831.

Viloria, A., Castillo, L., Garcia, J. A., Biomorgi, J. (2010). U.S. Patent No. 7,645,722. Washington, DC: U.S. Patent and Trademark Office.

Zojaji, I. (2020) "A review of the role of natural inhibitors to prevent calcium carbonate deposition" 9th National Conference on New Research in Chemical and Science and Engineering.

ارزیابی تأثیر شوری فاز آبی بر معدنی شدن دی‌اکسید کربن در طول فرآیند ذخیره‌سازی گاز

- برایات بریاکپوآ کیناته[1,*]، اوگونا دیکسون آمادی[2]، اولالکان کونل آکیندله[3]، جرمیاه ایفئانی اکرومه[4]

۴،۱. گروه مهندسی نفت، دانشگاه ایالتی ریورز، پورت هارکورت، نیجریه

۲. گروه نفت و گاز، دانشگاه سالفورد، منچستر، انگلستان

۳. گروه علوم داده، هوش مصنوعی و مدل‌سازی، دانشگاه هال، انگلستان

(ایمیل نویسنده مسئول: ahhassani@srb.iau.ir)

چکیـــــــده

در این پژوهش، تأثیر شوری فاز آبی بر فرآیند معدنی شدن دی‌اکسید کربن بررسی شده است. شوری فاز آبی تأثیر قابل توجهی بر میزان دی‌اکسید کربن به دام افتاده از طریق مکانیزم انحلالی دارد و همچنین ممکن است بر فرآیندهای انحلال و رسوب‌گذاری مواد معدنی تأثیر بگذارد. در حالی که روش‌های مختلف ذخیره‌سازی دی‌اکسید کربن از جمله ذخیره‌سازی ساختاری، باقیمانده، انحلالی و تا حدی معدنی به طور گسترده مطالعه شده‌اند، پتانسیل به دام‌اندازی معدنی و عوامل مؤثر بر آن کمتر مورد بررسی قرار گرفته‌اند. در این تحقیق، تأثیر تغییرات شوری فاز آبی بر معدنی شدن دی‌اکسید کربن از طریق شبیه‌سازی عددی بررسی شده است. این شبیه‌سازی با استفاده از یک شبیه‌ساز ژئوشیمیایی و یک مدل سه‌بعدی همگن از یک آبخوان با ابعاد ۰۱×۰۳×۰۳ (۰۰۰۹ بلوک شبکه‌ای) و عرض هر بلوک ۰۷ متر انجام شده است. شبکه تولید شده با ویژگی‌های پتروفیزیکی، شبکه‌بندی و خصوصیات سنگی پر شده است. چهار مدل با خصوصیات سنگ و سیال مشابه برای شرایط آب خالص و شوری‌های مختلف (۱۰۰۰۰ppm) ۰،۰۱ wt (۱۵۰۰۰ppm) ۰،۰۱۵ wt و (۲۰۰۰۰ppm) ۰،۰۲ wt به ترتیب شبیه‌سازی شدند. نتایج نشان داد که با افزایش شوری آب شور، میزان دی‌اکسید کربن حل‌شده کاهش می‌یابد. افزایش شوری باعث کاهش مول‌های دی‌اکسید کربن تبدیل‌شده به یون‌های محلول در آب و کاهش میزان انحلال در آب موجود می‌شود. همچنین، با افزایش مدت زمان تزریق دی‌اکسید کربن، نرخ رسوب‌گذاری کائولینیت و کلسیت افزایش یافته، در حالی که نرخ انحلال آنورتیت کاهش می‌یابد. تغییرات مولی مواد معدنی در مورد آنورتیت با افزایش سطح شوری افزایش یافته اما با افزایش مدت زمان تزریق دی‌اکسید کربن کاهش می‌یابد. از سوی دیگر، تغییرات مولی کلسیت و کائولینیت با افزایش سطح شوری و مدت زمان تزریق کاهش پیدا می‌کند. به طور کلی، با افزایش شوری فاز آبی، مقدار کلسیت و کائولینیت کاهش می‌یابد.

این مطالعه نشان داده است که واکنش‌پذیری مواد معدنی تشکیل‌دهنده مخزن نسبت به غلظت شوری متفاوت است که این امر نقش تعیین‌کننده‌ای در ظرفیت ذخیره‌سازی و به دام‌اندازی دی‌اکسید کربن دارد.

واژگان کلیدی: معدنی شدن، انحلال، مدل آبخوان، شوری فازی، ذخیره‌سازی

استفاده از تجزیه و تحلیل جامع سیستم‌های خبره برای بهبود انتخاب سیال اسیدکاری در تولید نفت

- محمد نوروزی دلاویز[1]، احمد ریگی[1]، سامان جهان‌بخشی[2*]

۱. کارشناسی ارشد مهندسی نفت، شرکت مدیریت پروژه‌های صنعتی ابدال، مرکز فناوری مپصا، تهران، ایران، کد پستی: ۸۳۶۴۶۷۳۹۹۱

۲. استادیار، دانشکده مهندسی معدن، دانشکدگان فنی، دانشگاه تهران، تهران، ایران

(ایمیل نویسنده مسئول: jahanbakhshi@ut.ac.ir)

چکیـــــــده

اسیدکاری چاه نقش مهمی در بهبود بازیابی نفت از طریق کاهش آسیب‌های مخزن ایفا می‌کند. با این حال، پیچیدگی انتخاب مناسب‌ترین سیال اسیدکاری، با توجه به شرایط مختلف مخزن، چالش قابل توجهی را ایجاد می‌کند. این مقاله بررسی می‌کند که چگونه استفاده از سیستم‌های خبره در بهبود فرآیند انتخاب سیال اسیدکاری موثر است. با مرور اثر، اجزا و مزایای سیستم‌های خبره، همراه با مطالعات موردی، مقاله نشان می‌دهد که چگونه این سیستم به تصمیم‌گیری موثرتر و اطلاعاتی بیشتر کمک می‌کند. در این بررسی، هشت نمونه از آسیب‌ها برای تجزیه و تحلیل با استفاده از سیستم خبره انتخاب شده است. پس از ارزیابی دقیق، یک سیال برای از بین بردن آسیب انتخاب شده است که کارایی سیستم خبره را نشان می‌دهد. ترکیب سیستم‌های خبره در مدل‌سازی و استنتاج تحت شرایط عدم قطعیت و دقت بالا، نقش اساسی در افزایش بهره‌وری، کاهش خطاها، پیش‌بینی رویدادها و اصلاح فرآیندهای تصمیم‌گیری دارد. این سیستم‌ها از الگوریتم‌ها و مدل‌های ریاضی پیشرفته برای مدل‌سازی و پیش‌بینی رویدادها در انواع مختلف برنامه‌ها استفاده می‌کنند، که باعث کمک به تصمیم‌گیری بهینه و سریع می‌شود.

واژگان کلیدی: اسیدکاری خمیره، انتخاب سیال اسیدکاری، آسیب سازند، سیستم‌های خبره، بهبود تولید نفت

مطالعه تطبیقی شیرابه تصفیه شده بیولوژیکی قبل و بعد از استفاده از AOP ها برای حذف COD و BOD و رنگ شیرابه

- صادق معتقد[۱]، امیرحسام حسنی[۲*]، سیدعلیرضا حاجی سید میرزاحسینی[۳]، سیدمسعود منوری[۲]، نبی اله منصوری[۲]

۱. دانشجوی دکتری، گروه مهندسی محیط زیست، دانشکده منابع طبیعی و محیط زیست، واحد علوم و تحقیقات، دانشگاه آزاد اسلامی، تهران، ایران

۲. استاد، گروه مهندسی محیط زیست، دانشکده منابع طبیعی و محیط زیست، واحد علوم و تحقیقات، دانشگاه آزاد اسلامی، تهران، ایران

۳. دانشیار، گروه مهندسی محیط زیست، دانشکده منابع طبیعی و محیط زیست، واحد علوم و تحقیقات، دانشگاه آزاد اسلامی، تهران، ایران

(ایمیل نویسنده مسئول: ahhassani@srb.iau.ir)

چکیـــــــده

در این تحقیق به بررسی مقایسه‌ای تصفیه شیرابه خروجی فرایند (UASB -AREATED LAGOON) قبل و بعد از اکسیداسیون پیشرفته (AOPs) پرداخته شده است و شاخص‌های آلاینده مانند COD, BOD و رنگ با لحاظ نمودن pH و دما و زمان تماس در معرض اکسید کنندگان مانند: ازن، H_2O_2/UV, UV و فتو فنتون مورد مطالعه و بررسی قرار گرفتند. زمان‌های تماس ۰، ۵، ۱۰، ۱۵، ۲۰، ۲۵ و ۳۰ دقیقه فرایند اکسیداسیون مدنظر قرار گرفته است. در میان AOPهای مورد مطالعه، UV/H_2O_2 بالاترین راندمان رنگ‌بری را نشان داد و تا ۹۸ درصد رسید. علاوه بر این، ازن زنی شیرابه اولیه منجر به حذف بهتر رنگ، COD و BOD نسبت به سایر فرایندهای AOP شد. به‌ویژه تصفیه با فتو فنتون بیشترین درصد حذف BOD را به خود اختصاص داد. ترتیب حذف COD در فرایند AOP عبارت بود از: PHOTO FENTON< O_3< UV < UV/H_2O_2. در حالی که ازن به‌عنوان عامل اکسیدکننده قوی مؤثر برای حذف COD و رنگ در شیرابه اولیه است اما فرایند UV/H_2O_2 در (pH = 6.4) بیشترین سرعت حذف رنگ را دارا بود و به‌عنوان کارآمدترین فرایند AOP برای حذف COD و رنگ ظاهر شد.

واژگان کلیدی: تجزیه، شیرابه زباله، تصفیه بیولوژیکی، اکسیداسیون شیمیایی

شبیه‌سازی عددی خط لوله گاز طبیعی در فازهای متراکم و ترکیبی

- مسلم ابروفراخ[۱]، مرتضی زیودار[۲*]، داود محبی کلهری[۳]

۱. دانشجوی دکتری، گروه مهندسی شیمی، دانشکده مهندسی، دانشگاه سیستان و بلوچستان، زاهدان، ایران

۲. استاد، گروه مهندسی شیمی، دانشکده مهندسی، دانشگاه سیستان و بلوچستان، زاهدان، ایران

۳. دانشیار، گروه مهندسی شیمی، دانشکده مهندسی، دانشگاه سیستان و بلوچستان، زاهدان، ایران

(ایمیل نویسنده مسئول: mzivdar@eng.usb.ac.ir)

چکیـــــــده

انتقال گاز طبیعی از طریق خطوط لوله به دلیل مقرون‌به‌صرفه بودن نسبت به سایر روش‌ها به‌طور گسترده مورد استفاده قرار می‌گیرد. با این حال، حمل گاز طبیعی از طریق خطوط لوله با چالش‌هایی مانند مصرف بالای انرژی، افت فشار قابل‌توجه و مشکلات جریان دوفازی مواجه است. در این مطالعه، انتقال گاز طبیعی در فازهای متراکم، ترکیبی (مناطق فاز متراکم و نزدیک به فاز متراکم) و دو فازی برای کاهش برخی از این محدودیت‌ها مورد بررسی قرار گرفت. علاوه بر این، مدل‌های ریاضی با فرم درجه دوم برای افت فشار در فاز متراکم و حالت ترکیبی بر اساس قطر، جریان جرمی و طول خط لوله پیشنهاد شدند. بر اساس این مدل‌ها، قطر خط لوله تأثیر بیشتری بر افت فشار نسبت به دبی و طول خط لوله داشت. نتایج همچنین نشان داد که مصرف انرژی مبدل حرارتی برای حالت ترکیبی ۳۵ درصد کمتر از فاز متراکم است. به‌طور متوسط، چگالی در فازهای متراکم و ترکیبی ۲/۵ برابر بیشتر از جریان دوفازی حاصل شد. افت فشار و سرعت در فازهای متراکم و ترکیبی ۲/۲ برابر کمتر از شرایط جریان دوفازی به دست آمد. همچنین، ظرفیت خط لوله برای انتقال گاز طبیعی در فازهای متراکم و ترکیبی ۵۲ درصد بیشتر از انتقال گاز در شرایط دوفازی محاسبه شد.

واژگان کلیدی: فاز متراکم، حالت هیبریدی، خط لوله، گاز طبیعی

کاربرد عصاره‌های گیاهی به‌عنوان بازدارنده رسوب باریت در عملیات تزریق آب

- امیرحسین ملکی[۱]، مستانه حاجی پور[۲*]، سیدجمال شیخ ذکریایی[۲]

۱. دانشجوی کارشناس ارشد، گروه مهندسی نفت، دانشکده نفت و مهندسی شیمی، واحد علوم و تحقیقات، دانشگاه آزاد اسلامی، تهران، ایران

۲. استادیار، گروه مهندسی نفت، دانشکده نفت و مهندسی شیمی، واحد علوم و تحقیقات، دانشگاه آزاد اسلامی، تهران، ایران

(ایمیل نویسنده مسئول: m.hajipour@srbiau.ac.ir)

چکیـــــــده

تزریق آب به مخازن نفتی یکی از روش‌های متداول جهت جبران افت فشار ناشی از تولید نفت می‌باشد. آب تزریقی معمولاً آب دریاست که حاوی یون‌هایی نظیر سولفات و کربنات است. آب سازندی اغلب دارای کاتیون‌هایی مانند کلسیم، باریم، استرانسیوم و غیره می‌باشد؛ بنابراین در اثر اختلاط آب تزریقی با آب سازندی، رسوبات معدنی تشکیل می‌شوند. یکی از مهم‌ترین مشکلات در عملیات تزریق آب، تشکیل رسوبات معدنی است که موجب آسیب به مخزن، کاهش تولید، افت فشار، استهلاک تجهیزات سرچاهی و در شرایط حاد بسته شدن چاه می‌گردد. استفاده از بازدارنده‌های رسوب روش مؤثری برای پیشگیری از تشکیل رسوبات است. در این مطالعه، عصاره برگ درخت زیتون به‌عنوان بازدارنده سبز جهت کاهش تشکیل رسوب باریت استفاده شد. برای این امر، نمونه آب‌ها بر اساس ترکیب یونی واقعی آب سازندی و آب تزریقی ساخته شدند و سپس در نسبت‌های مختلف حجمی با هم مخلوط شدند. عملکرد بازدارندگی عصاره برگ درخت زیتون در غلظت‌های مختلف ارزیابی شد. مشخصه یابی ترکیبات موجود در عصاره گیاهی مورد استفاده با آنالیز FTIR انجام شد. بیشترین مقدار رسوب سولفات باریم برابر با ۰/۳۷ gr/l در مخلوط حاوی ۹۰ درصد آب سازندی مشاهده شد. نتایج آزمایشگاهی نشان داد که مؤثرترین غلظت بازدارنده برای کاهش تشکیل رسوب، ۲۰ ml/l است. علاوه بر آن، تأثیر pH و شوری آب تزریقی نیز مورد بررسی قرار گرفت و بهترین عملکرد بازدارنده در شوری ۴۱۰۰ ppm و pH برابر با ۷/۷ مشاهده شد.

واژگان کلیدی: آسیب سازند، رسوبات معدنی، بازدارنده سبز، عصاره گیاهی

Iran Gas Institute

Journal of Gas Technology

VOLUME 9 • ISSUE 1 • SUMMER 2024

EISSN: 2588-5596

Contents